Internal Model Design for Power Electronic Controllers

By

Randupama Tharangani Gunasekara

A thesis submitted to the Faculty of Graduate Studies of
The University of Manitoba
in partial fulfilment of the requirements for the degree of

Master of Science

Department of Electrical and Computer Engineering
University of Manitoba
Winnipeg, Canada

Abstract

This thesis deals with the problem of control system design for power electronic controllers when high performance is desired despite unaccounted for internal and external conditions. Factors such as parameter variations, operating condition changes, and filtering and measurements delays, may adversely impact the performance of a circuit whose controller design is not immune to external and internal disturbances. The thesis explores the method of internal model design as a viable approach for designing controllers with superior performance despite system variations.

Following a presentation of the theoretical background of the internal model design, the thesis considers two examples of state variable models, improving the stability of a voltage source converter and speed control of an induction motor. Conclusions show the new control system is more stable and offers better controllability despite unexpected system variations, compared to classical control system.

Acknowledgments

This thesis is the outcome of two years of hard work and I might not have made it successfully if I had not got the support of some amazing people. It is an honor to express my gratitude to all of them at this point. First and foremost I would like to convey my sincere gratitude to my advisor, Professor Shaahin Filizadeh, for his supervision, invaluable advice and encouragement throughout my Master's program. His constant stimulating support helped me tremendously to be critical and analytical in every step required to finish this thesis.

I would like to thank all my lecturers for their support, help, and valuable advice. I am glad to thank my examination committee for accepting to review my thesis. I would also like to thank Prof. Filizadeh and the University of Manitoba for providing me with financial support and making it possible for me to complete this thesis.

I would also like to express my heartfelt gratitude to my parents and siblings who gave me support and strength throughout my life and made me able to pursue my goals. Last but not the least; I would like to thank all those who have offered a hand to the completion of this research directly or indirectly. Your contribution is appreciated and always remembered.

Randupama T. Gunasekara

Dedication

To my loving parents

Contents

List of Tables

List of Figures

List of Symbols

L	-	Inductance
C	-	Capacitance
V	-	Voltage
R	-	Resistance
$R(t)$	-	Reference
$U(t)$	-	Input
$Y(t)$	-	Output
$E(t)$	-	Error
$G(t)$	-	Process
$D(t)$	-	Disturbance
$\mathbf{x}$	-	State vector
$\tilde{\mathbf{x}}$	-	Estimate of the state x
ξ	-	Damping ratio
ω	-	Angular velocity

List of Abbreviations

DC	-	Direct Current
HVDC	-	High Voltage Direct Current
AC	-	Alternating Current
GTO	-	Gate Turn off Thyristor
BJT	-	Bipolar Junction Transistor
MOSFET	-	Metal-Oxide Semiconductor Field-Effect Transistor
IGBT	-	Insulted gate bipolar transistor
UPS	-	Uninterruptible Power Supply
SITH	-	Static Induction Thyristor
MCT	-	MOS Controlled Thyristor
PSCAD	-	Power System Computer Aided Design
EMTDC	-	Electromagnetic Transients including DC
VSC	-	Voltage Source Converter
PID	-	Proportional Integral Derivative
NDI	-	Nonlinear dynamic inversion
IMC	-	Internal Model Controller
SCR	-	Silicon Controlled Rectifier
PLL	-	Phase Locked Loop

Chapter 1

Introduction

1.1 Power Electronic Controllers

One of the main developments that has revolutionized the electrical engineering industry is the advent of power electronics. Power electronics can be defined as the engineering study of switching electronic circuits that convert electrical power from one form to another. During the last few decades, power electronics has enjoyed a massive growth in manufacturing, aerospace [1]-[4], domestic [5], commercial [6]-[8] and military applications [6], [9]. With this rapid evolution, not only have the reliability and the performance of power electronic devices increased but also the size and the cost have been reduced. With these improved features, power electronics has conquered almost every corner of the electrical engineering industry. Virtually everywhere, the generated power is reprocessed through some form of power electronics before it is finally used.

The technology behind almost all the switching power supplies and other applications such as power converters [10], inverters [11], motor drives, incandescent lamp dimming [12], heating applications [8] and motor soft starters [13], is power electronics. It pro-

vides solutions from very small mobile phones to huge turbines and trains; the power range can vary from milliWatts to GigaWatts. This technological advancement has enabled the rise of new applications and appropriate control systems designed for particular applications to obtain desired performance.

1.2 Semiconductor Devices and Their Applications

Power semiconductor devices are the core of power electronics [14] and are used in power electronic circuits for processing of energy and regulating the voltage or current as desired. In power electronics, semiconductor devices are often used as switches where they are either on or off depending on the output requirement. This is unlike low-power electronic circuits in which semiconductor devices are typically used in their active operating region as amplifiers. Semiconductor devices can be classified in to three main categories, as detailed bellow, based on how much ability they offer to the designer in controlling their on/off states.

1.2.1 Uncontrolled semiconductor devices

The on and off processes of these devices cannot be controlled and the device attains its on/off states depending on the surrounding circuit's behaviour. A diode is a semiconductor device with uncontrolled characteristics. Figure 1-1 shows the circuit symbol and *v-i* characteristics of a diode.

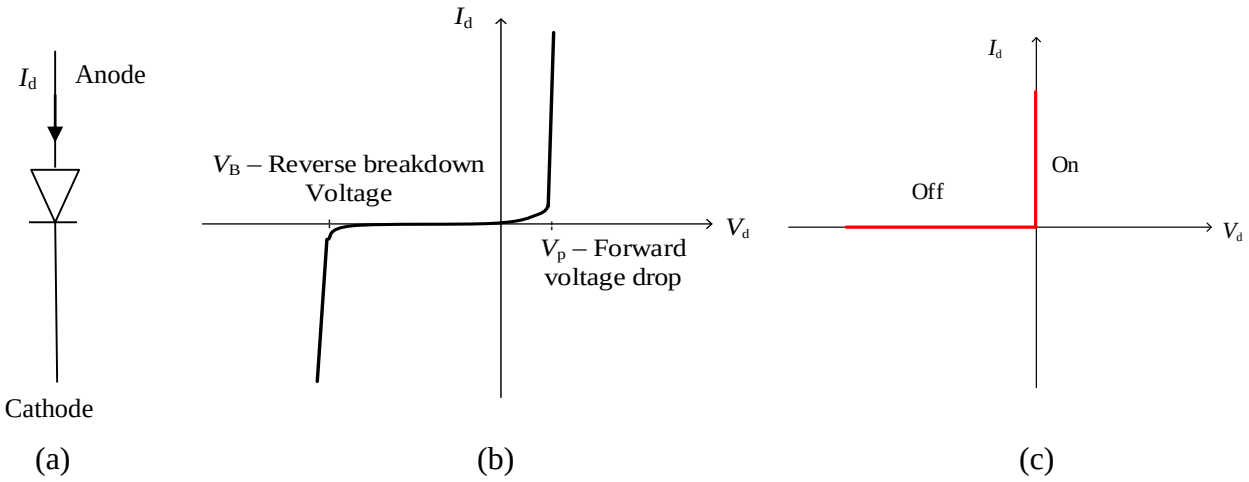

Figure 1-1 – Diode (a) circuit symbol, (b) *v-i* characteristics, (c) ideal *v-i* characteristics

When the device is in the on state the voltage across the device is very small or ideally zero at any current and when it is in the off state the current flowing through it is very small or ideally zero at any voltage.

1.2.2 Semi-controlled semiconductor devices

Semi-controlled semiconductor devices are turned on by an external control circuit and once they are turned on the off state of the device will depend on the surrounding circuit's conditions.

Modern power electronics was initiated with the invention of the thyristor, which is a semi-controlled semi-conductor device. Since then it has been widely applied in a large number of electrical engineering applications, such as power supplies [14], [15], static Var compensators [16], [17], chopper-fed dc drives, HVDC conversion [18], ac machine drives [19], heating control [20], [21], lighting and welding control and solid state circuit breakers [22].

Thyristors have a rapid turn on when a gate signal is applied to trigger the device. For a proper turn-on the gate signal must meet a minimum current requirement over a certain length of time. Figure 1-2 shows the circuit symbol and the *v-i* characteristics of a thyristors.

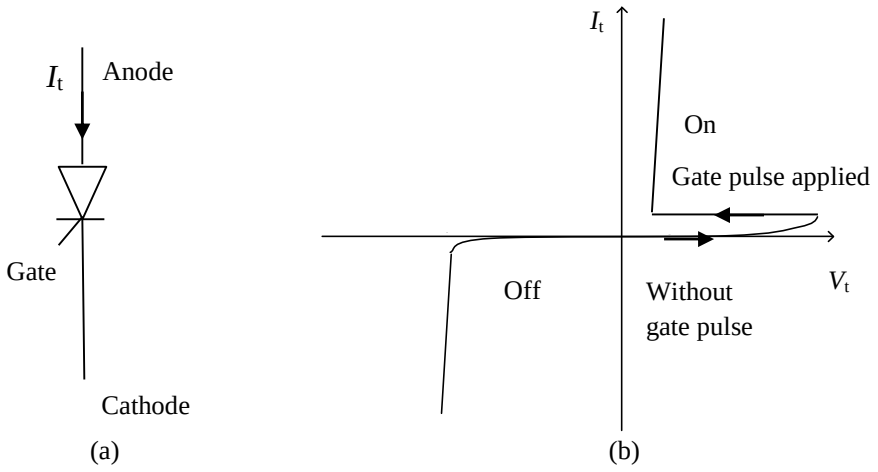

Figure 1-2 – Thyristor (a) Circuit symbol, (b) *v-i* characteristics

Furthermore thyristors require a certain amount of time to obtain forward blocking capability following a turn-off. If this time is not provided to the thyristor, and the voltage across the device is forward biased, it will start conducting even without a gate pulse. This phenomenon is called commutation failure and is to be avoided in normal operation.

1.2.3 Fully-controlled semiconductor devices

Fully controlled semiconductor devices have the capability of controlling both on and off states. These devices differ from each other in many ways such as switching frequency, gate requirements, capability of blocking the reverse voltage, and available power ratings. Some of the fully controlled semiconductor devices are gate turn off thyristors (GTO) [23], bipolar junction transistors (BJT), power MOSFETs, insulted gate bipolar transis-

tors (IGBT), silicon induction thyristors (SITH) and MOS controlled thyristors (MCT). These semiconductor devices are used in a variety of power electronic applications as detailed bellow.

GTOs are mainly used in high-power applications such as ac machine drives, uninterrupted power systems, photovoltaic and fuel cell inverters and static Var compensators [24]. BJTs are mostly used in voltage-fed choppers and inverters with frequencies from 10 to 15 kilo-Hertz. IGBTs are used in medium power applications such as relays, power supplies and drivers for solenoids, contactors, dc and ac motor drives and UPS systems.

Advancements in power electronic devices have created a remarkable impact in the development of modern converters. With this trend power converters have become increasingly capable of providing reliable power with less loss. Power electronic converters need proper controllers to regulate their operation to obtain desired output when the input to the system or the operating conditions of the system is changed.

The following figure shows a block diagram of a generic power electronic system.

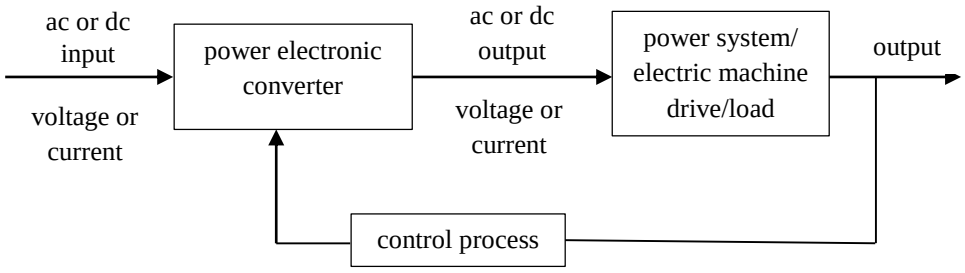

Figure 1-3 - Block diagram of a power electronic controller

As shown in the above figure, the input provided to the high-power system has been regulated using a power electronic converter under the guidance of a feedback control system to obtain the desired output.

To obtain the desired performance of these applications, power electronic converters need to be properly controlled. The performance of converters largely relies on the effectiveness of the associated controllers; therefore, it is important to apply an appropriate control system to the converter to obtain desired output.

To design an effective control system it is essential to have proper knowledge about the dynamics of the entire system and controlling methodologies. In this research, the control process of a voltage-source converter (VSC) has been considered. A voltage-source converter is a popular type of power-electronic converter used in conversion between ac and dc. There are different methods that can be used to control this type of converters. Direct control and decoupled control are two methods that are practiced commonly. In this research a decoupled control strategy has been used (as discussed in detail in Chapter 3). Furthermore a novel controller consisting of an internal model design to improve the controller performance of the voltage source converter is presented.

1.3 Motivation

Control systems are often designed with the assumptions of linearity and time invariance, as these assumptions lower the burden and complexity of the design process. However, in reality, endogenous conditions such as system parameter changes and exogenous conditions, such as undesired disturbances affecting the plant behaviour and the time delays of the feedback parameters, may result in control systems providing unexpected results. In this research, to overcome these effects, the existing control system of a VSC to control power transfer and vector control system of an induction machine to control its speed

have been modified using an internal model design (which is a predictive loop). The new control system offers better controllability even in the presence of unexpected situations.

1.4 Objectives of the research

The main objective of this research is to develop advanced decoupled control systems for VSCs using internal model design techniques. The examples shown include internal model design for a VSC and a control system to regulate the speed of an induction motor. These control systems allow the system output to follow a reference time-variant input even when un-modeled dynamics are considered.

To carry out this task, several steps are required.

i. Identification of the endogenous and exogenous factors that affect control systems of a power electronic application;
ii. Study the behaviour of the internal model designs, and carry out few simple examples;
iii. Check the performance of the modified control systems under different scenarios;
iv. Look for alternative methods that can provide expected results under different circumstances;
v. Design of a modified decoupled controller with an internal model for a voltage source converter connected to a power system;
vi. Design of a modified indirect vector controller with an internal model for an induction machine to regulate the speed;

vii. Implementation of the control system and the power system model in simulation software;

viii. Tuning controllers to achieve expected output;

ix. Check the performance by testing the simulation case under different scenarios;

x. Compare the results with the existing control system.

1.5 Software tools

The software program used for simulation of the system model in this thesis is the PSCAD/EMTDC software. PSCAD stands for Power System CAD and EMTDC stands for Electromagnetic Transients including DC. PSCAD/EMTDC is one of the most popular electromagnetic transient simulation software packages and it is developed at the Manitoba HVDC Research Center. This software tool is being used in high power industrial applications such as power system planning, operation, commissioning and research.

EMTDC is the computational engine of the simulator and numerically solves the differential equations of the electrical power system network. PSCAD provides the graphical user interface. Running simulation cases, analysing results, schematically constructing circuits and presenting the data in an integrated graphical environment are features of this simulation tool

1.6 Thesis outline

Chapter 2 of the thesis presents a literature survey, which describes the status of the subject presently available in the literature.

Chapter 3 describes different control strategies used for tracking a reference given to the controller. Furthermore, Chapter 3 illustrates how to design a compensator that provides asymptotic tracking with zero steady state error. It also includes a discussion of designing internal models for a number of simple examples including several alternative methods.

Chapter 4 describes a voltage-source converter and its power system applications, which will be controlled by the new controller. Furthermore mathematical modeling of the voltage source converter is described. How to design the decoupled controller and the modified controller with the internal model design are also described in this chapter. Additionally system models implemented in the PSCAD/EMTDC software, which show the performance under different circumstances such as delays in the feedback system and circuit parameter variations are presented.

Chapter 5 describes the design of a control system to regulate the speed of an induction machine. A dynamic model of an induction motor is reviewed and equations for the current, voltage, and torque in a rotting dq0 frame are derived. An indirect vector control strategy is designed for the induction machine to track a set machine speed. Then an internal model controller is added to the existing control system and its performance is evaluated. As the rotor resistance of an induction machine can change over time and during operation, controller performance is checked with and without an internal model design to observe how it responds to system parameter changes.

Chapter 6 describes the conclusions and it presents future directions along which further research can be conducted.

Chapter 2

Background and Literature Review

2.1 Introduction

A control system is the linking mechanism of components forming a power system configuration that provides a desired output in response to a reference input. Effective control requires understanding and modeling of the system to be controlled. Originally, control theory was limited to enhance the performance and stability of single-input single-output (SISO) systems; additionally time-variant plant conditions were often not considered. These simplifying assumptions were often applied even when the actual system did not fully manifest such properties. With the increasingly strict operating conditions of modern power systems control systems had to be designed to control complex power ap-

plications, which include uncertainties in the system. These control systems should be robust and provide the expected output not only under predefined system conditions but also under unexpected system conditions (up to certain limits). These uncertainties depend on different operating conditions of the system and its applications. If it is a power system application, system parameter changes may include variations of inductor, resistor or capacitance values due to aging of parameters or temperature. Fault conditions or addition of system components such as electric machinery, converters and distributed generators can also introduce uncertainties to the power systems. The adverse impacts of these unexpected situations can be partly eliminated by designing the system with large safety margins, which will adversely affect their cost, or they can be tackled through proper control systems.

One major problem that may cause instability or otherwise undesirable performance of a feedback control system is time delay [25]. When the delay is small conventional controllers (such as proportional-integral-derivative (PID) controllers) could be used but with the increase of the delay, the process delivers poor performance as it requires significant detuning to maintain the stability of the control system. Therefore, to overcome these problem researchers have come up with several alternative control methods [26].

For proper control of a power system, measurements should be fed to the control system. To carry out this task variables must be properly measured. However, system variables may not always be properly measured due to system uncertainties, or it may not be possible to directly measured them; to overcome this issue, researchers have developed methodologies to *observe* the states of a power system. These state observers are used to

enhance the performance of the existing control systems by providing reliable estimations of crucial variables without directly measuring them.

Kalman filtering is one approach used to estimate the unknown variables of a system more precisely than the readings based on a single measurement [27]. It uses a series of measurements of the states of the system over time to provide the estimate. More importantly it provides better performance compared to ordinary feedback controllers under noisy system conditions. The Smith predictor algorithm is another type of algorithm that is used to design controllers where system variables need to be observed [28]. It provides better results compared to ordinary feedback controllers for systems with pure time delays. These state observer methodologies control the system using the predicted output rather than the actual output. Therefore the implementation is dependent mostly on the accuracy of the prediction. Most of the controllers deliver optimal responses in absence of predicted model uncertainties.

Internal model controller (IMC) design is another methodology to observe the states of a power system for the purpose of its control. The IMC structure was initially developed for chemical process applications. It became popular as a robust control method for other control engineering practice, such as disk drive servomechanisms [29] and it is widely used in robotic applications where trajectory tracking is involved [30]. Several internal model designs were developed for disturbance compensation in different applications [31]. Internal model designs have been modified to perform different tasks. For instance some applications require disturbance rejection internal designs whereas other applications concentrate more on reducing the effect of time delays in systems. Though

there have been plenty of IMC techniques developed, still certain enhancements and advances are possible to improve the performance of IMC based controllers.

2.2 Internal Model Design Structure

Figure 2-1 illustrates the configuration of a classical feedback structure. The difference between the reference value and the output (error $E(s)$) is sent through the controller ($C(s)$). Then the controlled input $U(s)$ is fed to the process. Finally the output is compared with the reference and the process continues. The disturbance $D(s)$ denotes inputs to the systems that are not controllable by the operator; for example these may include loading conditions that are imposed externall and to which the system has to react.

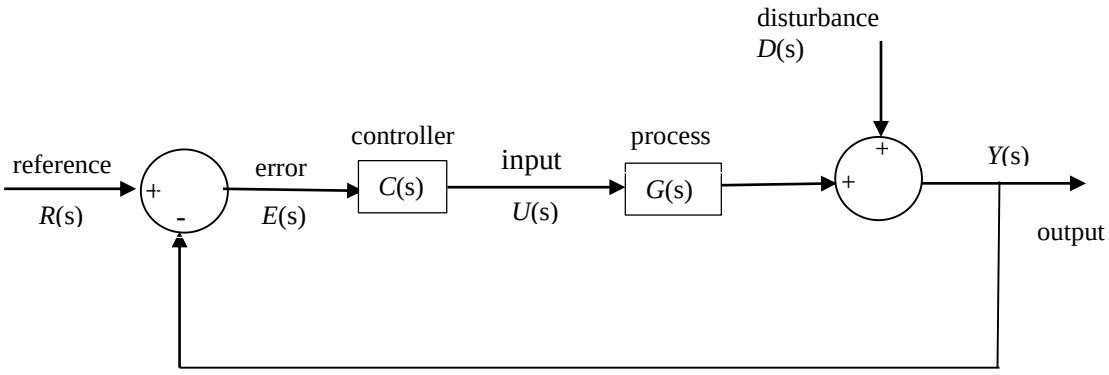

Figure 2-1 - Classical feedback structure

Internal model designs can be implemented by modifying the classical feedback control system. Figure 2-2 illustrates the modified version of the classical control system, which incorporates an internal model.

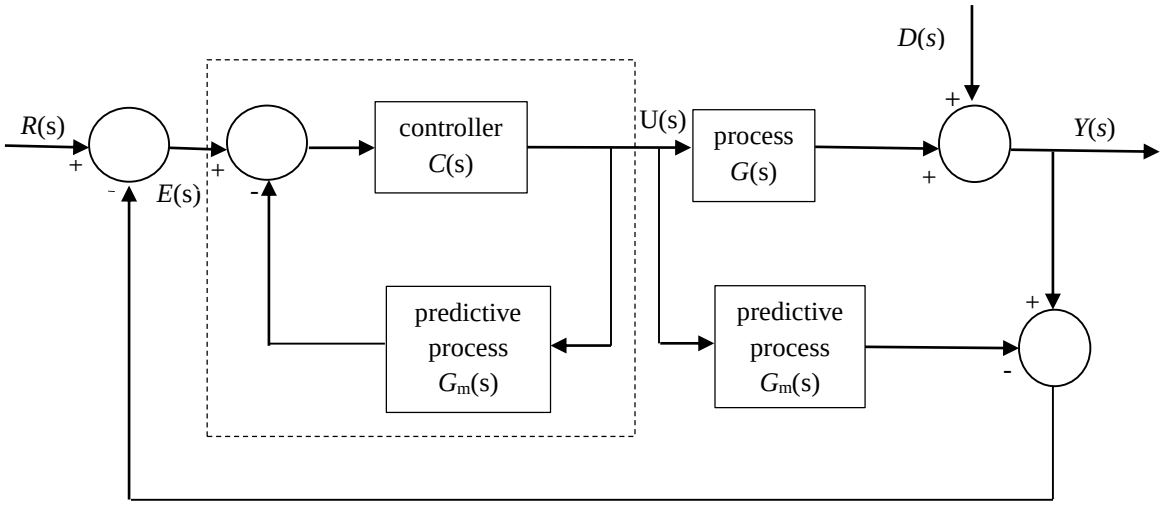

Figure 2-2 - Modified Classical feedback structure

As per Figure 2-2, it can be seen that a predictive process model of the actual process is added and subtracted to/from the classical control structure of Figure 2-1. The controller (C(s)) and the predictive process (G_m(s)) (shown together inside the dashed box) can be represented as a new controller (C_n(s)) as shown in Figure 2-3.

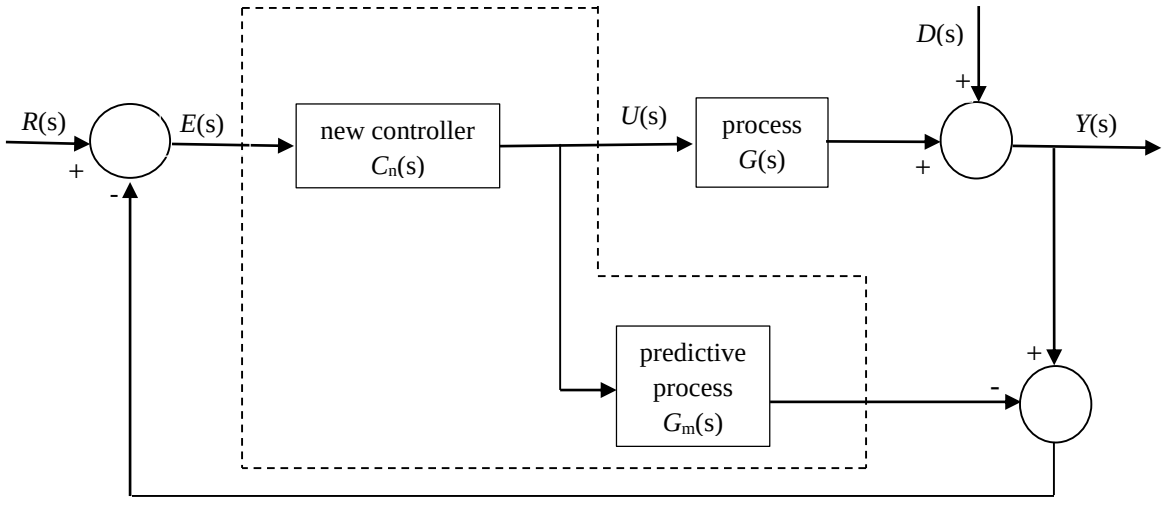

Figure 2-3 - Simplified version of Figure 2.2

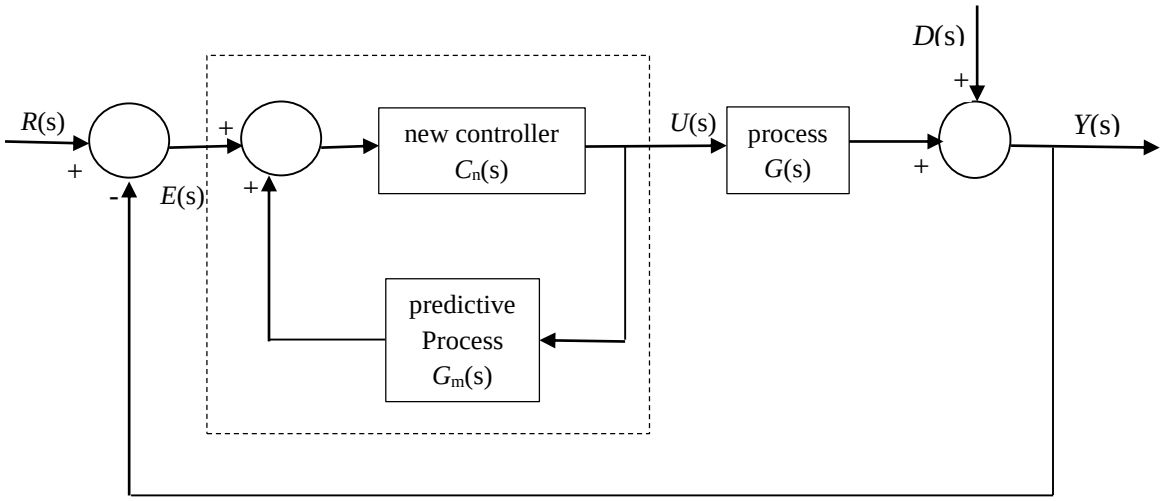

Figure 2-4 - Simplified version of Figure 2-3

Figure 2-4 shows an equivalent arrangement, in which the predictive process is moved in parallel with the controller $C_n(s)$.

As per Figure 2-4, the new controller $C_n(s)$ and the internal model are encircled by the dashed box; this illustrates that the predictive model of the process is fed back to the new controller as an internal loop and provide the controlled input to the process.

From Figure 2-1, the following equations can be obtained.

$$E(s)C(s) = U(s) \tag{2.1}$$

Similarly, the following equations are obtained from Figure 2-4,

$$(E(s)+U(s)G_m(s))C_n(s) = U(s) \tag{2.2}$$

Using (2.1) and (2.2) following Equations can be derived:

$$C_n(s) = \frac{C(s)}{1+G_m(s)C(s)} \tag{2.3}$$

$$C(s) = \frac{C_n(s)}{1-G_m(s)C_n(s)} \tag{2.4}$$

According to equation (2.4) it can be seen that the internal model control system shown in Figure 2-4 can be characterized as a control mechanism consisting of the new controller $C_n(s)$ and a predictive model $G_m(s)$ of the plant. The internal model controls the input provided to the process by controlling the difference between the output of the process and the reference value. This error can occur due to disturbances or other mismatches of the model.

From Figure 2-4, the output of the system can be expressed as:

$$Y(s) = U(s)G(s) + D(s) \tag{2.5}$$

Using equation (2.1), $Y(s)$ can be expressed as:

$$Y(s) = E(s)C(s)G(s) + D(s) \tag{2.6}$$

Error $E(s)$ is:

$$E(s) = R(s) - Y(s) \tag{2.7}$$

Using equation (2.7), $Y(s)$ can be expressed as:

$$Y(s) = (R(s) - Y(s))C(s)G(s) + D(s) \tag{2.8}$$

By rearranging the equation (2.8), $Y(s)$ can be expressed as:

$$Y(s) = \frac{G(s)R(s)}{1 + C(s)G(s)} + \frac{D(s)}{1 + C(s)G(s)} \tag{2.9}$$

Using equation (2.4) the output of the system can be expressed as follows.

$$Y(s) = \frac{G(s)C_n(s)R(s)}{1 + C_n(s)(G(s) - G_m(s))} + \frac{(1 - G_m(s)C_n(s))D(s)}{1 + C_n(s)(G(s) - G_m(s))} \tag{2.10}$$

If the plant can be modeled correctly where $G_m(s)$ is equal to $G(s)$ and if the disturbance is absent, from (2.10) the system becomes an open loop one. Based on the stability of $C_n(s)$ and $G(s)$, closed-loop stability is characterized.

According to (2.4) it can be seen that the closed-loop stability is dependent on the stability of the new controller $C_n(s)$ and the model of the process $G(s)$. If the process model and the predictive model are equal and the new controller is the inverse of the process $C_n(s) = G(s)^{-1}$ the system can be controlled to obtain the expected output from the system given that the model of the system is stable. Therefore IMC is a useful concept, which allows an open-loop controller to provide closed-loop performance. Thus the IMC structure offers better performance to obtain expected results from a process compared to a classical feedback controller. However, selection or design of a compensator is a critical task as it can create instability in the presence of disturbances and plant model mismatches. Filters are used in power system controllers to make them more robust and to help in minimizing the discrepancies between the plant and the model. But as a consequence it produces delays in the system and leads to decrease the efficiency of the controller. Therefore designing a controller for a power system has become a critical task.

In this research, a controller has been designed including an internal model design to control a VSC and an induction machine. This controller is a dynamic compensator that can be used for set point tracking applications providing expected results.

Chapter 3

The Method of Internal Model Design

3.1 Main Controlling Strategies

The choice of a particular electronic control scheme for power electronic system depends on several factors such as reference inputs, which can be either controllable or uncontrollable, measurability of the output system parameters, and controllability and observability of the system. Controlling the output of a system to achieve asymptotic tracking of prescribed trajectories, commonly referred to as trajectory tracking, is a critical problem in control theory. As it has attracted considerable attention from control researchers, three main possibilities to approach the issue have been introduced. These can be characterized as (i) tracking by dynamic inversion [32], (ii) adaptive tracking [33], and (iii) tracking via internal models [34].

Tracking by dynamic inversion has been often used for control of nonlinear systems such as robotic applications [32]. Nonlinear dynamic inversion (NDI) process requires comprehensive knowledge about the tracking trajectory as it consists of massive complex

calculations for computation of the initial conditions and the feedback of the system. In adaptive tracking, the controller structure consists of a feedback loop and a controller with an adjustable gain [33]. This method can effectively handle parameter uncertainties, but the knowledge of the entire trajectory is needed to be used for designing the adaptation algorithm. Therefore these approaches are not well-suited for applications with unknown trajectories.

Internal model-based tracking, which is used in this research, has the capability of handling uncertainties simultaneously in the plant parameters as well as in the trajectory to be followed. Furthermore, time delays, which can occur due to external conditions, can be compensated by this method for proper functionality of the control system. Filtering of output parameters, which are extracted from the system to feed to the controller, is an external condition that can cause time delay. Moreover it has been proven that a controller designed with an internal model is able to secure asymptotic decay to zero of the tracking error for every possible trajectory and it can perform robustly with respect to parameter uncertainties of the system [35]. Therefore internal model control design is a very promising method that can be used for many power system applications. However the controllers designed using IMC concept can be costly due to the additional sensors that are needed to measure the system parameters for internal loop feedback, and they may also slow down the controller process. In this chapter the fundamentals of the internal model-based design method are presented.

3.2 Internal model design

A controller can face a great deal of unexpected environment changes of its applications in real time implementation. These unpredicted phenomena could occur due to endogenous conditions such as system parameter variations, or exogenous conditions, such as additional undesired inputs affecting the plant behaviour and the time delays of the feedback parameters.

In this section, the design of a compensator that provides asymptotic tracking of a reference input with zero steady state error is considered. Reference inputs considered include steps, ramps, sinusoids, etc. If the plant can be modeled as a linear, finite-dimensional, time-invariant system, the controller can be developed as follows. Suppose that the model of the plant is a set of first-order linear differential equations, written in the form.

$$\dot{\mathbf{x}} = \mathbf{A}\,\mathbf{x} + \mathbf{B}\,u \tag{3.1}$$

$$y = \mathbf{C}\,\mathbf{x} \tag{3.2}$$

where $\mathbf{x}$ is the state vector, u is the input and y is the output.

Let a reference input $\boldsymbol{r}$ to be generated by a linear system be of the form,

$$\dot{\mathbf{x}}_r = \mathbf{A}_r\mathbf{x}_r \tag{3.3}$$

$$r = \mathbf{d}_r\mathbf{x}_r \tag{3.4}$$

When the input is a step response, then:

$$\dot{x}_r = 0 \tag{3.5}$$

$$r = x_r \tag{3.6}$$

Or equivalently,

$$\dot{r} = 0 \tag{3.7}$$

The tracking error (e(t)) can be defined as follows,

$$e = y - r \tag{3.8}$$

Taking the time derivative of the error yields:

$$\dot{e} = \dot{y} \tag{3.9}$$

Taking the time derivative of (3.2) yields:

$$\dot{y} = \mathbf{C}\dot{\mathbf{x}} \tag{3.10}$$

Let two intermediate variables $\mathbf{v}$ and ω be defined as follows:

$$\mathbf{v} = \dot{\mathbf{x}} \tag{3.11}$$

$$\omega = \dot{u} \tag{3.12}$$

From (3.11) and (3.12) the following state-space representation can be obtained.

$$\begin{pmatrix} \dot{e} \\ \dot{\mathbf{v}} \end{pmatrix} = \begin{pmatrix} 0 & \mathbf{C} \\ 0 & \mathbf{A} \end{pmatrix} \begin{pmatrix} e \\ \mathbf{v} \end{pmatrix} + \begin{pmatrix} 0 \\ \mathbf{B} \end{pmatrix} \omega \tag{3.13}$$

If (3.13) is controllable, feedback can be written in the following form so that the above equation will be stable.

$$\omega = -K_1 e - \mathbf{K}_2 \mathbf{v} \tag{3.14}$$

where K_1 and $\mathbf{K_2}$ are constants

Stability of the equation (3.13) implies the tracking error stability; therefore, the objective of asymptotic tracking with zero steady state error can be achieved. The control input can be found using above equation (3.14) as shown below,

$$u(t) = -K_1 \int_0^t e(\tau)\, d\tau - \mathbf{K}_2 \mathbf{x}(t) \tag{3.15}$$

The corresponding block diagram of the developed scheme is shown in Figure 3-1.

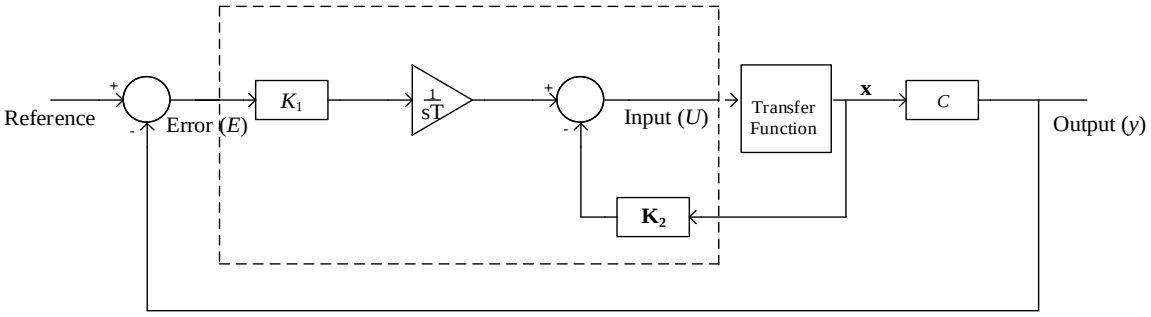

Figure 3-1 - Block diagram of the modified control system

As per the diagram, the error (E) which is the difference between the reference and the output, is multiplied by a constant and sent through an integrator. After that, the result is subtracted from the state parameter generated by the system and then fed to the system as the real input. The dashed box represents the controller including the internal model.

3.3 Internal model design examples

3.3.1 Example 1

In this section, a first-order system is used to demonstrate the performance of the internal model concept from Section 3.2. First a classical controller is designed and then it is modified using the internal model concept.

Consider the following first-order single-input, single-output system.

$$\dot{\mathbf{x}} = 5\mathbf{x} + 2u \tag{3.16}$$

$$y = 2\mathbf{x} \tag{3.17}$$

In Laplace domain,

$$s\mathbf{x} = 5\mathbf{x} + 2u \tag{3.18}$$

and the system transfer function can be written as follows.

$$\mathbf{x} = \frac{2u}{s - 5} \tag{3.19}$$

To compare the performance of the modified controller and the classical system three system models have been built with different controlling strategies.

3.3.1.1 Case 1 (Classical control system)

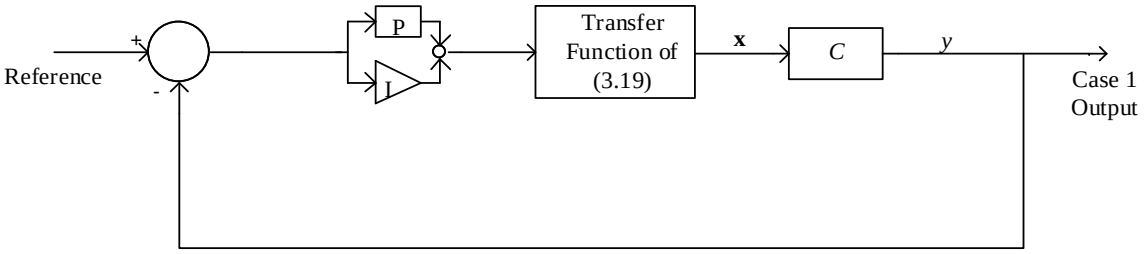

Figure 3-2 - Classical control system, designed for example 1

Figure 3-2 shows a classical control system built to control the output of the system. As shown a simple proportional-integral (PI) controller has been used to control the error between the reference and the output. The PI controller has been well tuned to follow the reference. The reference is varied as shown in the Figure 3-3.

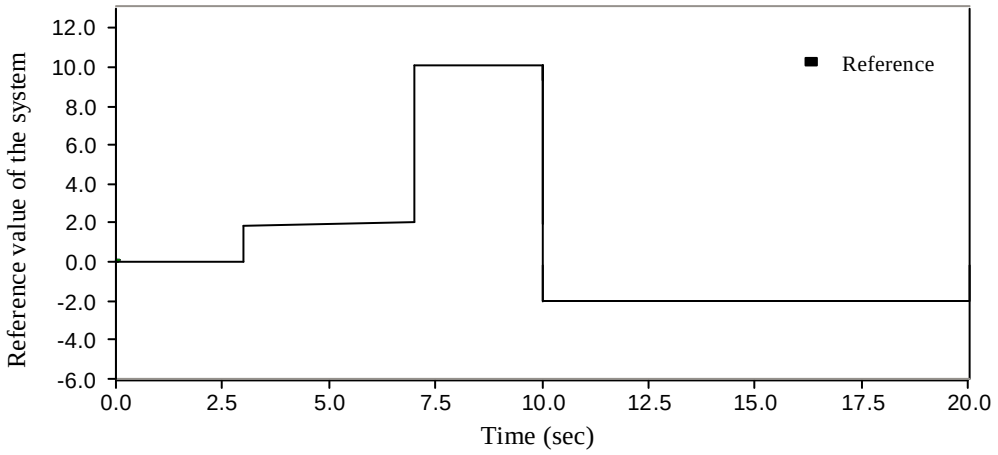

Figure 3-3 - Step reference input given to the system

3.3.1.2 Case 2 (control system with an internal model)

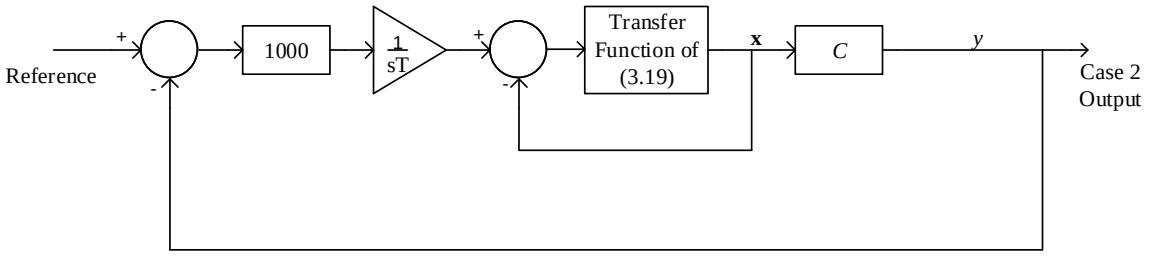

Figure 3-4 - Modified control system, designed for example 1

Figure 3-4 shows the control system built with an internal model design. The integrator is well tuned, output to follow the reference shown by Figure 3-3 and obtain better performance compared to classical control system.

3.3.1.3 Case 3 (control system with an internal model and the observer)

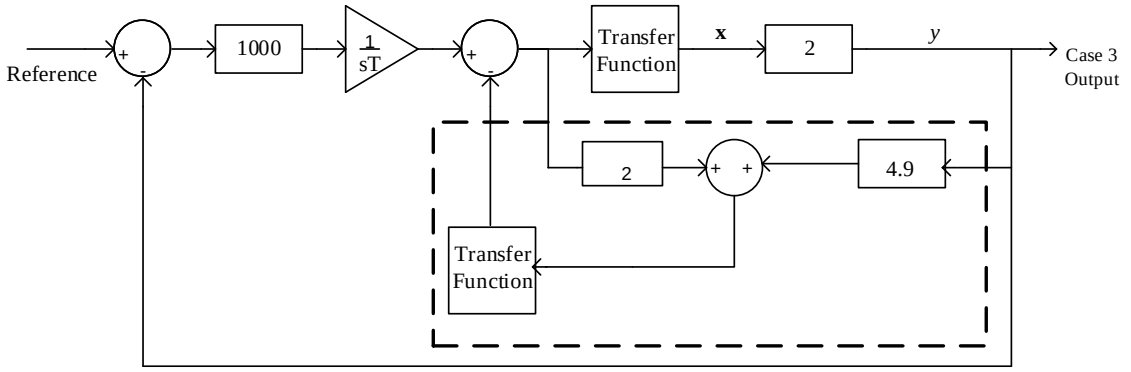

Figure 3-5 - Modified control system, designed for example 1 with the state space observer

The configuration shown in Figure 3-5 has been designed similar to case 2 with a modified state feedback generated using a state observer. The state observer is shown within the dashed box in Figure 3-5.

3.3.1.3.1 Controllability and observability

One of the key questions that arises while developing a state variable compensator is whether the system is controllable. This has to do with whether the poles of a closed-loop system can be arbitrary placed in the complex plane (the poles of a closed loop system are equivalent to the eigen-values of the system matrix in state variable format). The concept of controllability and observability was heavily investigated by Kalman in 1960 [36], [37].

Consider a system given as follows.

$$\dot{\mathbf{x}} = \mathbf{A}\mathbf{x} + \mathbf{B}u \tag{3.20}$$

$$y = \mathbf{C}\mathbf{x} \tag{3.21}$$

The controllability can be determined as follows. If the matrix **A** is an *n* x *n* matrix and if it is a multi-input system, matrix **B** can be an *n* x *m* matrix where *m* is the number of inputs to the system. For a single input, single output system the controllability matrix is defined as follow in terms of **A** and **B**,

$$\mathbf{P}_c = \left[\mathbf{B} \quad \mathbf{AB} \quad \mathbf{A}^2\mathbf{B} \quad \ldots \quad \mathbf{A}^{n-1}\mathbf{B}\right] \tag{3.22}$$

If $\mathbf{P}_c$ is an *n* x *n* matrix and the determinant is non-zero, the system is controllable [38].

E. g. $\mathbf{A} = \begin{pmatrix} -2 & 0 \\ 2 & -3 \end{pmatrix}$ $\mathbf{B} = \begin{pmatrix} 1 \\ 0 \end{pmatrix}$ $\mathbf{C} = \begin{pmatrix} 0 & 1 \end{pmatrix}$

$$\mathbf{AB} = \begin{pmatrix} -2 \\ 2 \end{pmatrix}$$

Therefore $\mathbf{P}_c = \begin{pmatrix} 1 & -2 \\ 0 & 2 \end{pmatrix}$

and the determinant of the $\mathbf{P}_c$ matrix is 2 therefore the system is controllable.

Consider the single input, single output system given by,

$$\dot{\mathbf{x}} = \mathbf{A}\mathbf{x} + \mathbf{B}u \tag{3.23}$$

$$y = \mathbf{C}\mathbf{x} \tag{3.24}$$

where **C** is a 1 x *n* row vector and x is an *n* x 1 column vector. For the above system, the observability matrix can be written as follows.

$$\mathbf{P}_o = \begin{pmatrix} \mathbf{C} \\ \mathbf{CA} \\ \cdot \\ \cdot \\ \cdot \\ \mathbf{CA}^{n-1} \end{pmatrix}$$

Po is an *n* x *n* matrix.

For $\mathbf{A} = \begin{pmatrix} 0 & 1 & 0 \\ 0 & 0 & 1 \\ \mathbf{-X} & \mathbf{-Y} & \mathbf{-Z} \end{pmatrix}$ and $\mathbf{C} = \begin{pmatrix} 1 & 0 & 0 \end{pmatrix}$

$\mathbf{CA} = \begin{pmatrix} 0 & 1 & 0 \end{pmatrix}$ and $\mathbf{CA}^2 = \begin{pmatrix} 1 & 0 & 0 \end{pmatrix}$ thus it is observed that:

$$\mathbf{P}_o = \begin{pmatrix} 1 & 0 & 0 \\ 0 & 1 & 0 \\ 0 & 0 & 1 \end{pmatrix}$$

where the determinant of $\mathbf{P}_o$ is 1. Therefore the system is observable.

3.3.1.3.2 State observer design

In designing a state observer process, first assume that all the states are available for the feedback. According to Luenberger [39], a full state observer for the system,

$$\dot{\mathbf{x}} = \mathbf{A}\mathbf{x} + \mathbf{B}u \tag{3.25}$$

$$y = \mathbf{C}\mathbf{x} \tag{3.26}$$

is given as follows.

$$\dot{\tilde{\mathbf{x}}} = \mathbf{A}\tilde{\mathbf{x}} + \mathbf{B}u + \mathbf{L}(y - \mathbf{C}\tilde{\mathbf{x}}) \tag{3.27}$$

where $\tilde{\mathbf{x}}$ denotes the estimate of the state $\mathbf{x}$ and the matrix $\mathbf{L}$ is the observer gain matrix, which will be determined as part of the observer design. In this case the observer provides an estimate ($\tilde{\mathbf{x}}$) so that it will reach x asymptotically. The estimation error can be written as follows.

$$\mathbf{e}(t) = \mathbf{x}(t) - \tilde{\mathbf{x}}(t) \tag{3.28}$$

To achieve the goal of the observer, the $\mathbf{L}$ matrix is designed so that the tracking error will be asymptotically stable as the error $\boldsymbol{e}(t)$ tends to zero.

Taking the time derivative of the error shown by equation (3.28),

$$\dot{\mathbf{e}} = \dot{\mathbf{x}} - \dot{\tilde{\mathbf{x}}} \tag{3.29}$$

By combining equations (3.27) and (3.29)

$$\dot{\mathbf{e}} = \mathbf{A}\mathbf{x} + \mathbf{B}u - \mathbf{A}\tilde{\mathbf{x}} - \mathbf{B}u - \mathbf{L}(y - \mathbf{C}\tilde{\mathbf{x}}) \tag{3.30}$$

$$\dot{\mathbf{e}}(t) = (\mathbf{A} - \mathbf{L}\mathbf{C})\mathbf{e}(t) \tag{3.31}$$

If the characteristic equation $\det(\lambda\mathbf{I} - (\mathbf{A} - \mathbf{L}\mathbf{C})) = 0$ has negative roots, then for any ini-

tial tracking error $\mathbf{e}(t_0)$, the $\mathbf{e}(t)$ will tend to zero with time. The **L** matrix will be calculated such that the characteristic equation's (3.31) roots lie on the left half plane.

For a faster response with a lower over-shoot, suppose the characteristic equations can be written as [40],

$$\Delta(\lambda) = (\lambda + \xi\omega_n) \tag{3.32}$$

where ξ is the damping ratio and ω_n is the angular velocity.

According to example 1 data (Section 3.3.1),

$\mathbf{A} = 5$, $\mathbf{C} = 2$,

$$\det(\lambda\mathbf{I} - (\mathbf{A} - \mathbf{LC}) = 0) \tag{3.33}$$

By substituting the values in equation (3.33),

$$\left|\lambda - (5 - 2L)\right| = 0$$

$$\lambda - 5 + 2L = 0 \tag{3.34}$$

Let ω_n is 6 and ξ to be 0.8 for minimal overshoot [40], using equation (3.34),

$L = 4.9$

Therefore the observer equation is,

$$\dot{\tilde{\mathbf{x}}} = 5\tilde{\mathbf{x}} + 2u + 4.9\,(y - 2\tilde{\mathbf{x}}) \tag{3.35}$$

The configuration shown in Figure 3-5 has been designed with a modified controller where the state estimator is designed using above calculated values.

3.3.1.4 Simulation results for Example-1

For the system defined in example 1, a varying step reference was given as shown in Figure 3-3. The following results were observed for all the 3 cases defined above.

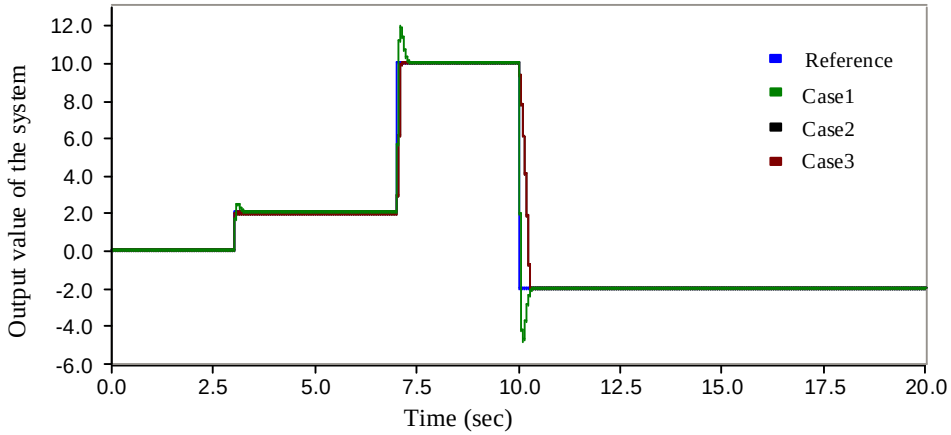

Figure 3-6 – Output of the three control strategies designed for example 1

Figure 3-6 illustrates how each control system behaves with time when the same reference input is given to the system. According to the above graph, it can be seen that every case has generally followed the reference value but in slightly different ways. The graph shown in Figure 3-7 gives a closer view of the behaviour of three cases during the transient period.

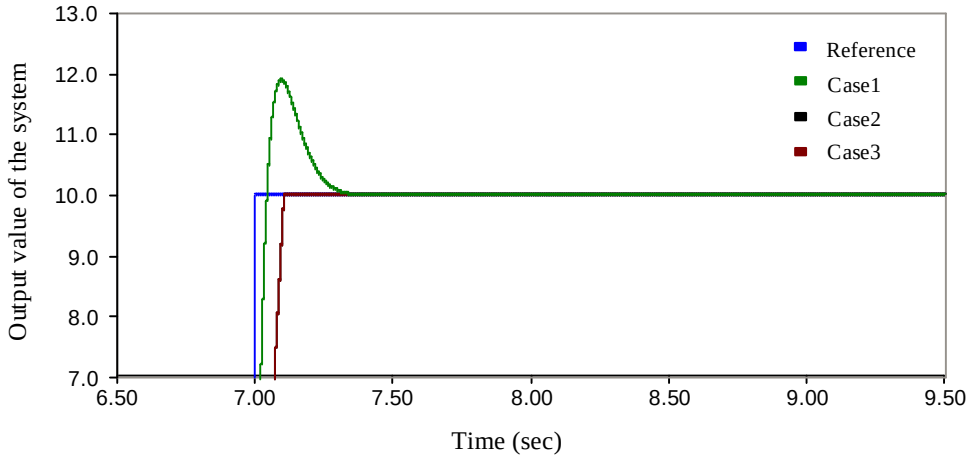

Figure 3-7 - Output of example 1 when the reference is changed to 10

According to this graph, during the transient period, the classical control system (case 1) has a significant overshoot whereas the modified control systems (case 2 and case3) follow the reference more closely. Furthermore it can be seen that case 2 and case 3 (modified controllers) have produced almost the same output. Hence for this system configuration (given by example 1) the modified control system has performed well compared to the classical system.

3.3.2 Example 2

In this section, a second order system equation is used to check the performance of the internal model concept discussed in Section 3.2. First a classical controller is designed to the system and then it is modified using the internal model. Then the case is implemented in PSCAD/EMTDC software and output results are observed.

The system equation are as follows.

$$\dot{\mathbf{x}} = \begin{pmatrix} 2 & 3 \\ -1 & 4 \end{pmatrix}\begin{pmatrix} \mathbf{x}_1 \\ \mathbf{x}_2 \end{pmatrix} + \begin{pmatrix} u_1 \\ u_2 \end{pmatrix} \tag{3.36}$$

$$y = \begin{pmatrix} 1 & 0 \\ 0 & 1 \end{pmatrix}\begin{pmatrix} \mathbf{x}_1 \\ \mathbf{x}_2 \end{pmatrix} \tag{3.37}$$

Taking the Laplace transform of equation (3.36),

$$s\mathbf{x}_1 = 2\mathbf{x}_1 + 3\mathbf{x}_2 + u_1 \tag{3.38}$$

$$s\mathbf{x}_1 = -\mathbf{x}_1 + 4\mathbf{x}_2 + u_2 \tag{3.39}$$

Using equation (3.38) and (3.39) transfer functions can be written as,

$$\mathbf{x}_1 = \frac{3\mathbf{x}_2 + u_1}{s - 2} \tag{3.40}$$

$$\mathbf{x}_2 = \frac{-\mathbf{x}_1 + u_2}{\mathrm{s} - 4} \tag{3.41}$$

This case has been implemented in PSCAD/EMTDC software to observe the response of the output. To compare the performance of the modified controller and the classical system, three system models have been built with different controlling strategies as in Example 1.

3.3.2.1 Case 1 (Classical control system)

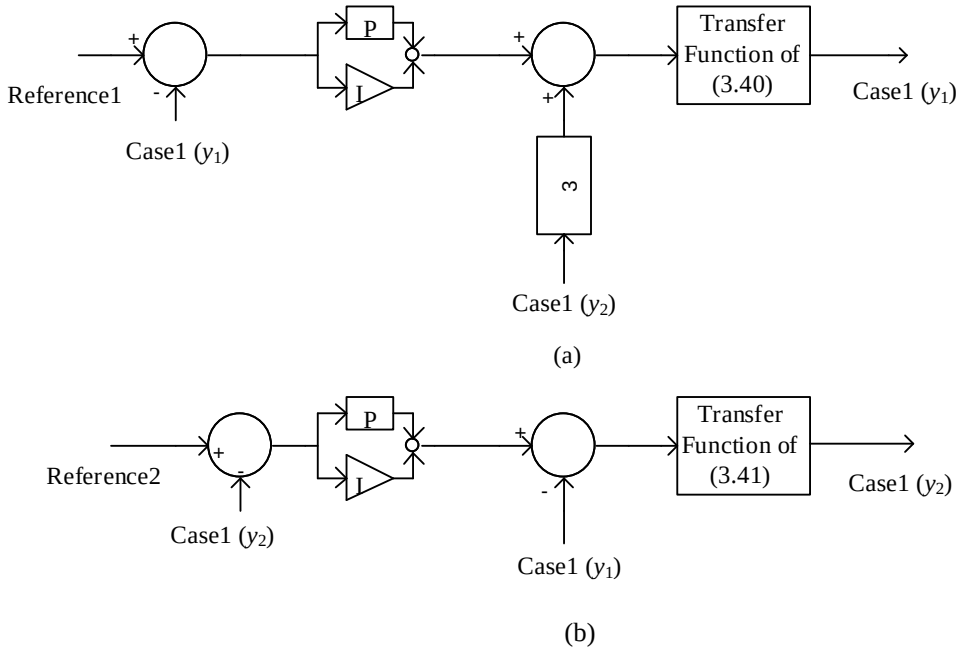

Figure 3-8 - Classical control system designed for Example 2 (a) controlled input 1 to the system (b) controlled input 2 to the system

Figure 3-8 shows a classical control system built to control the input of the system. As per the Figure 3-8, PI controller has been used and it has been well tuned to follow the reference which is given as a step sequence as shown in Figure 3-9.

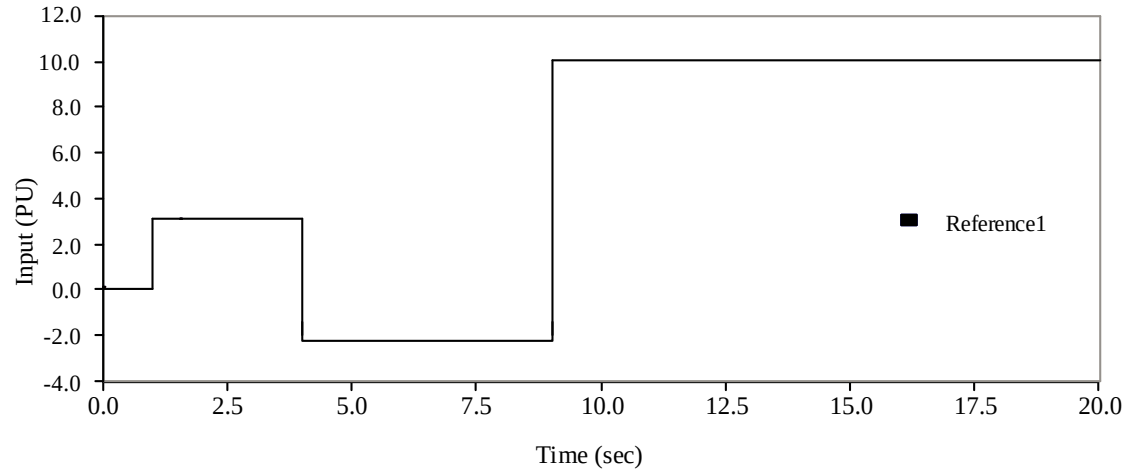

(a)

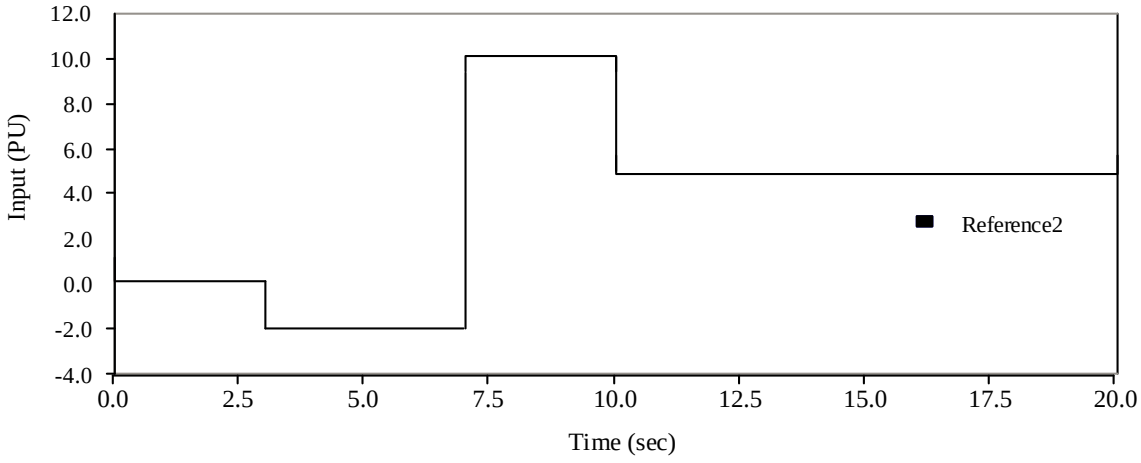

(b)

Figure 3-9 – (a) Reference 1, (b) Reference 2, inputs given to the example 2

The two reference inputs shown in Figure 3-9 are fed to the three control strategies designed for Example 2 to check the controllers' responses.

3.3.2.2 Case 2 (control system with an internal model)

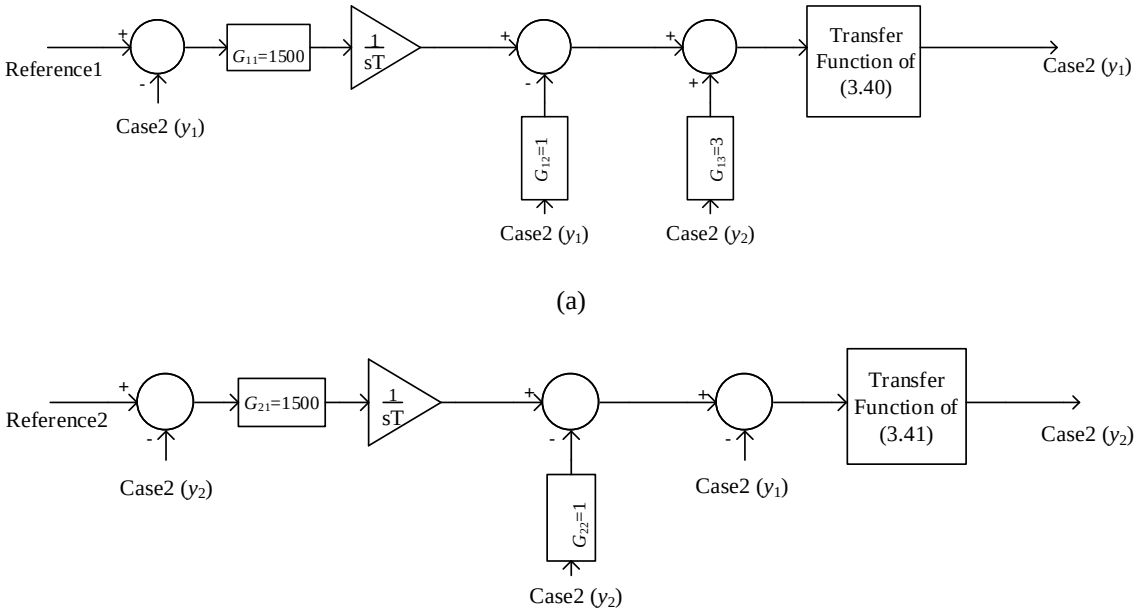

Figure 3-10 - Modified control system designed for (a) input 1 (b) input 2, for Example 2

Figure 3-10 shows the modified controller built with an internal model control design. G_{11}, G_{12}, G_{13} and G_{21}, G_{22} are proportional gains of the controller. The integrator is tuned for the output of the system to follow the reference shown by Figure 3-9 and to obtain better performance from the above configuration.

3.3.2.3 Case 3 (control system with an internal model and the observer)

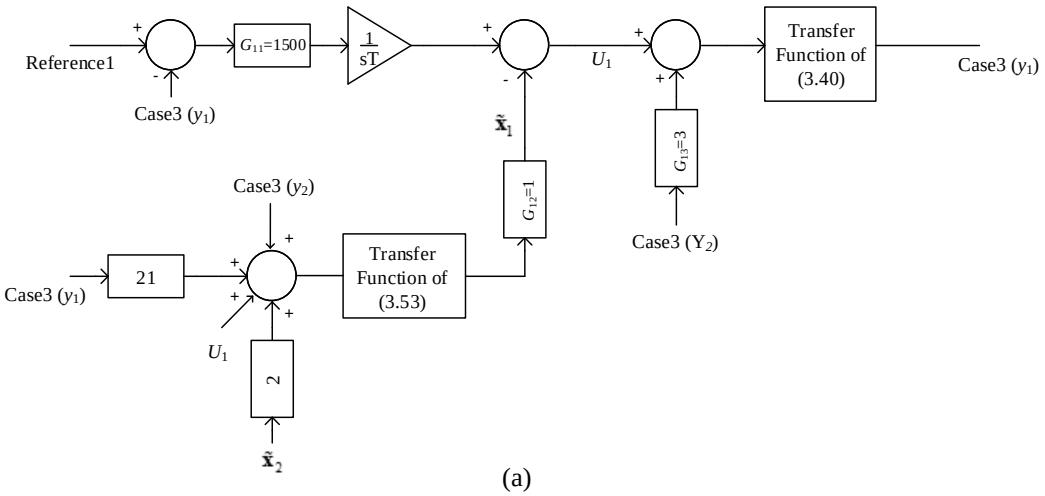

(a)

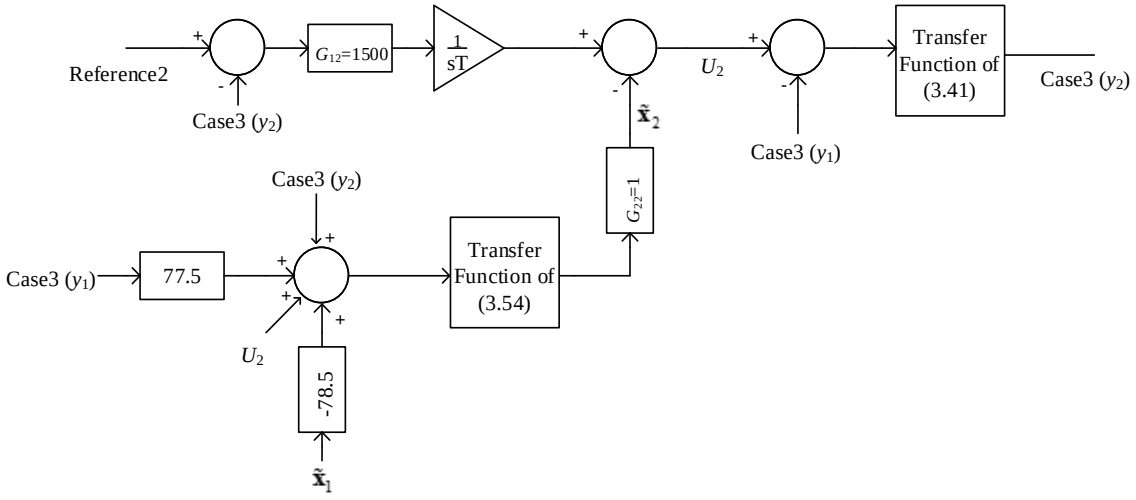

(b)

Figure 3-11 - Modified control systems designed for (a) input 1 (b) input 2, of Example 2 using the state observer

Configuration shown in Figure 3-11 has been designed same as case 2, but the state feed-back is given using a state observer. G_{11}, G_{12}, G_{13} and G_{21}, G_{22} are proportional gains of the controller.

3.3.2.3.1 Observer Design

To design the observer shown above, the gain matrix and other parameters were calculated as bellow.

$$\mathbf{A} = \begin{pmatrix} 2 & 3 \\ -1 & 4 \end{pmatrix} \qquad \mathbf{C} = \begin{pmatrix} 1 & 0 \\ 0 & 1 \end{pmatrix} \qquad \mathbf{B} = \begin{pmatrix} 1 & 0 \\ 0 & 1 \end{pmatrix}$$

The state observer equation is given bellow.

$$\dot{\tilde{\mathbf{x}}} = \mathbf{A}\tilde{\mathbf{x}} + \mathbf{B}\,u + \mathbf{L}\,(y - \mathbf{C}\tilde{\mathbf{x}}) \tag{3.42}$$

Where $\tilde{\mathbf{x}}$ denotes the estimate of the state **x** and the **L** matrix is the observer gain matrix which will be determined as the part of the observer design.

Estimation error can be written as,

$$\mathbf{e}(t) = \mathbf{x}(t) - \tilde{\mathbf{x}}(t) \tag{3.43}$$

Taking the time derivative of error given by equation (3.43),

$$\dot{\mathbf{e}} = \dot{\mathbf{x}} - \dot{\tilde{\mathbf{x}}} \tag{3.44}$$

By combining equations (3.42) and (3.44) the following equation can be obtained,

$$\dot{\mathbf{e}} = \mathbf{A}\mathbf{x} + \mathbf{B}u - \mathbf{A}\tilde{\mathbf{x}} - \mathbf{B}u - \mathbf{L}(y - \mathbf{C}\tilde{\mathbf{x}}) \tag{3.45}$$

$$\dot{\mathbf{e}}(t) = (\mathbf{A} - \mathbf{L}\mathbf{C})\mathbf{e}(t) \tag{3.46}$$

The characteristic equation is:

$$\det(\lambda\,\mathbf{I} - (\mathbf{A} - \mathbf{L}\mathbf{C})) = 0 \tag{3.47}$$

For a faster response with a lower over shoot, suppose the characteristic equation of equation (3.47) can be written as bellow [40],

$$\Delta(\lambda) = \lambda^2 + 2\xi\omega_n\lambda + \omega_n^2 \tag{3.48}$$

where ξ is the damping ratio and ω_n is the angular velocity. According to the dimensions of the system given in this example, the gain matrix (**L**) can be written as,

$$\begin{pmatrix} L_1 & L_2 \\ L_3 & L_4 \end{pmatrix}$$

By substituting the values to the equation (3.47),

$$\left| \lambda \begin{pmatrix} 1 & 0 \\ 0 & 1 \end{pmatrix} - \left(\begin{pmatrix} 2 & 3 \\ -1 & 4 \end{pmatrix} - \begin{pmatrix} L_1 & L_2 \\ L_3 & L_4 \end{pmatrix} \begin{pmatrix} 1 & 0 \\ 0 & 1 \end{pmatrix} \right) \right| = 0$$

$$\left| \begin{pmatrix} \lambda & 0 \\ 0 & \lambda \end{pmatrix} - \left(\begin{pmatrix} 2 & 3 \\ -1 & 4 \end{pmatrix} - \begin{pmatrix} L_1 & L_2 \\ L_3 & L_4 \end{pmatrix} \right) \right| = 0$$

$$\left| \begin{pmatrix} \lambda & 0 \\ 0 & \lambda \end{pmatrix} - \left(\begin{pmatrix} 2 - L_1 & 3 - L_2 \\ -1 - L_3 & 4 - L_4 \end{pmatrix} \right) \right| = 0$$

$$\left| \begin{pmatrix} \lambda - 2 + L_1 & 3 + L_2 \\ 1 + L_3 & \lambda - 4 + L_4 \end{pmatrix} \right| = 0$$

$$(\lambda - 2 + L_1)(\lambda - 4 + L_4) - (L_2 - 3)(L_3 + 1) = 0 \tag{3.49}$$

Assume L_2 and L_4 to are 1 (for the simplicity of the calculations)

$$\Delta(\lambda) = \lambda^2 + \lambda\,(L_1 - 5) + 2L_3 - 3L_1 + 8 \tag{3.50}$$

Let ω_n be 10 and select ξ to be 0.8 for minimal overshoot [40], using equation (3.49) and (3.50), L_3 and L_1 can be found.

$$L_1 - 5 = 16$$

$$L_1 = 21$$

and

$$2L_3 - 3L_1 + 8 = 100 \tag{3.51}$$

By substituting the value of L_1 to equation (3.51), L_3 can be found.

$$L_3 = 77.5$$

By substituting the values for the observer equation (3.42),

$$\dot{\tilde{\mathbf{x}}} = \begin{pmatrix} 2 & 3 \\ -1 & 4 \end{pmatrix} \tilde{\mathbf{x}} + \begin{pmatrix} 1 & 0 \\ 0 & 1 \end{pmatrix} u + \begin{pmatrix} 21 & 1 \\ 77.5 & 1 \end{pmatrix} (y - \mathbf{C}\tilde{\mathbf{X}}) \tag{3.52}$$

Taking the Laplace transform of the above equation,

$$s\tilde{\mathbf{x}}_1 = 2\tilde{\mathbf{x}}_1 + 3\tilde{\mathbf{x}}_2 + u_1 + 21y_1 - 21\tilde{\mathbf{x}}_1 + y_2 - \tilde{\mathbf{x}}_2$$

$$\tilde{\mathbf{x}}_1 = \frac{u_1 + y_2 + 21\,y_1 + 2\,\tilde{\mathbf{x}}_2}{s + 19} \tag{3.53}$$

And

$$s\tilde{x}_2 = -\tilde{\mathbf{x}}_1 + 4\tilde{\mathbf{x}}_2 + u_2 + 77.5y_1 - 77.5\tilde{\mathbf{x}}_1 + y_2 - \tilde{\mathbf{x}}_2$$

$$\tilde{\mathbf{x}}_2 = \frac{u_2 + y_2 + 77.5\,y_1 - 78.5\,\tilde{\mathbf{x}}_1}{s - 3} \tag{3.54}$$

The configuration shown in Figure 3-11 has been designed with a modified controller where the state estimator is designed using the above calculated values.

3.3.2.4 Simulation results for Example 2

For the system defined in example 2, a varying step reference was given as shown in Figure 3-9. Following results have been obtained for all the three cases defined above.

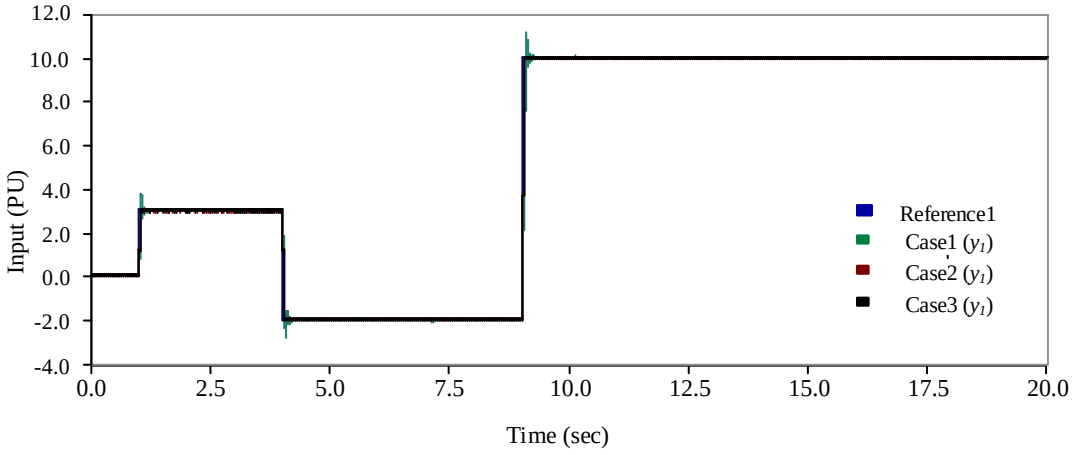

(a)

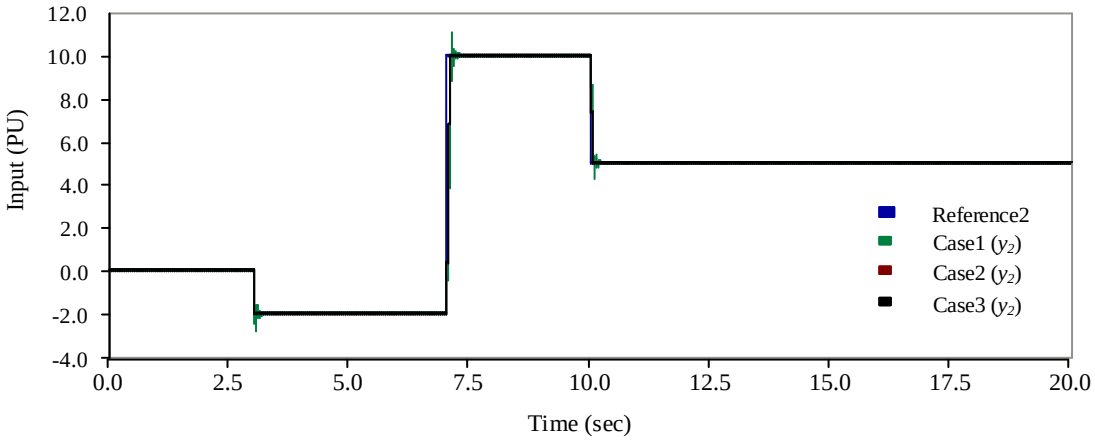

(b)

Figure 3-12 – (a) Output 1 (y_1), (b) Output 2 (y_2), of three control strategies designed for example 2

Figure 3-12 illustrates how each control system behaves with time when the same reference input is given to the three cases. According to the above graph, it can be seen that, each case has exactly followed the reference value but in a different manner. The Figure 3-13 and 3-14 give a closer look of the behaviour of three cases during the transient period.

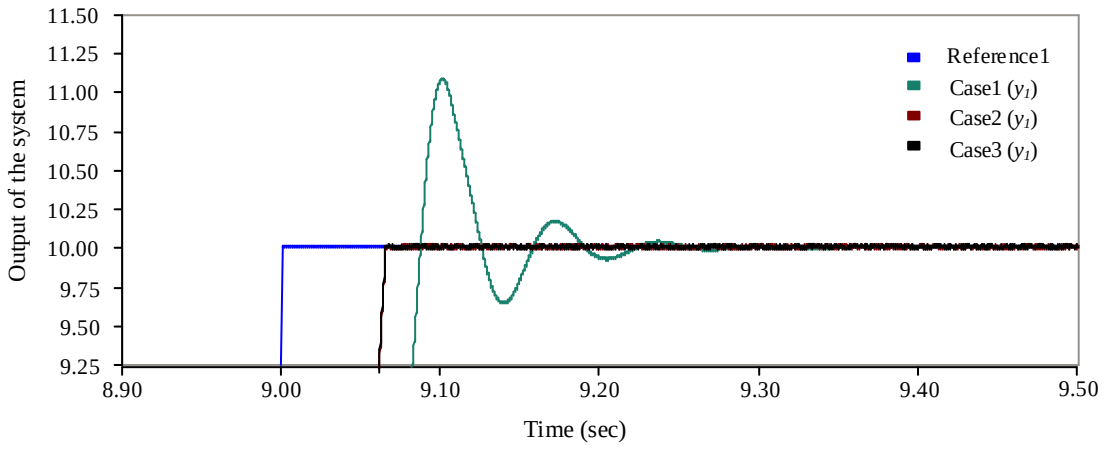

Figure 3-13 - Output 1 (y_1) of example 2 when the reference is changed to 10

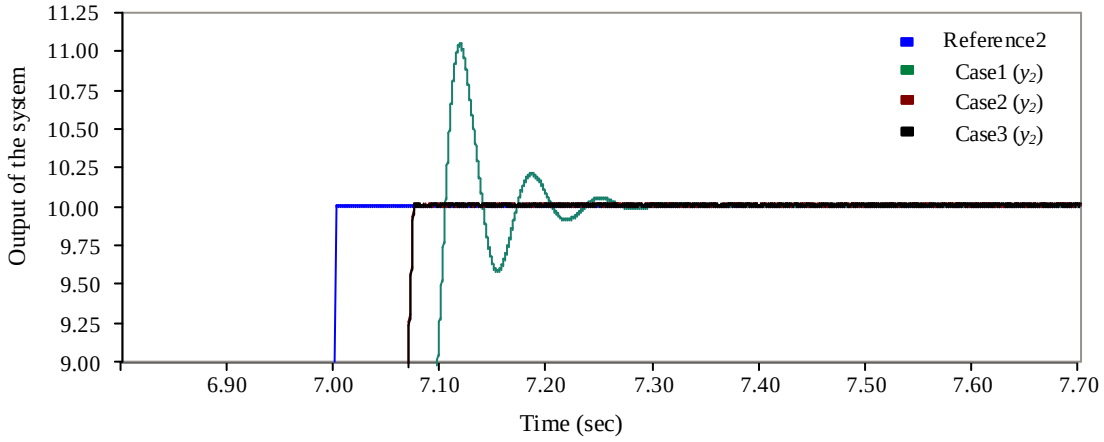

Figure 3-14 - Output 2 (y_2) of example 2 when the reference is changed to 10

Figures 3-13 and 3-14 are zoomed in versions of Figure 3-12 and it shows the behaviour of the three control systems when the reference value is 10. According to the graph, during the transient period, it can be seen that the classical control system (case 1) has a significant overshoot whereas the modified control systems (case 2 and case3) follow the exact reference. Output 1 (y_1) given by Figure 3-7 shows that the settling time of case 1 is 9.32s whereas case 2 and 3 have settled at 9.06s. Therefore modified case has stabilized 0.25s faster than the classical system. Output 2 (y_2) shown in Figure 3-7 illustrates that

the settling time of case 1 is 7.32s whereas case 2 and 3 have settled at 7.07s. Therefore the modified case has stabilized 0.25s faster than the classical system. Furthermore it can be seen that case 2 and case 3 (modified controllers) have given almost identical outputs.

To observe the controller behaviors, a disturbance was applied to the system described in Example 2 and the following results were obtained. Here a random number generator has been used to give random noise which vary from (-2) to (+2) as shown below.

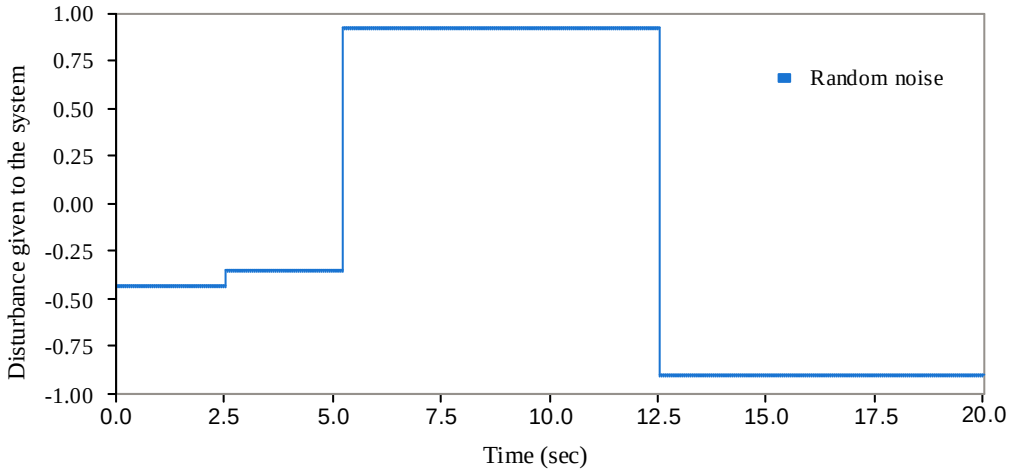

Figure 3-15 – Random noise given to system given by example 2

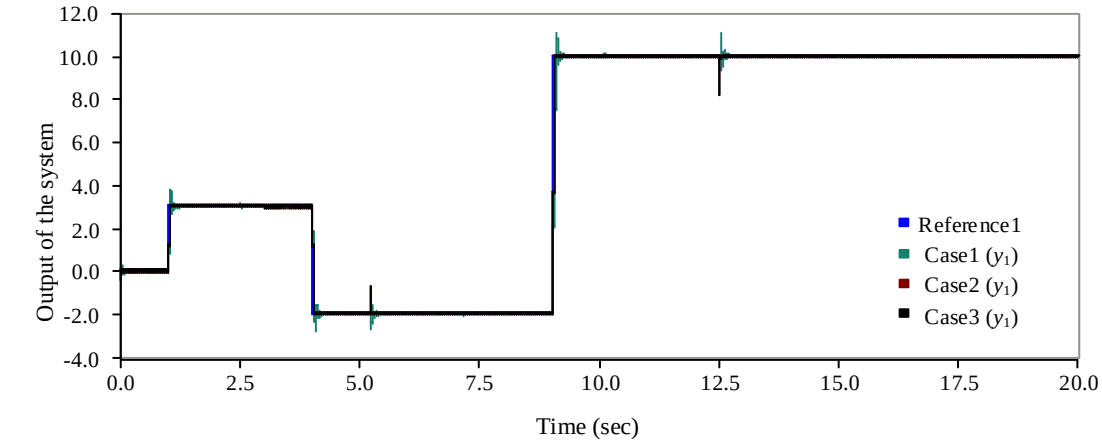

(a)

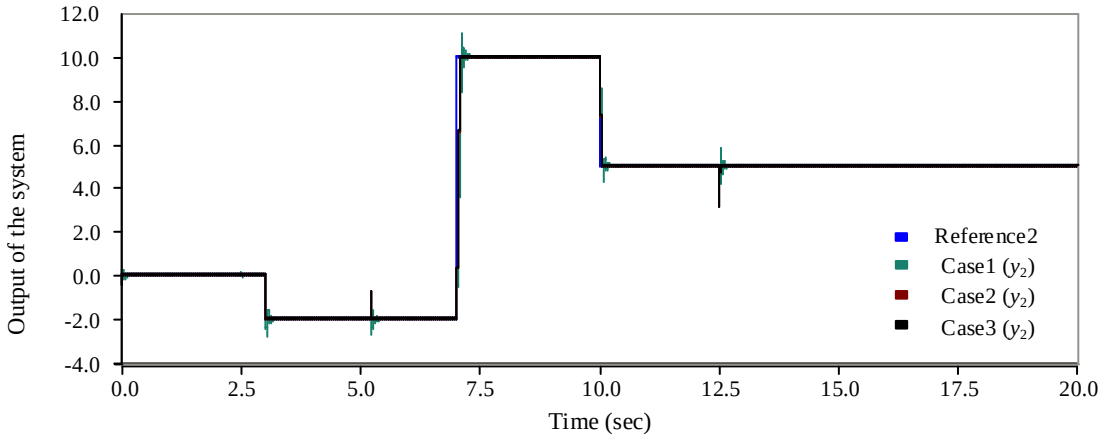

(b)

Figure 3-16 – (a) Output 1 (y_1), (b) Output 2 (y_2), of the three control strategies designed for example 2 when a random noise is applied

Figure 3-16 shows how the random noise has affected the output of the system.

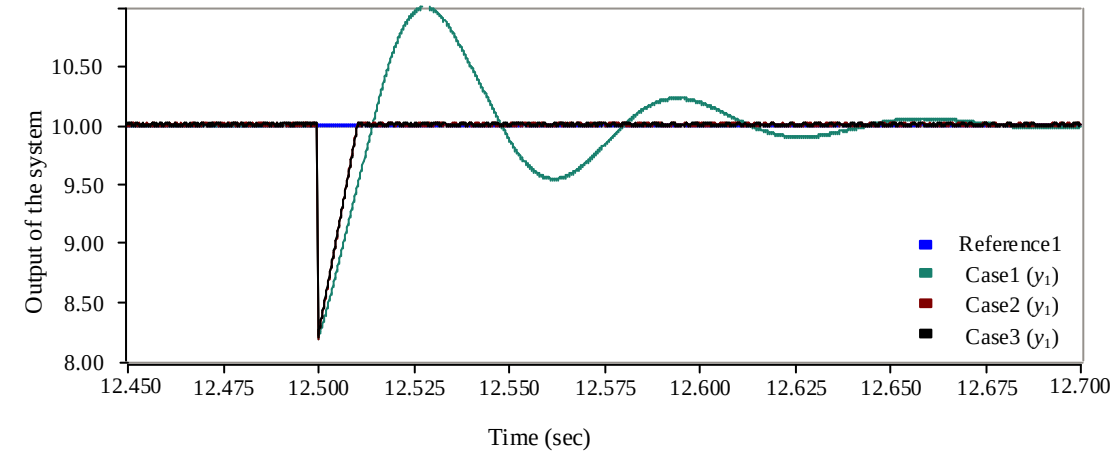

(a)

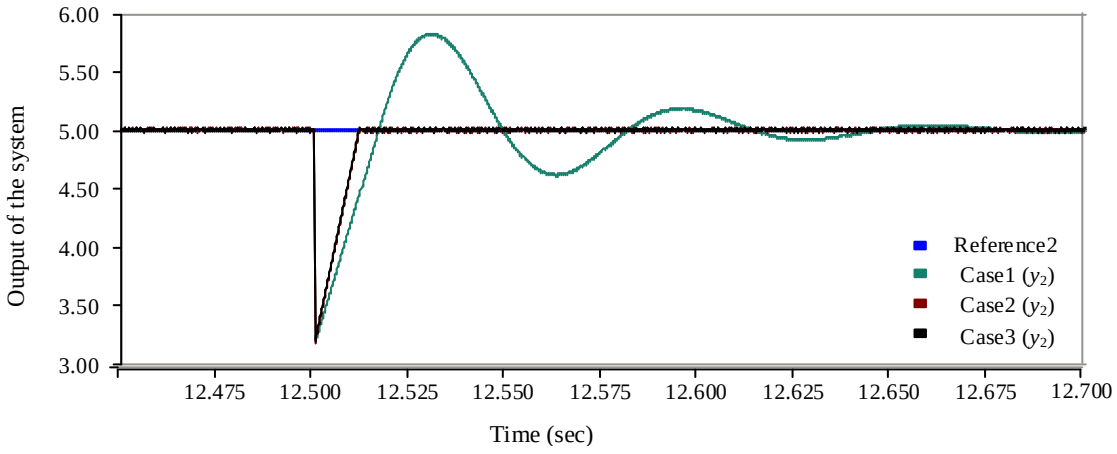

(b)

Figure 3-17 – (a) Output 1 (y_1), (b) Output 2 (y_2), of three control strategies designed for example 2, when the random noise is applied

Figure 3-17 is a zoomed in version of Figure 3-16 where the disturbance is applied to the system and the controllers' responses are shown. As per the graph it can be seen that the case 2 and case 3 controllers stabilize faster than the classical case. Therefore it can be concluded that the modified controller is more fitting for real time power system implementations than the classical method.

For the system given by Example 2, a low pass filter was also applied before feeding the system. The purpose of this modification was to observe the behaviour of the control

systems when there is a delay in the feedback parameter. This often occurs in real case scenarios as when the filters are used to extract the system output, there will be a significant delay in the feedback system. Therefore PID controllers will be detuned and will not perform as expected. In this case a 0.05s time delay has given to the outputs of the system. This time delay was provided using a $\frac{1}{1+sT}$ transfer function, where T denotes the delay time constant.

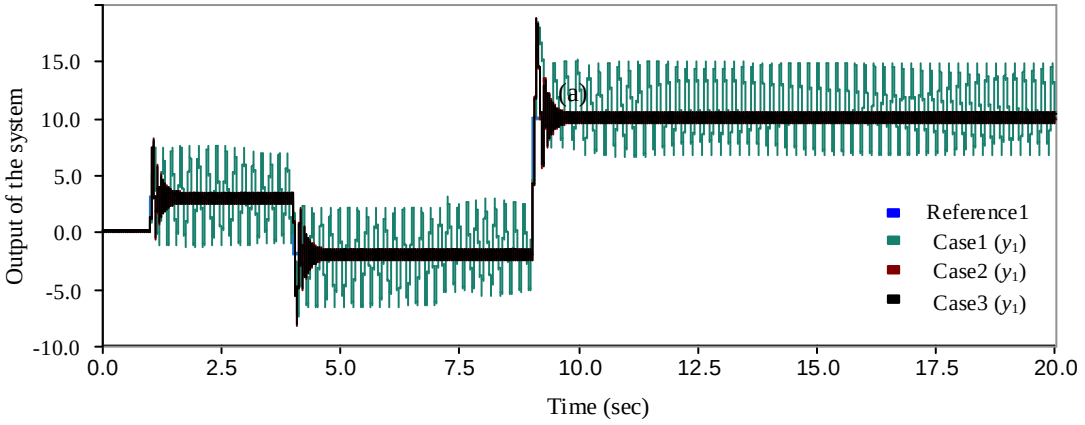

(a)

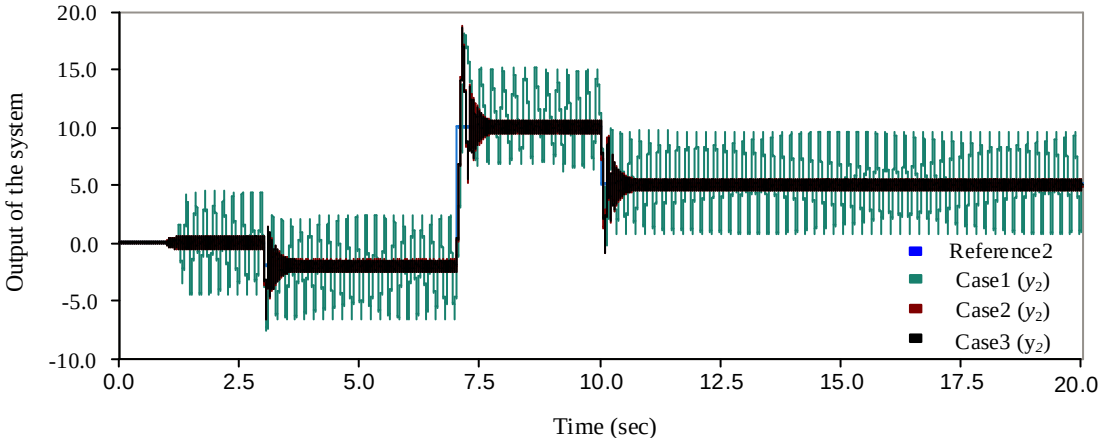

(b)

Figure 3-18 – (a) Output 1 (y_1), (b) Output 2 (y_2), of the three control strategies designed for of example 2 when a filter is added to the system

Examining Figure 3-18 it can be seen that the classical case (case 1) has not performed as expected.

Decoupling refers to the situation where two or more physically coupled systems operate without affecting each other's performance. In this example the two states of the system are coupled and each state has an effect on each other, as seen by variations of one when the other one is given a new command. By using a decoupling control technique each state can be controlled individually. Close examnitaion of the waveforms in Figure 3-18 (a) around t =7.5s shows that when the reference 2 is changed (as shown in Figure 3-18 (b)), the output 1 undergoes a transient. This means with the addition of delay, classical controller has shown lack of decoupling capability.

Comparing to case 1, the other two cases have given the results desired. Therefore it can again be concluded that the modified controller is more fitting for real time power system implementations than the classical method.

Chapter 4

Modified Control System for Active and Reactive Power Control of a Voltage-Source Converter

4.1 Voltage Source Converter

Voltage-source converter circuits are capable of converting a dc voltage to an ac voltage. These circuits are designed using fully-controlled semiconductor devices such as GTO thyristors, transistors, or IGBTs. The input dc source can be either from an independent dc source such as a battery bank or can be provided from the rectified output of an ac power supply stabilized by means of large capacitors. A VSC is capable of delivering an output with adjustable frequency, magnitude and phase shift. As most power system applications require sinusoidal waveforms, VSCs mostly generate sinusoidal waveforms at their output. This is however accompanied by a certain amount of harmonics, which need to be removed or reduced.

4.2 Introduction of the application

In this research, a voltage source converter is used with an external dc circuit to improve the stability of the connected power system by providing real and reactive power as it is required by the power system. Depending on the storage of the dc link, the active power that can be provided to the system can be varied. In this study a basic control strategy has been designed to control the converter. This basic controller represents a system that enables the converter to follow changes in the reference active and reactive power given by an outer loop system. The two main control parameters of the controller are active and reactive power of the system. To achieve independent control of active and reactive power, a decoupled control strategy based on dq0 transformation has been used [41]. This decoupling strategy of active and reactive current is applicable only for the linear systems and if the parameters of the system are time invariant. However any additional control action can lead to a reduction of system performance.

In this research, to enhance the performance of the classical decoupled control system, an internal model design has been added to the existing control system. This internal model design has been developed using the methodology discussed in Chapter 3. To analyse the performance of the basic and modified control systems, a generalized mathematical model of the converter shown in Figure 4-1 is used.

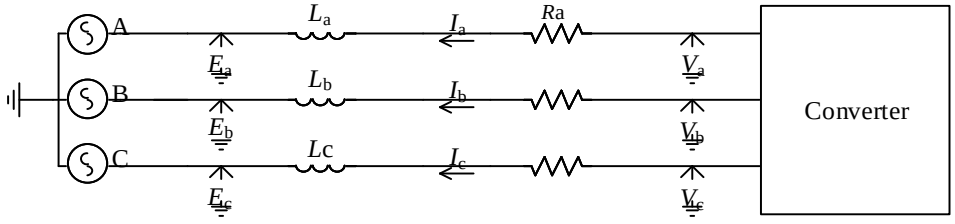

Figure 4-1- Equivalent circuit diagram of the converter connected to the power system

According to Figure 4-1, the converter is connected to the power system represented by a sinusoidal waveform and it is connected to the system with a series resistance and series inductance, which represents the line and transformer required for connection. To control active and reactive current independently abc to dq0 transformation technique was used.

Direct–quadrature–zero (dq0) transformation is a mathematical transformation that rotates the reference frame of a three-phase systems. When the three phase circuit is a balanced, application of the dq0 transform reduces the three AC quantities in to two DC quantities. This transformation simplifies the analysis of three-phase circuits and the calculations can then be carried out on these DC quantities before performing the inverse transform to obtain the actual three-phase results. In dq0 domain time varying parameters of systems become constants, which make the calculations easier; it will also be easier to see the system behaviour compared to the three phase domain. Therefore in most of the electrical engineering applications, such as machine drives and converters, this techniques is used.

In this power system application, to track the phase angle of the voltage, a phase-locked loop (PLL) block has been used and then it is fed to the dq0 block for current and voltage transformations from the three-phase abc domain to the dq0 domain. The feedback to the controller is the current of the power system, which will be transformed to the dq0 domain before feeding to the system. Designing of the decoupled controller is described in Section 4.3.

4.3 Mathematical Modeling of the Basic Decoupled Control System

The following equations were developed with the assumption that the three-phase system is fully balanced.

Let $R = R_a = R_b = R_c$ and $L = L_a = L_b = L_c$

Kirchhoff's voltage law (KVL) in the main loop of the circuit shown in Figure 4-1 yields:

$$V_a = E_a + R_a I_a + L_a \frac{dI_a}{dt} \tag{4.1}$$

$$V_b = E_b + R_b I_b + L_b \frac{dI_b}{dt} \tag{4.2}$$

$$V_c = E_c + R_c I_c + L_c \frac{dI_c}{dt} \tag{4.3}$$

After rearranging the equations (4.1), (4.2) and (4.3),

$$\frac{dI_a}{dt} = -\frac{R}{L} I_a + \frac{1}{L}(V_a - E_a) \tag{4.4}$$

$$\frac{dI_b}{dt} = -\frac{R}{L} I_b + \frac{1}{L}(V_b - E_b) \tag{4.5}$$

$$\frac{dI_c}{dt} = -\frac{R}{L} I_c + \frac{1}{L}(V_c - E_c) \tag{4.6}$$

Equation (4.4), (4.5) and (4.6) can be written in matrix form as follows,

$$\begin{pmatrix} \frac{dI_a}{dt} \\ \frac{dI_b}{dt} \\ \frac{dI_c}{dt} \end{pmatrix} = \begin{pmatrix} \frac{-R}{L} & 0 & 0 \\ 0 & \frac{-R}{L} & 0 \\ 0 & 0 & \frac{-R}{L} \end{pmatrix} \begin{pmatrix} I_a \\ I_b \\ I_c \end{pmatrix} + \frac{1}{L} \begin{pmatrix} V_a - E_a \\ V_b - E_b \\ V_c - E_c \end{pmatrix} \tag{4.7}$$

The decoupled control system has been designed using a new domain, which consists of two dimensions in this scenario as mentioned in Section 4.2. Parks transformation shown by (4.8) is used to transfer the system of abc three-phase quantities into the dq0 frame.

$$\mathbf{T}=\frac{2}{3}\begin{pmatrix} \cos(\theta) & \cos(\theta-\frac{2\pi}{3}) & \cos(\theta+\frac{2\pi}{3}) \\ \sin(\theta) & \sin(\theta-\frac{2\pi}{3}) & \sin(\theta+\frac{2\pi}{3}) \\ \frac{1}{2} & \frac{1}{2} & \frac{1}{2} \end{pmatrix} \tag{4.8}$$

Real power P can be written as shown below in dq0 domain,

$$P = \frac{3}{2}(V_d\ I_d - V_q\ I_q) \tag{4.9}$$

Reactive power Q can be written as shown below in dq0 domain,

$$Q = \frac{3}{2}\ (V_q\ I_d - V_d\ I_q) \tag{4.10}$$

Let the source voltage in three phase domain is given by following equations,

$$V_a = V_m \sin\ (\omega t) \tag{4.11}$$

$$V_b = V_m \sin(\omega t - \frac{2\pi}{3}) \tag{4.12}$$

$$V_c = V_m \sin(\omega t + \frac{2\pi}{3}) \tag{4.13}$$

where V_m is the peak value of the source voltage

Using the transformation matrix **T**, source voltage can be transferred to dq0 domain,

$$\begin{pmatrix} V_d \\ V_q \\ 0 \end{pmatrix} = \mathbf{T}\begin{pmatrix} V_a \\ V_b \\ V_c \end{pmatrix} \tag{4.14}$$

After substituting the values of the equation (4.14), V_d and V_q can be calculated.

$$V_d = V_m \tag{4.15}$$

$$V_q = 0 \tag{4.16}$$

After substituting the values of equation (4.9) and (4.10) active and reactive power can be found as shown below,

$$P = \frac{3}{2} V_d \, I_d = \frac{3}{2} V_m \, I_d \tag{4.17}$$

$$Q = -\frac{3}{2} V_d I_q = -\frac{3}{2} V_m I_q \tag{4.18}$$

After applying KVL to the system, the following generalized equation can be formed,

$$\mathbf{E}_{a,b,c} = -\mathbf{R}.\mathbf{I}_{a,b,c} - \mathbf{L}\frac{d\mathbf{I}_{a,b,c}}{dt} + \mathbf{V}_{a,b,c} \tag{4.19}$$

Using Park's transformation, equation (4.19) can be written as below,

$$\mathbf{E}_{d,q,0} = \mathbf{T} \, . \, \mathbf{E}_{a,b,c} \tag{4.20}$$

By substituting values of the equation (4.20), the following equations are derived,

$$\mathbf{E}_{d,q,0} = \mathbf{T}(-\mathbf{R}.\mathbf{I}_{a,b,c} - \mathbf{L}\frac{d\mathbf{I}_{a,b,c}}{dt} + \mathbf{V}_{a,b,c}) \tag{4.21}$$

$$\mathbf{E}_{d,q,0} = -\mathbf{R}.\mathbf{T}.\mathbf{I}_{a,b,c} - \mathbf{L}.\mathbf{T}.\frac{d\mathbf{I}_{a,b,c}}{dt} + \mathbf{T}.\mathbf{V}_{a,b,c} \tag{4.22}$$

$$\mathbf{E}_{d,q,0} = -\mathbf{R}.\mathbf{I}_{d,q,0} - \mathbf{L}(\mathbf{T}.\mathbf{T}^{-1}.\frac{d\mathbf{I}_{d,q,0}}{dt} + \mathbf{T}\frac{d\mathbf{T}^{-1}}{dt}\mathbf{I}_{d,q,0}) + \mathbf{T}.\mathbf{V}_{a,b,c} \tag{4.23}$$

Calculating the derivative of the transformation matrix,

$$\frac{d\mathbf{T}^{-1}}{dt} = \frac{d}{d\theta}\begin{pmatrix} \cos(\theta) & \sin(\theta) & 1 \\ \cos(\theta-\frac{2\pi}{3}) & \sin(\theta-\frac{2\pi}{3}) & 1 \\ \cos(\theta+\frac{2\pi}{3}) & \sin(\theta+\frac{2\pi}{3}) & 1 \end{pmatrix}\frac{d\theta}{dt} \tag{4.24}$$

$$\frac{d\mathbf{T}^{-1}}{dt} = \begin{pmatrix} -\sin(\theta) & \cos(\theta) & 1 \\ -\sin(\theta-\frac{2\pi}{3}) & \cos(\theta-\frac{2\pi}{3}) & 1 \\ -\sin(\theta+\frac{2\pi}{3}) & \cos(\theta+\frac{2\pi}{3}) & 1 \end{pmatrix}\omega \tag{4.25}$$

$$\mathbf{T}.\frac{d\mathbf{T}^{-1}}{dt} = \frac{2}{3}\begin{pmatrix} \cos(\theta) & \cos(\theta-\frac{2\pi}{3}) & \cos(\theta+\frac{2\pi}{3}) \\ \sin(\theta) & \sin(\theta-\frac{2\pi}{3}) & \sin(\theta+\frac{2\pi}{3}) \\ \frac{1}{2} & \frac{1}{2} & \frac{1}{2} \end{pmatrix}\begin{pmatrix} -\sin(\theta) & \cos(\theta) & 1 \\ -\sin(\theta-\frac{2\pi}{3}) & \cos(\theta-\frac{2\pi}{3}) & 1 \\ -\sin(\theta+\frac{2\pi}{3}) & \cos(\theta+\frac{2\pi}{3}) & 1 \end{pmatrix}\omega \tag{4.26}$$

$$\mathbf{T}.\frac{d\mathbf{T}^{-1}}{dt} = \begin{pmatrix} 0 & 1 & 0 \\ -1 & 0 & 0 \\ 0 & 0 & 0 \end{pmatrix}\omega \tag{4.27}$$

By simplifying equation (4.23), the following equations can be derived,

$$\mathbf{E}_{d,q,0} = -\mathbf{R}.\mathbf{I}_{d,q,0} - \mathbf{L}(\mathbf{I}.\frac{d\mathbf{I}_{d,q,0}}{dt} + \mathbf{T}\frac{d\mathbf{T}^{-1}}{dt}\mathbf{I}_{d,q,0}) + \mathbf{V}_{d,q,0} \tag{4.28}$$

$$E_d = -R.I_d - L\frac{dI_d}{dt} + \omega I_q + V_d \tag{4.29}$$

$$E_q = -R.I_q - L\frac{dI_q}{dt} - \omega I_d + V_q \tag{4.30}$$

Equations (4.29) and (4.30) can be rearranged as shown below,

$$\frac{dI_{\mathrm{d}}}{dt} = -\frac{R}{L} I_{\mathrm{d}} + \omega I_{\mathrm{q}} + \frac{1}{L}(V_{\mathrm{d}} - E_{\mathrm{d}}) \tag{4.31}$$

$$\frac{dI_{\mathrm{q}}}{dt} = -\frac{R}{L} I_{\mathrm{q}} - \omega I_{\mathrm{d}} + \frac{1}{L}(V_{\mathrm{q}} - E_{\mathrm{q}}) \tag{4.32}$$

By rewriting the equations (4.31) and (4.32) in matrix form,

$$\begin{pmatrix} \frac{dI_{\mathrm{d}}}{dt} \\ \frac{dI_{\mathrm{q}}}{dt} \end{pmatrix} = \begin{pmatrix} -\frac{R}{L} & \omega \\ -\omega & -\frac{R}{L} \end{pmatrix} \begin{pmatrix} I_{\mathrm{d}} \\ I_{\mathrm{q}} \end{pmatrix} + \frac{1}{L} \begin{pmatrix} V_{\mathrm{d}} - E_{\mathrm{d}} \\ V_{\mathrm{q}} - E_{\mathrm{q}} \end{pmatrix} \tag{4.33}$$

For a given dynamical system, the internal state variables are the smallest (in number) subset of system variables that can be used to represent the complete state of the power system at any given time if the input to the system is also known. The general form of the state space representation of a linear time-invariant system is as follows:

$$\dot{\mathbf{x}} = \mathbf{A}\,\mathbf{x} + \mathbf{B}\,u \tag{4.34}$$

where $\mathbf{x}$ is the state variable and u is the input of the system.

Considering equations (4.33) and (4.34), it can be seen that equation (4.33) follows the state space equation format.

I_{d} and I_{q} are the state variables and $\frac{1}{L}(V_{\mathrm{d}} - E_{\mathrm{d}})$ and $\frac{1}{L}(V_{\mathrm{q}} - E_{\mathrm{q}})$ are the inputs to the system.

Let,

$$U_1 = \frac{1}{L}(V_d - E_d) \tag{4.35}$$

$$U_2 = \frac{1}{L}(V_q - E_q) \tag{4.36}$$

By rearranging the equations (4.31) and (4.32), the following equations are derived,

$$\frac{dI_d}{dt} = -\frac{R}{L} I_d + \omega I_q + U_1 \tag{4.37}$$

$$\frac{dI_q}{dt} = -\frac{R}{L} I_q - \omega I_d + U_2 \tag{4.38}$$

After subjecting U_1 and U_2, equations (4.37) and (4.38) can be written as:

$$U_1 = (\frac{dI_d}{dt} + \frac{R}{L} I_d) - \omega I_q \tag{4.39}$$

$$U_2 = (\frac{dI_q}{dt} + \frac{R}{L} I_q) + \omega I_d \tag{4.40}$$

Considering the above equations, controlled input to the system can be represented as bellow,

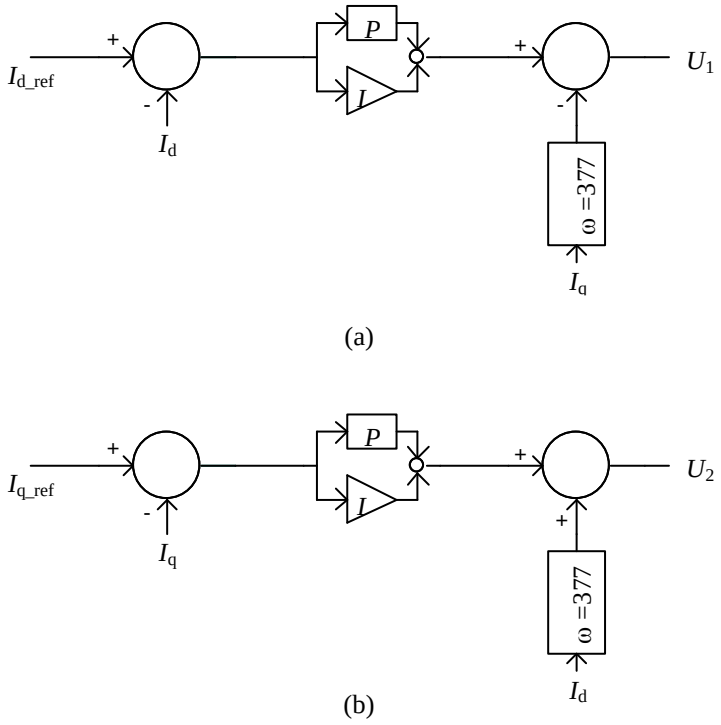

Figure 4-2 - Controlled (a) input 1 (b) input 2, to the system

Figure 4-2 illustrates the controlled inputs U_1 and U_2 of the system. I_{d_ref} and I_{q_ref} are the reference input currents given to the control system shown by Figure 4-3 and I_d, I_q are the system currents in the dq0 domain. According to the Figure 4-2, it can be seen that the system current transferred to dq0 frame has been fed to the controller and then the current errors ((I_{d_ref}-I_d) and (I_{q_ref}-I_q)) have been sent through a PI controller. After that the decoupling terms have been added to the result coming through the PI controller to obtain the controlled input to the system.

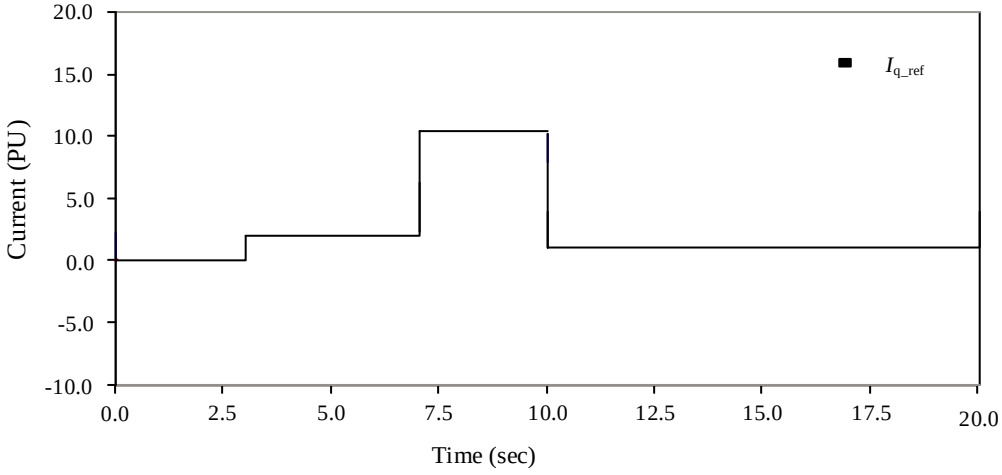

(a)

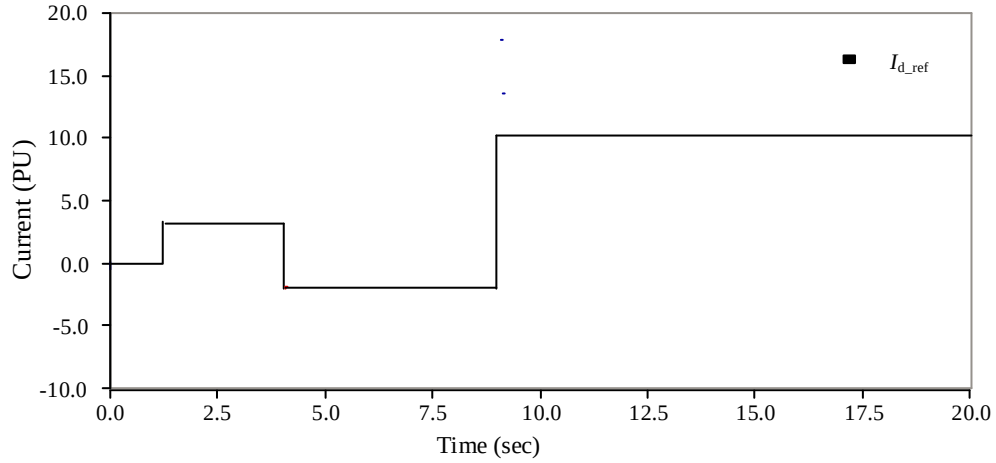

(b)

Figure 4-3- Reference input currents (a) I_{q_ref}, (b) I_{d_ref} , given to the system

Taking the Laplace transform of equations (4.37) and (4.38),

$$I_d = \frac{U_1 + \omega I_q}{s + \frac{R}{L}} \tag{4.41}$$

$$I_q = \frac{U_2 - \omega I_d}{s + \frac{R}{L}} \tag{4.42}$$

Equations (4.41) and (4.42), can be represented as block diagrams shown in Figure 4-4.

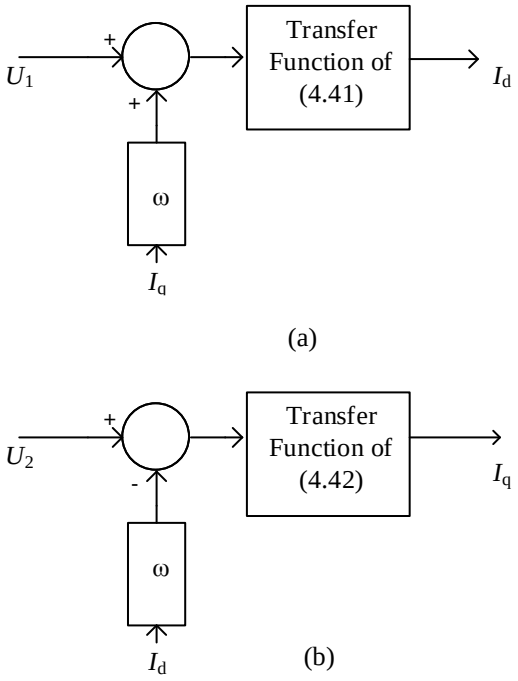

Figure 4-4 - Representation of the power system equations (a) (4-41) and (b) (4-42) in block diagrams

The power system equivalent system shown in Figure 4-5 is controlled using the controllers by block diagrams shown by Figure 4-2 and Figure 4-4.

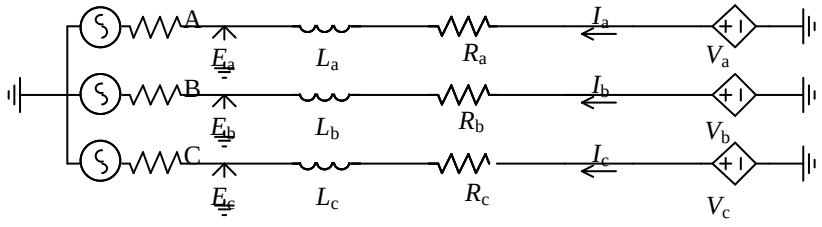

Figure 4-5- Representation of the power system

Figure 4-5 is a representation of the power system and V_a, V_b and V_c are the voltages supplied to the system by the converter. E_a, E_b and E_c are the source voltages of the power system and the system parameter values are shown in Table 4-1.

Table 4-1 - Voltage source converter system parameters

Parameter	Value
$E_a = E_b = E_c$	230kV
$R_a = R_b = R_c$	0.01Ω
$L_a = L_b = L_c$	0.001H

A model of this system along with its control circuitry was implemented in PSCAD/EMTDC transient simulation software to check the performance of the system shown in Figure 4-5 with the controller, which was modeled as follows in Figure 4-6.

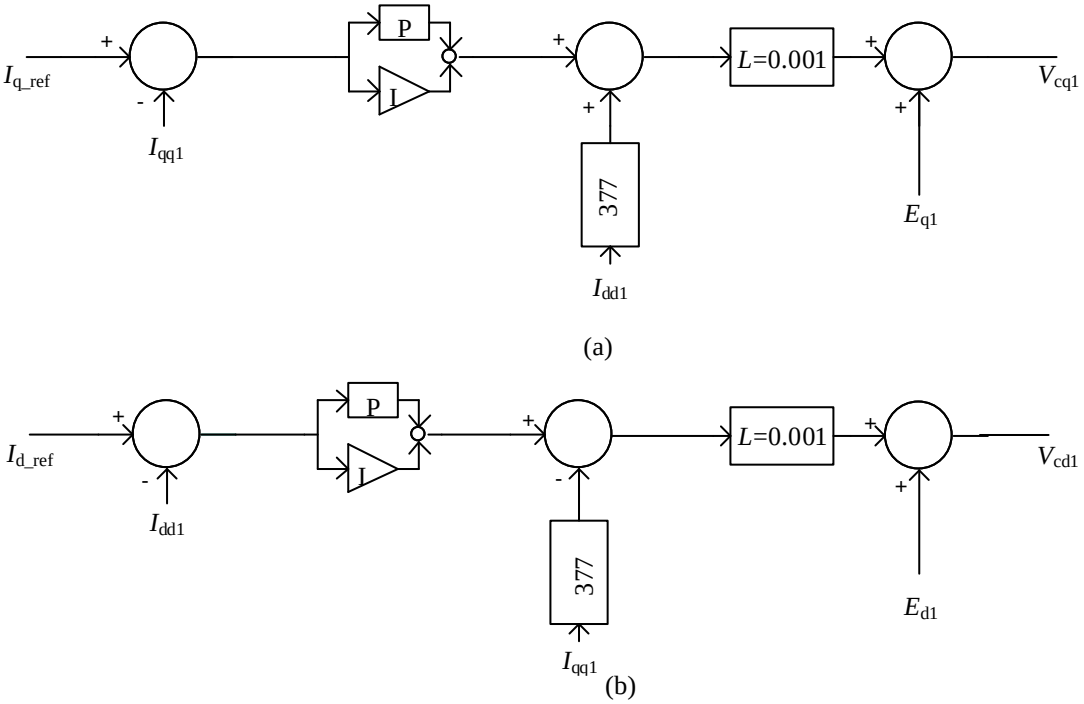

Figure 4-6 - Classical control system (a) d axis (b) q axis, designed for the power system

E_{d1}, E_{q1} are the source voltages of the power system and I_{dd1}, I_{qq1} are the system current in dq0 domain. L is the inductance of the system. An abc-dq0 transformation has been used to transfer abc parameters to dq0 domain and the transformation angle was fed to the dq0 transfer tool using a phase locked loop (PLL). V_{cd1} and V_{cq1} are the converter end voltages in dq0 domain. After transferring V_{cd1} and V_{cq1} to abc domain V_a, V_b, V_c are

supplied to the power system as shown in Figure 4-5. PI controllers of the system were tuned using trial and error to obtain the system current similar to the reference current input. The above simulation cases were simulated for 20 seconds and results shown in Figure 4-7 were obtained.

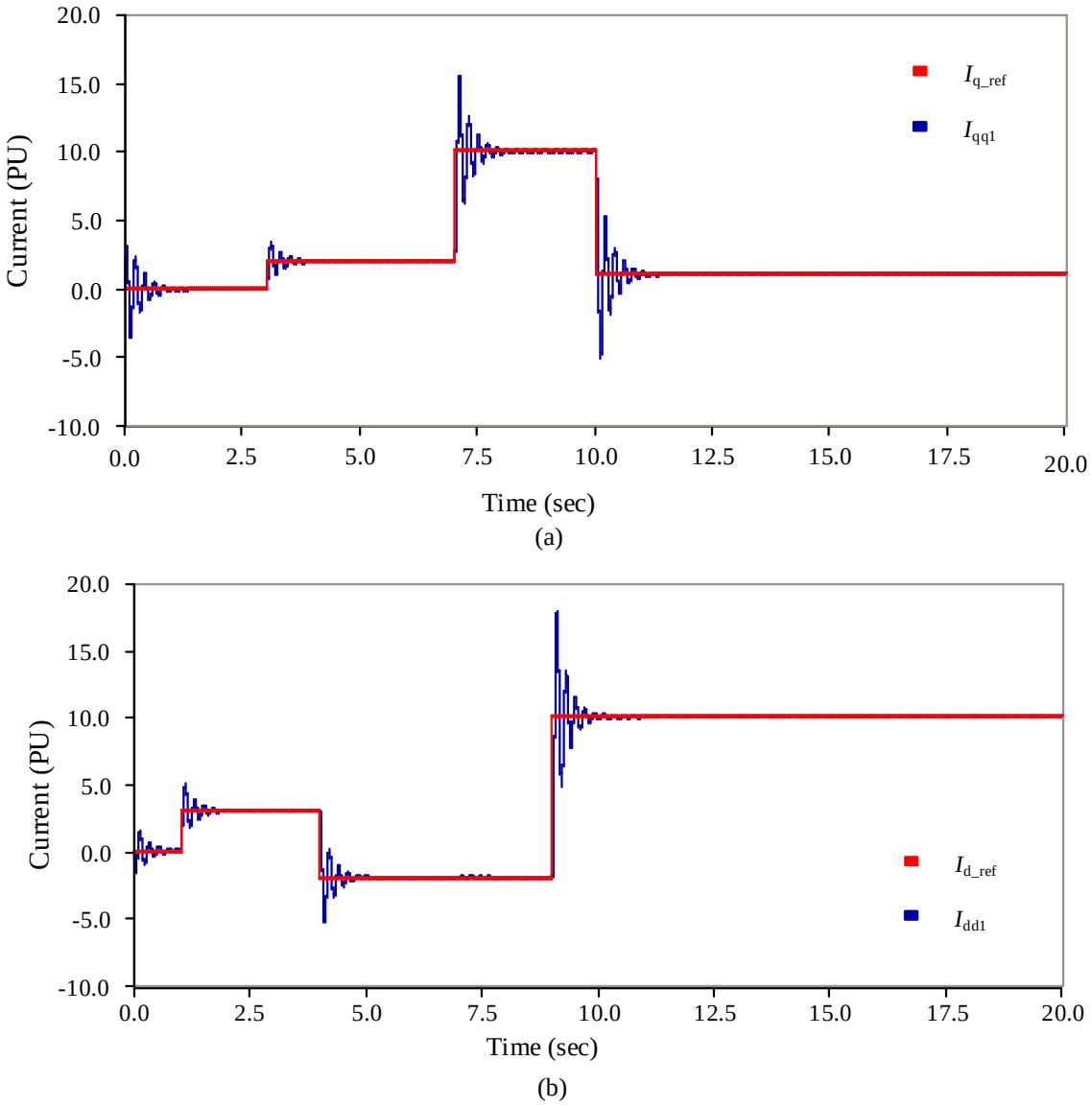

Figure 4-7 – Reference and system currents (a) in q axis, (b) in d axis, of the classical control system

I_{dd1} and I_{qq1} are the system current in dq0 frame and I_{d_ref} and I_{q_ref} are the reference current input to the controller. According to the Figure 4-7, it can be seen that even

though there is a small transient period, the output currents follow the reference value as expected and the system is decoupled accurately.

4.4 Mathematical modeling of the internal model design

As described in Chapter 3, an internal model is designed to improve the performance of the classical decoupled control system. System parameter values were used as shown in Table 4-1. To develop an internal model design, two methods are used.

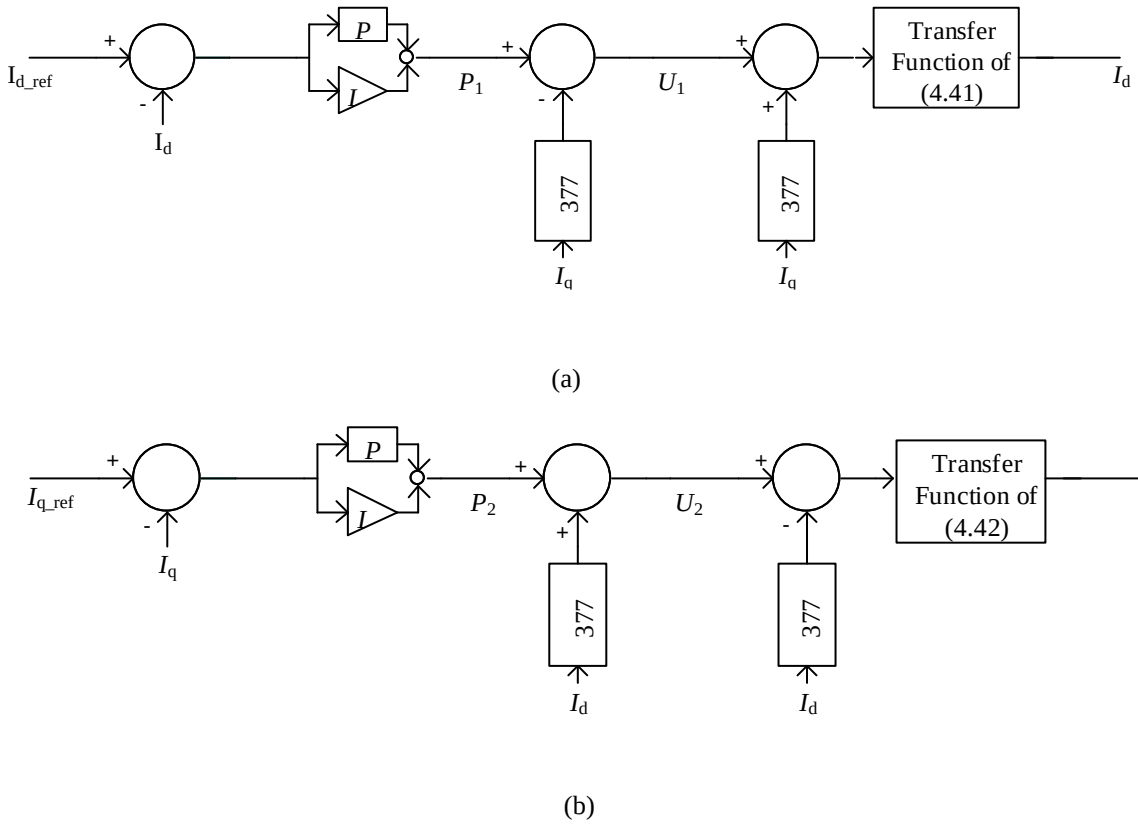

Figure 4-8 - Representation of the classical control system (a) d axis (b) q axis, with equivalent model of the power system

4.4.1 Method 1: (control system with an internal model design)

Figure 4-8 is used to calculate state variables I_d and I_q that would be generated in the power system at a given time. The following equations were then developed by writing equivalences to I_d, I_q and U_1, U_2.

$$I_q = (U_2 - \omega I_d)\frac{1}{(s + \frac{R}{L})} \tag{4.43}$$

$$I_d = (U_1 + \omega I_q)\frac{1}{(s + \frac{R}{L})} \tag{4.44}$$

$$P_2 + \omega\, I_d = U_2 \quad \text{so that} \quad P_2 = U_2 - \omega\, I_d \tag{4.45}$$

$$P_1 - \omega\, I_q = U_1 \text{ so that } P_1 = U_1 + \omega\, I_q \tag{4.46}$$

Therefore to predict the output currents I_d and I_q considering equations (4.43) and (4.44), it can be seen that by multiplying equations (4.45) and (4.46) by $(s + \frac{R}{L})$ factors I_q and I_d can be obtained.

Therefore the predictive state variables can be written as:

$$P_2 \frac{1}{(s + \frac{R}{L})} = I_q \tag{4.47}$$

$$P_1 \frac{1}{(s + \frac{R}{L})} = I_d \tag{4.48}$$

The modified control system with the predictive state feedback is shown as in Figure 4-9.

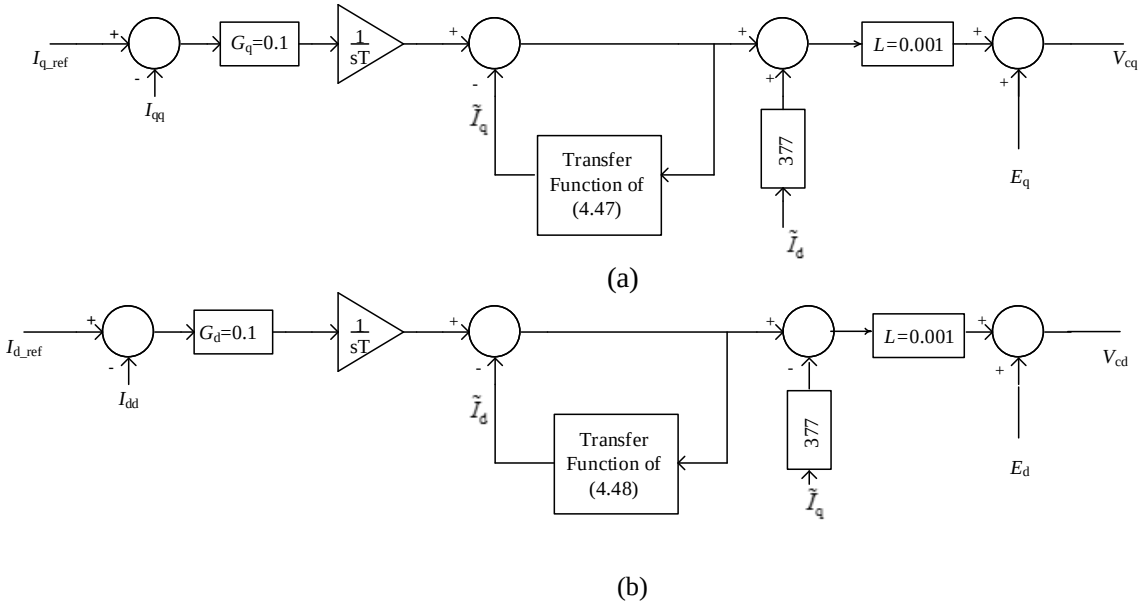

Figure 4-9 – (a) d axis (b) q axis, modified control systems with internal model designs

E_d and E_q are the source voltages of the power system and I_{dd}, I_{qq} are the system currents in dq0 domain. L, G_d, and G_q are the inductance of the system and the proportional gains of d axis and q axis current controllers, respectively. An abc dq0 transformation has used to transfer abc parameters to dq0 domain in PSCAD/EMTDC simulation software. The transformation angle was fed to the dq0 transfer tool using a phase locked loop (PLL). V_{cd} and V_{cq} are the converter end voltages in dq0 domain. After transferring V_{cd} and V_{cq} to abc domain V_a, V_b, V_c are supplied to the power system. PI controllers of the system were tuned using trial and error to obtain the system current similar to the reference current input. This simulation case was simulated for 20 seconds and results shown in Figure 4-10 were obtained. Reference currents shown in Figure 4-3 were given to the modified controller so that a clear comparison over each case can be achieved.

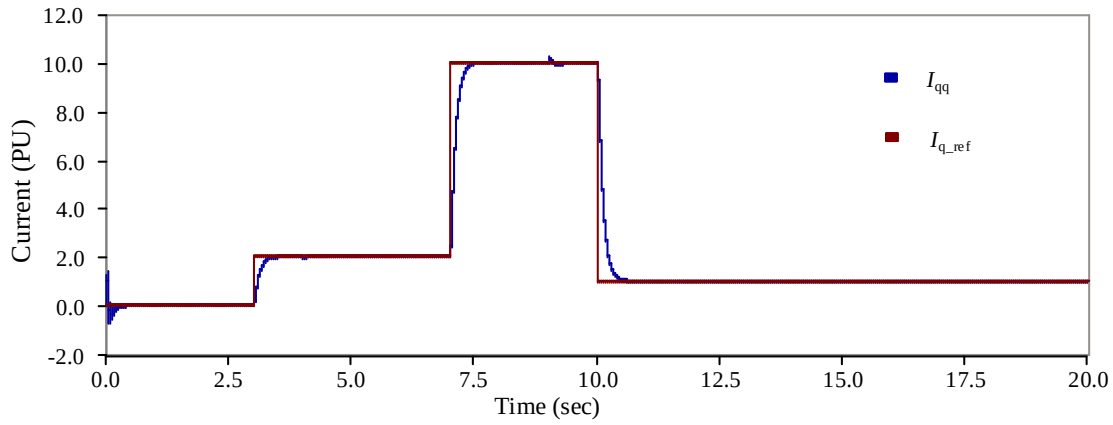

(a)

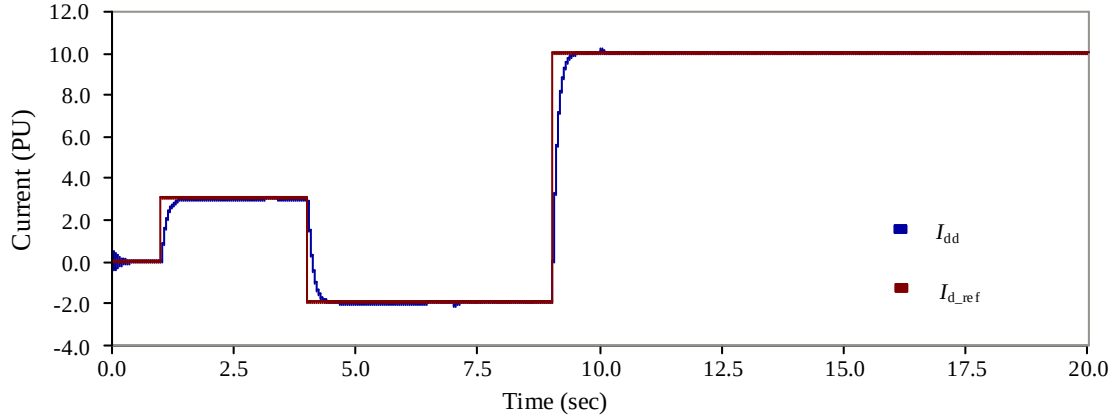

(b)

Figure 4-10 - Reference currents given to the controllers and the system currents (a) in q axis, (b) in d axis

I_{dd} and I_{qq} are the system currents in dq0 frame and I_{d_ref} and I_{q_ref} are the reference current input to the modified controller. According to the Figure 4-10, it can be seen that the output currents follow the reference values as expected and the system is decoupled accurately. Therefore it can be concluded that the new controller has provided expected results.

4.4.2 Method 2: (control system with the state observer)

In this method, to provide the state feed back to the controller in this particular application, a different state observer concept has been used [28]. This method has been discussed in detail in chapter 3 with two examples.

In designing of state observer process, first assumption was that all the states are available for the feedback.

The system equation for this particular application can be stated as follows:

$$\begin{pmatrix} \frac{dI_d}{dt} \\ \frac{dI_q}{dt} \end{pmatrix} = \begin{pmatrix} -\frac{R}{L} & \omega \\ -\omega & -\frac{R}{L} \end{pmatrix} \begin{pmatrix} I_d \\ I_q \end{pmatrix} + \begin{pmatrix} 1 & 0 \\ 0 & 1 \end{pmatrix} \begin{pmatrix} U_1 \\ U_2 \end{pmatrix} \tag{4.49}$$

By substituting the values from Table 4-1 in to equation (4.49),

$$\dot{\mathbf{x}} = \begin{pmatrix} -10 & 377 \\ -377 & -10 \end{pmatrix} \begin{pmatrix} \mathbf{x}_1 \\ \mathbf{x}_2 \end{pmatrix} + \begin{pmatrix} u_1 \\ u_2 \end{pmatrix} \tag{4.50}$$

$$y = \begin{pmatrix} 1 & 0 \\ 0 & 1 \end{pmatrix} \begin{pmatrix} \mathbf{x}_1 \\ \mathbf{x}_2 \end{pmatrix} \tag{4.51}$$

To design the observer, the gain matrix and other parameters were calculated as below.

$$\mathbf{A} = \begin{pmatrix} -10 & 377 \\ -377 & -10 \end{pmatrix} \qquad \mathbf{C} = \begin{pmatrix} 1 & 0 \\ 0 & 1 \end{pmatrix} \qquad \mathbf{B} = \begin{pmatrix} 1 & 0 \\ 0 & 1 \end{pmatrix}$$

The state observer equation is given bellow.

$$\dot{\tilde{\mathbf{x}}} = \mathbf{A}\tilde{\mathbf{x}} + \mathbf{B}u + \mathbf{L}(y - \mathbf{C}\tilde{\mathbf{x}}) \tag{4.52}$$

where $\tilde{\mathbf{x}}$ denotes the estimate of the state $\mathbf{x}$ and the $\mathbf{L}$ matrix is the observer gain matrix

which will be determined as part of the observer design. The estimation error can be written as:

$$\mathbf{e}(t) = \mathbf{x}(t) - \tilde{\mathbf{x}}(t) \tag{4.53}$$

Taking the time derivative of the error given by equation (4.53),

$$\dot{\mathbf{e}} = \dot{\mathbf{x}} - \dot{\tilde{\mathbf{x}}} \tag{4.54}$$

By combining equations (4.52) and (4.54), the following equation can be obtained,

$$\dot{\mathbf{e}} = \mathbf{A}\mathbf{x} + \mathbf{B}u - \mathbf{A}\tilde{\mathbf{x}} - \mathbf{B}u - \mathbf{L}(y - \mathbf{C}\tilde{\mathbf{x}}) \tag{4.55}$$

$$\dot{\mathbf{e}}(t) = (\mathbf{A} - \mathbf{LC})\mathbf{e}(t) \tag{4.56}$$

Characteristic equation of equation (4.56) can be written as below,

$$\det(\lambda\mathbf{I} - (\mathbf{A} - \mathbf{LC})) = 0 \tag{4.57}$$

For a faster response with a lower overshoot, suppose the characteristic equations can be written [40] as:

$$\Delta(\lambda) = \lambda^2 + 2\xi\omega_n\lambda + \omega_n^2 \tag{4.58}$$

where ξ is the damping ratio and ω_n is the angular velocity. According to the dimensions of the system given in this example the gain matrix (**L**) can be written as:

$$\begin{pmatrix} L_1 & L_2 \\ L_3 & L_4 \end{pmatrix}$$

By substituting the values of Table 4-1 in equation (4.57),

$$\left| \lambda \begin{bmatrix} 1 & 0 \\ 0 & 1 \end{bmatrix} - \left(\begin{bmatrix} -10 & 377 \\ -377 & -10 \end{bmatrix} - \begin{bmatrix} L_1 & L_2 \\ L_3 & L_4 \end{bmatrix} \begin{bmatrix} 1 & 0 \\ 0 & 1 \end{bmatrix} \right) \right| = 0$$

$$\left| \begin{bmatrix} \lambda & 0 \\ 0 & \lambda \end{bmatrix} - \left(\begin{bmatrix} -10 - L_1 & 377 - L_2 \\ -377 - L_3 & -10 - L_4 \end{bmatrix} \right) \right| = 0$$

$$\left|\left(\begin{bmatrix} \lambda+10+L_1 & -377+L_2 \\ 377+L_3 & \lambda+10+L_4 \end{bmatrix}\right)\right|=0$$

$$(\lambda+10+L_1)(\lambda+10+L_4)-(L_2-377)(L_3+377)=0 \tag{4.59}$$

Assume L_2 and L_4 are 1 (for the simplicity of the calculations)

$$\Delta(\lambda)=\lambda^2+\lambda(L_1+21)+11(10+L_1)+376(L_3+377) \tag{4.60}$$

Let ω_n be 10 and select ξ to be 0.8 for minimal overshoot [40], using equations (4.58) and (4.60), L_3 and L_1 can be found.

$$L_1-21=16$$

$$L_1=-5 \text{ and}$$

$$11(10+L_1)+376\,(L_3+377)=100 \tag{4.61}$$

By substituting the value of L_1 in to equation (4.61), L_3 can be found.

$$L_3=-376.88$$

By substituting the values from Table 4-1 for the observer equation (4.52),

$$\dot{\tilde{\mathbf{x}}}=\begin{bmatrix} -10 & 377 \\ -377 & -10 \end{bmatrix}\tilde{\mathbf{x}}+\begin{bmatrix} 1 & 0 \\ 0 & 1 \end{bmatrix}u+\begin{bmatrix} -5 & 1 \\ -376.88 & 1 \end{bmatrix}(y-\mathbf{C}\tilde{\mathbf{x}}) \tag{4.62}$$

Taking the Laplace transform of the above equation,

$$s\tilde{\mathbf{x}}_1=-10\tilde{\mathbf{x}}_1+377\tilde{\mathbf{x}}_2+u_1-5y_1-21\tilde{\mathbf{x}}_1+y_2-\tilde{\mathbf{x}}_2$$

$$\tilde{\mathbf{x}}_1=\frac{u_1+y_2-5y_1+376\tilde{\mathbf{x}}_2}{s+5} \tag{4.63}$$

And $s\tilde{\mathbf{x}}_2=-377\tilde{\mathbf{x}}_1-10\tilde{\mathbf{X}}_2+u_2-376.88y_1+376.88\tilde{\mathbf{x}}_1+y_2-\tilde{\mathbf{x}}_2$

$$\tilde{\mathbf{x}}_2=\frac{u_2+y_2-376.88y_1-0.12\tilde{\mathbf{x}}_1}{s+11} \tag{4.64}$$

The modified control system with the predictive state feedback can be shown by Figure 4-11. The state estimator was designed using the above calculated values.

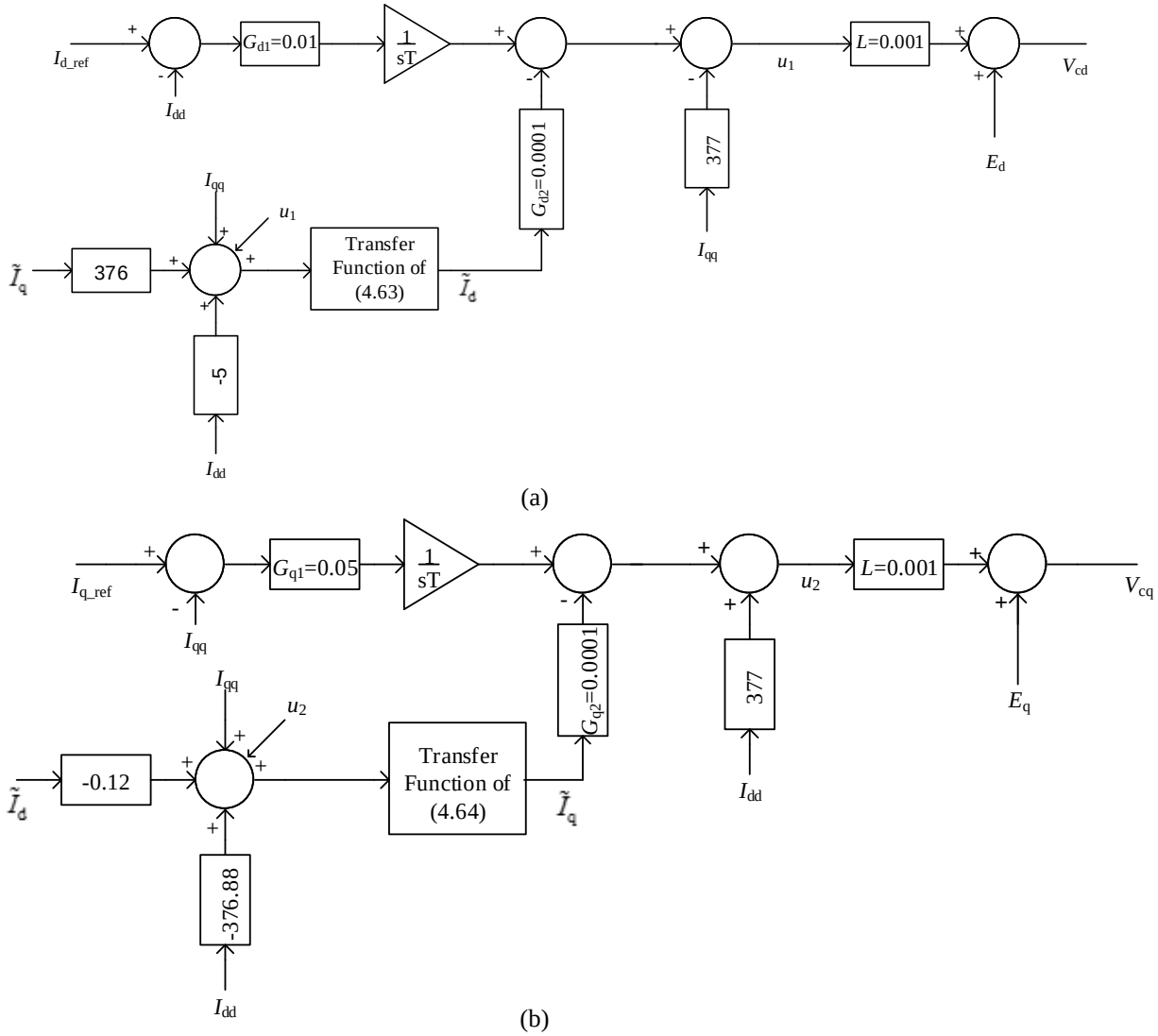

Figure 4-11 - (a) d axis (b) q axis, modified control systems with state observer

E_d, E_q are the source voltages of the power system and I_{dd}, I_{qq} are the system currents in dq0 domain. L is the system inductance and G_{d1}, G_{d2}, $G_{q1,}$ G_{q2} are the d and q axis current controller gains.The transformation angle was fed to the dq0 transfer tool using a phase locked loop (PLL). V_{cd} and V_{cq} are the converter end voltages in dq0 domain. After fer-

ring V_{cd} and V_{cq} to abc domain V_a, V_b, V_c are supplied to the power system. PI controllers of the system were tuned to obtain the system current similar to the reference current inputs shown in Figure 4-3. These simulation cases were simulated for 20 seconds and the results shown in Figure 4-12 were obtained.

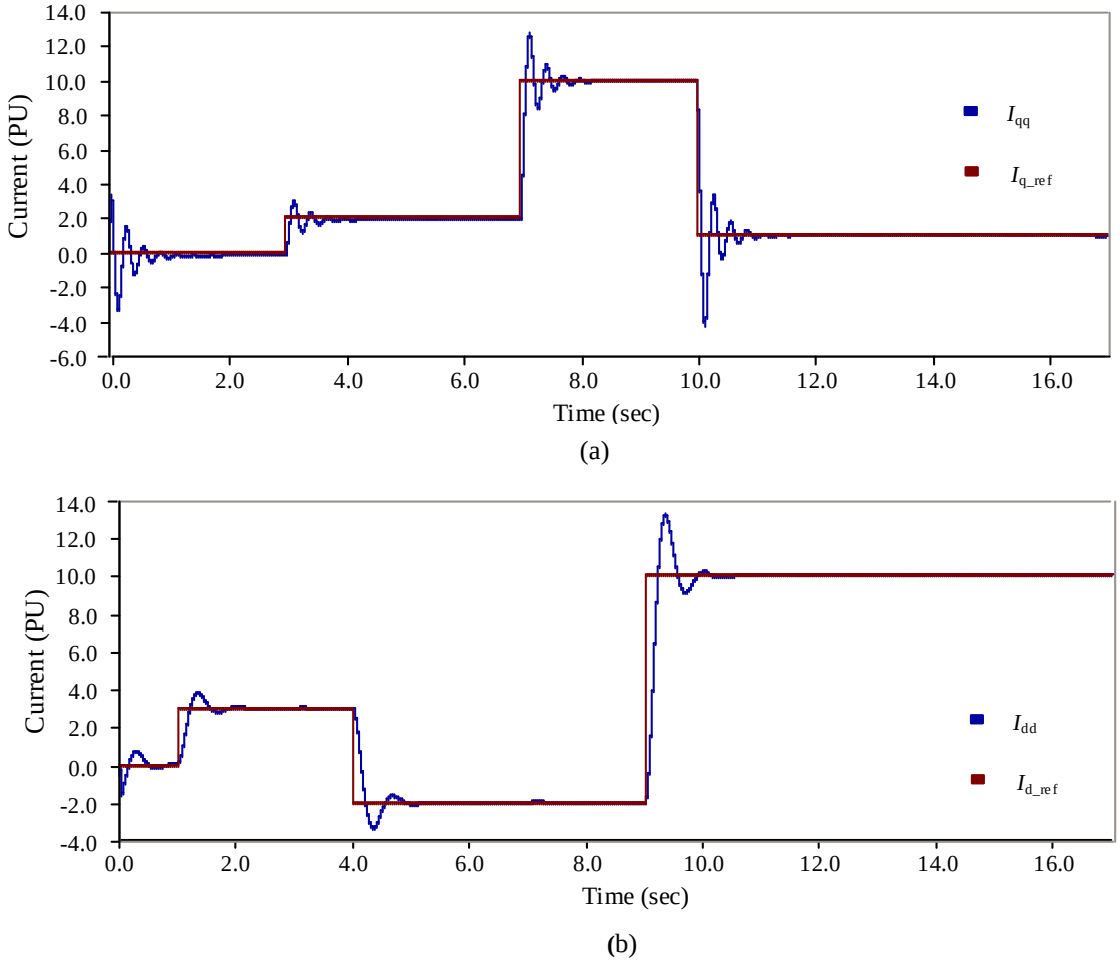

Figure 4-12 - Reference currents given to the controllers and system currents (a) in q axis, (b) in d axis

I_{dd} and I_{qq} are the system currents in dq0 frame and I_{d_ref} and I_{q_ref} are the refrence current input to the modified controller. According to Figure 4-12, it can be seen that the output currents of the new controller follow the reference values as expected and the system is decoupled accurately.

4.5 Simulation results

Simulation cases shown by Figures 4-6 and 4-9 were simulated for 20 seconds where each case was fed with references shown in Figure 4-3, plotted in the same graph shown by Figure 4-13, so that a clear comparison over each case can be achieved.

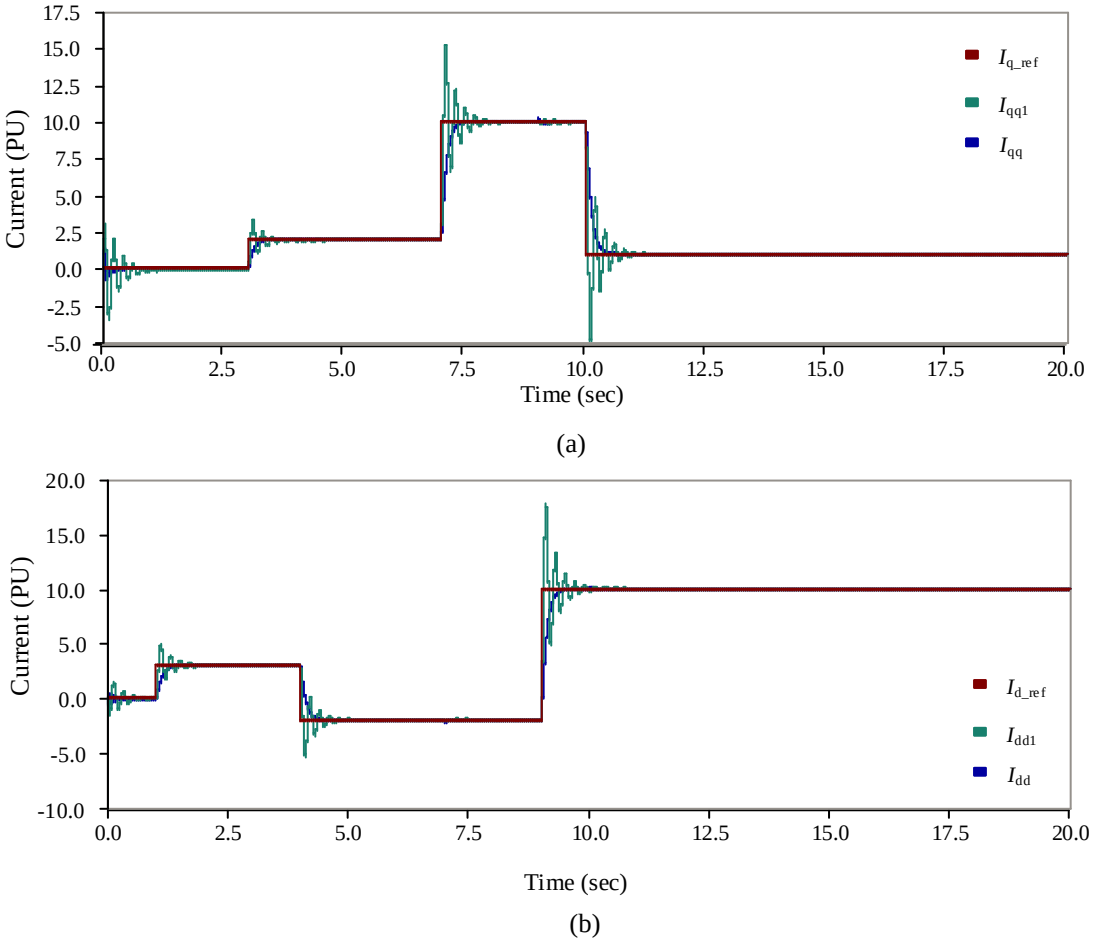

Figure 4-13 - Reference currents and the system currents (a) in q axis, (b) in d axis when the classical controller and the modified controller (using method 1) are used

I_{dd} and I_{qq} are the system currents in dq0 frame when the I_{d_ref} and I_{q_ref} are given as the reference input to the modified controller with the predictive control loop using

method 1 calculation and I_{dd1} and I_{qq1} are the system current in dq0 frame when the classical controller is connected to the system.

Simulation cases shown by Figures 4-6 and Figure 4-11 were simulated for 20 seconds where each case was fed with references shown in Figure 4-3, plotted in the same graph shown by the following figures so that a clear comparison over each case can be achieved.

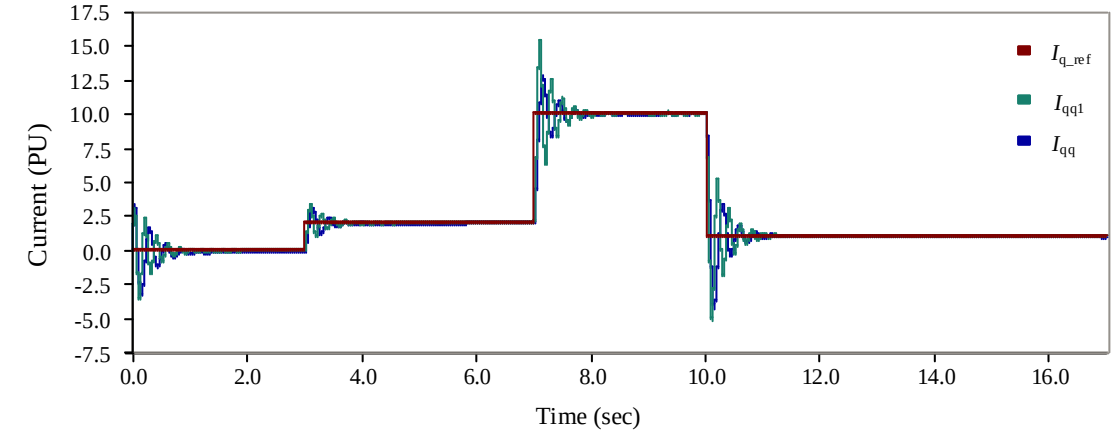

(a)

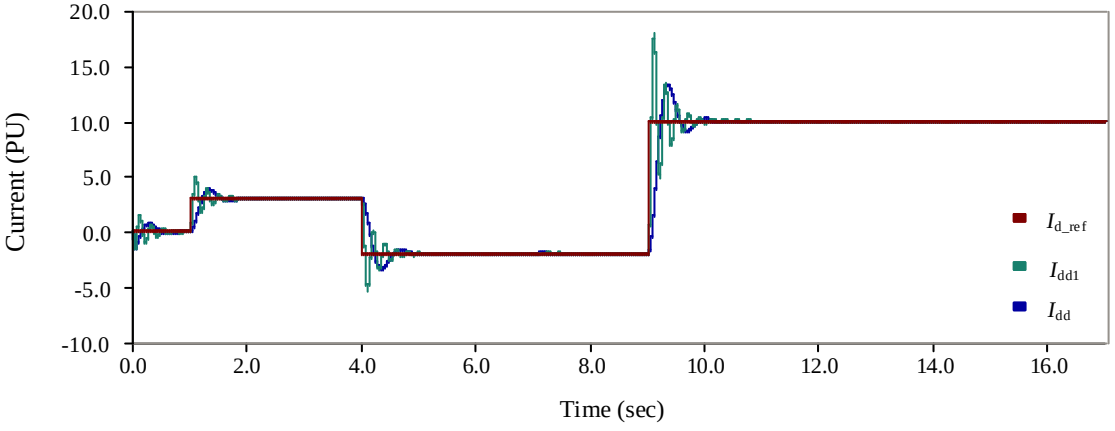

(b)

Figure 4-14 - Reference currents and the system currents (a) in q axis, (b) in d axis when the classical controller and the modified controller (using method 2) are used

I_{dd} and I_{qq} are the system currents in dq0 frame when the I_{d_ref} and I_{q_ref} are given as the reference input to the modified controller which comprised with the predictive control loop using method 2 calculations and I_{dd1} and I_{qq1} are the system current in dq0 frame when the classical controller is connected to the system.

According to Figures 4-13 and 4-14, it can be see that all the controllers have delivered expected results and the controller with the state estimator which was calculated using the procedure described in method 1, has given better results compared to other control methods. When considering the transient period, the classical control system has lot of fluctuations whereas the controller with the internal model, which was designed using method 1, follows the reference without unexpected fluctuations. The controller designed using the calculations described in method 2 has also provided better results compared to the classical control system but could not reach the performance level provided by the controller designed using the calculations described in method 1.

To check the behaviour of the system current when the modified controller was connected to the power system over the classical controller scenario, under different circumstances the following simulations shown in Figure 4-15 were carried out using PSCAD/EMTDC software.

4.5.1 System current behavior after adding a filter to the system

Filtering of output parameters, which are extracted from the system to feed to the controller, is an external condition that can cause time delay. Therefore in this section a filter which provides 0.5ms time delay in the feedback system has been added to the system.

The following simulation results were obtained to observe the behaviour of the classical controller and the modified controllers.

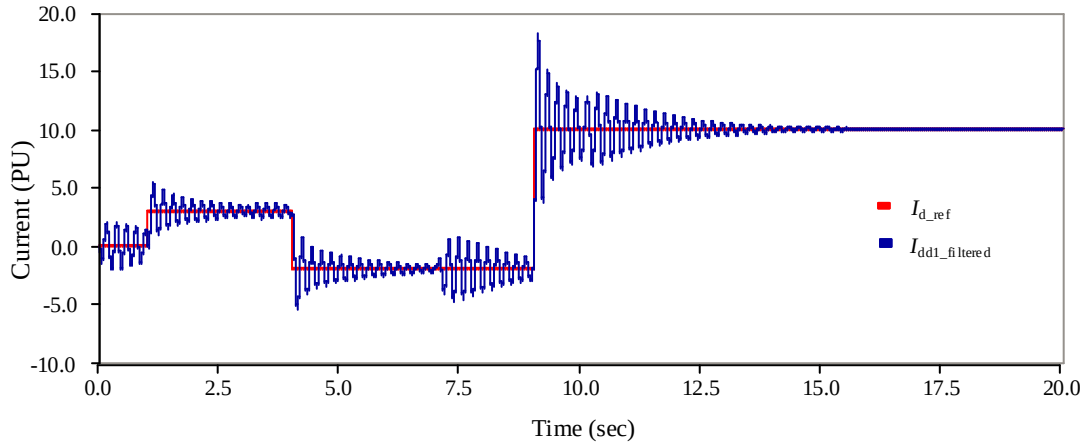

(a)

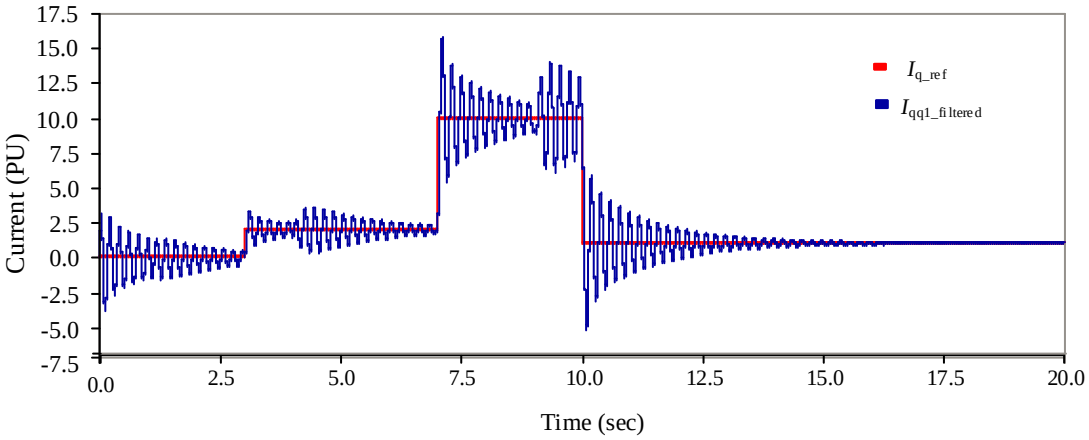

(b)

Figure 4-15 - Reference currents and the filtered system currents (a) in q axis, (b) in d axis when the classical controller is used

$I_{dd1\_filtered}$ and $I_{qq1\_filtered}$ are the system current in dq0 frame when the I_{d_ref} and I_{q_ref} are given as the reference current inputs to the classical controller. Comparing Figure 4-15 with Figure 4-7 it can be observed that, with the delay in the system due to the filter, the classical controller has given unexpected results comprised of a lot of fluctuations and lack of decoupling capability.

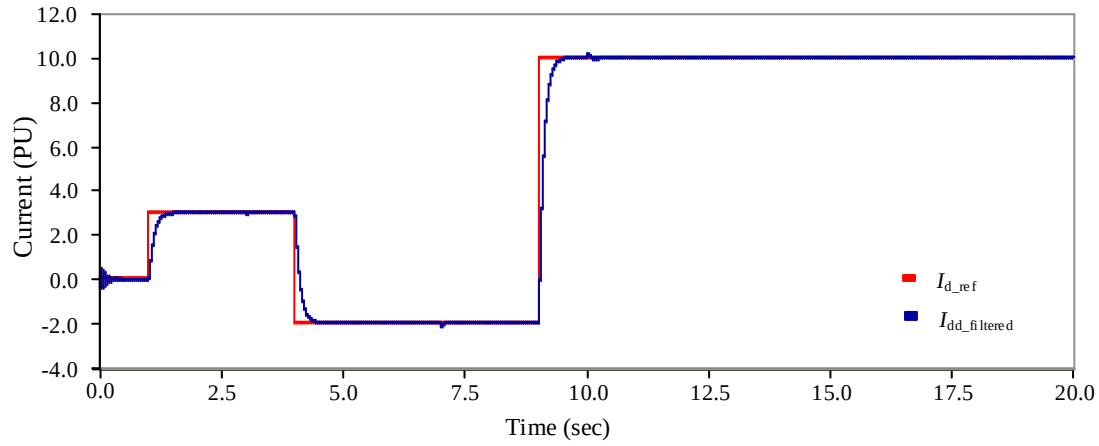

(a)

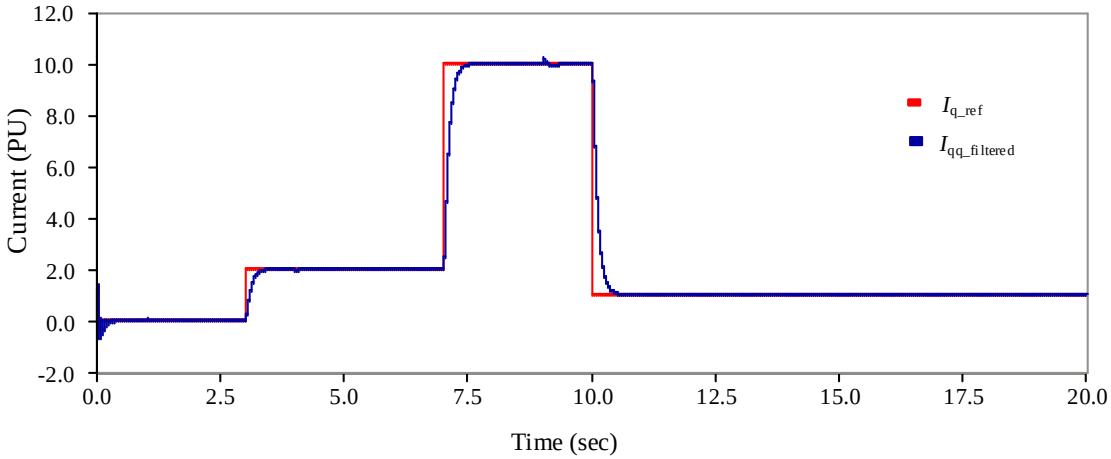

(b)

Figure 4-16 - Reference currents and the filtered system currents (a) in q axis, (b) in d axis, of the modified controller designed using method 1

$I_{dd\_filtered}$ and $I_{qq\_filtered}$ are the system current in dq0 frame when the I_{d_ref} and I_{q_ref} are given as the reference current inputs to the modified controller which was designed as described in method 1. Comparing Figure 4-10 with Figure 4-16 it can be observed that, even with the delay in the system due to the filter, the controller modified using method 1, has given expected results.

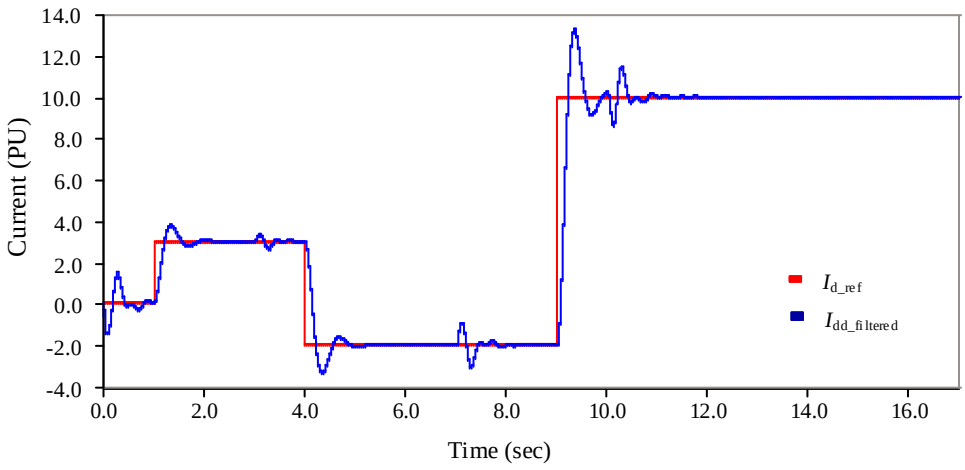

(a)

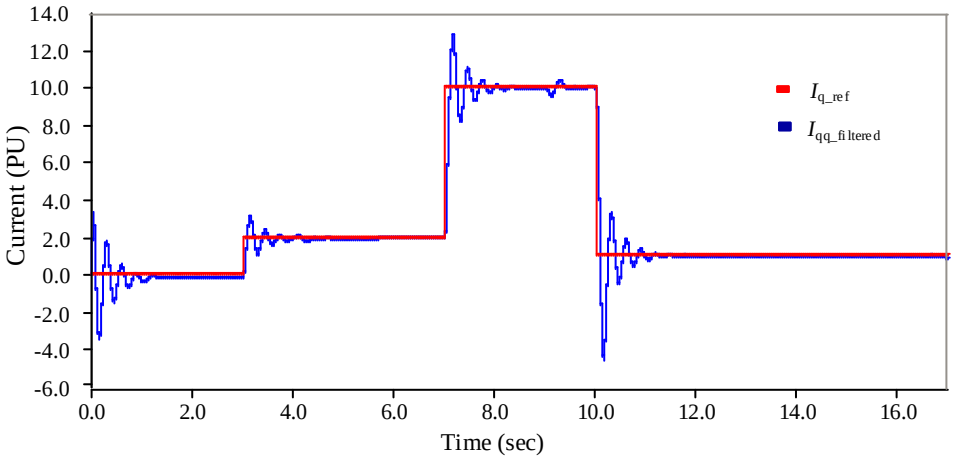

(b)

Figure 4-17 - Reference currents and the filtered system currents (a) in q axis, (b) in d axis, of the modified controller designed using method 2

$I_{dd\_filtered}$ and $I_{qq\_filtered}$ are the system current in dq0 frame when the I_{d_ref} and I_{q_ref} are given as the reference current inputs to the modified controller which was designed as described in method 2. Comparing Figure 4-12 with Figure 4-17 it can be observed that, with the delay in the system the controller modified using method 2, has given better results compared to the classical control system but it is not decoupled as desired. Further-

more it can be seen that the controller modified using method 1 has higher decoupling capability and less transients compared to controller designed as described by method 2.

4.5.2 System current behavior after changing the inductance of the system by 1 percent without adding the filter

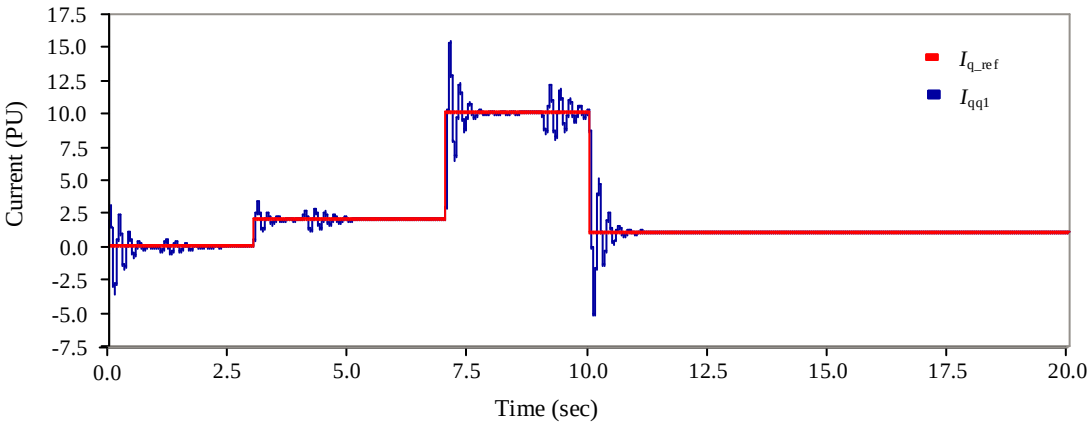

(a)

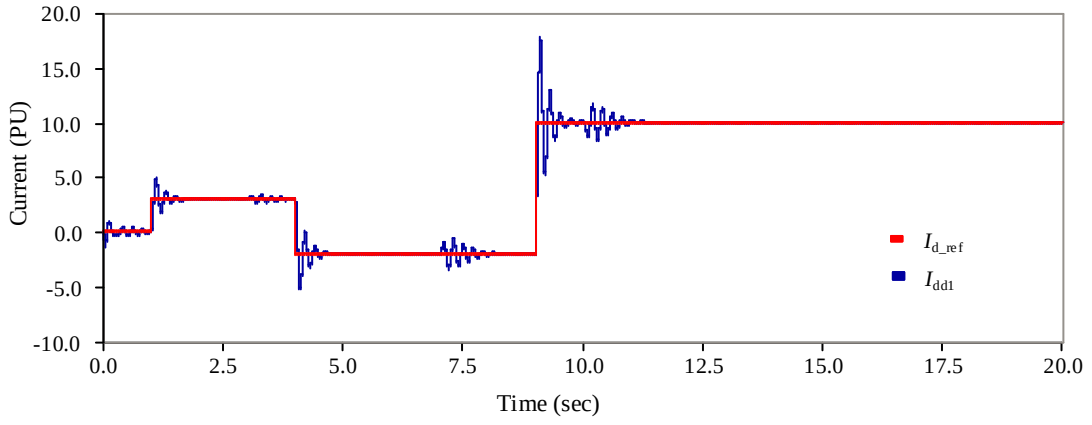

(b)

Figure 4-18 - Reference currents and the system currents (a) in q axis, (b) in d axis when the classical controller is used (with 1% inductance change and without adding a filter)

I_{dd1} and I_{qq1} are the system current in dq0 frame when the I_{d_ref} and I_{q_ref} are given as the reference current inputs to the classical controller. When comparing Figure 4-18 with

Figure 4-7 it can be observed that, with the inductance change in the system, the classical controller has given unexpected results including unpredicted fluctuations and lack of de-coupling capability.

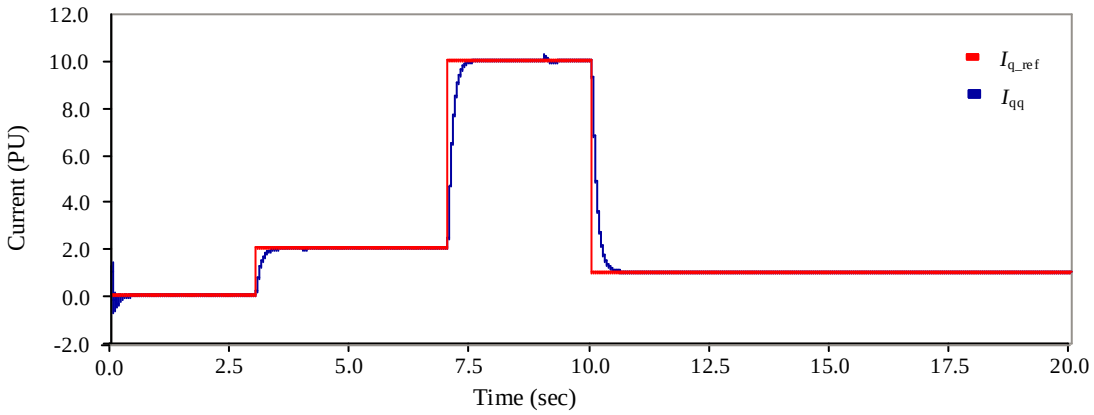

(a)

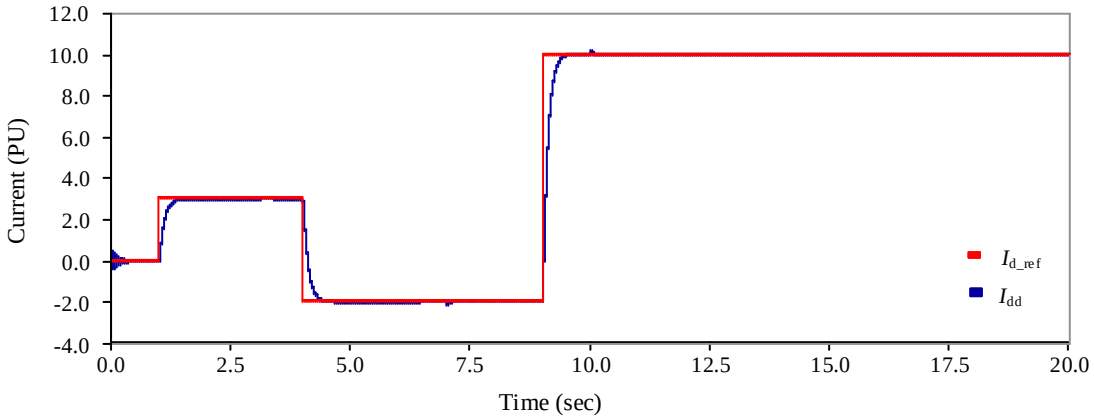

(b)

Figure 4-19 - Reference currents and the system currents (a) in q axis, (b) in d axis, of the modified controller designed using method 1 (with 1% inductance change and without adding a filter)

I_{dd} and I_{qq} are the system current in dq0 frame when the I_{d_ref} and I_{q_ref} are given as the reference current inputs to the modified controller which was designed using the calculations described by method 1. The inductance was changed by 1 percent from its orig-

inal value. Comparing Figure 4-19 with Figure 4-10 it can be observed that, even with the inductance change in the system, the modified controller has given the expected results.

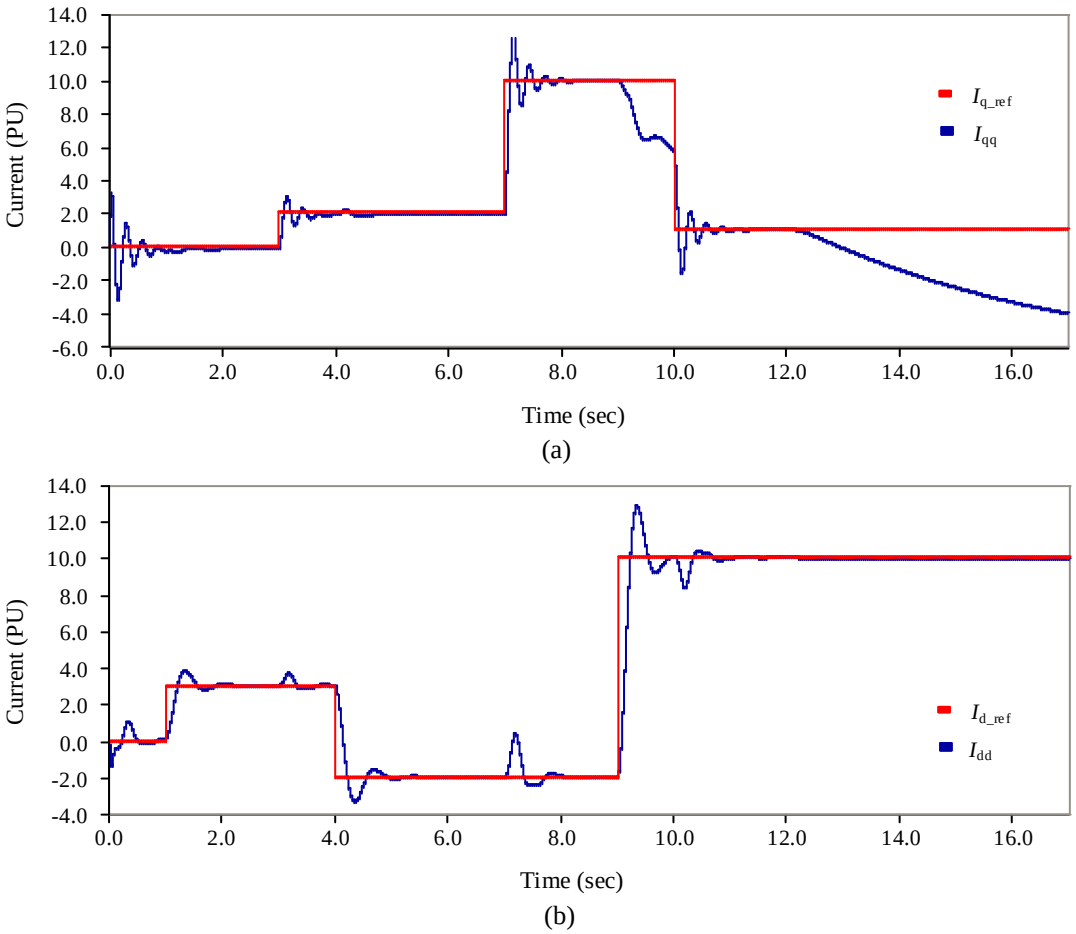

Figure 4-20 - Reference currents and the system currents (a) in q axis, (b) in d axis, of the modified controller designed using method 2 (with 1% inductance change and without adding the filter)

I_{dd} and I_{qq} are the system current in dq0 frame when the I_{d_ref} and I_{q_ref} are given as the reference current inputs to the modified controller designed using the calculations described by method 2. Comparing Figure 4-20 with Figure 4-12 it can be observed that, with the inductance change in the system, the modified controller has given unexpected results including unpredicted fluctuations and lack of decoupling capability. The control-

ler performance modified using method 2 has deteriorated from its reference inputs given to the controller.

4.5.3 System current behavior after changing the inductance of the system by 5 percent without adding the filter

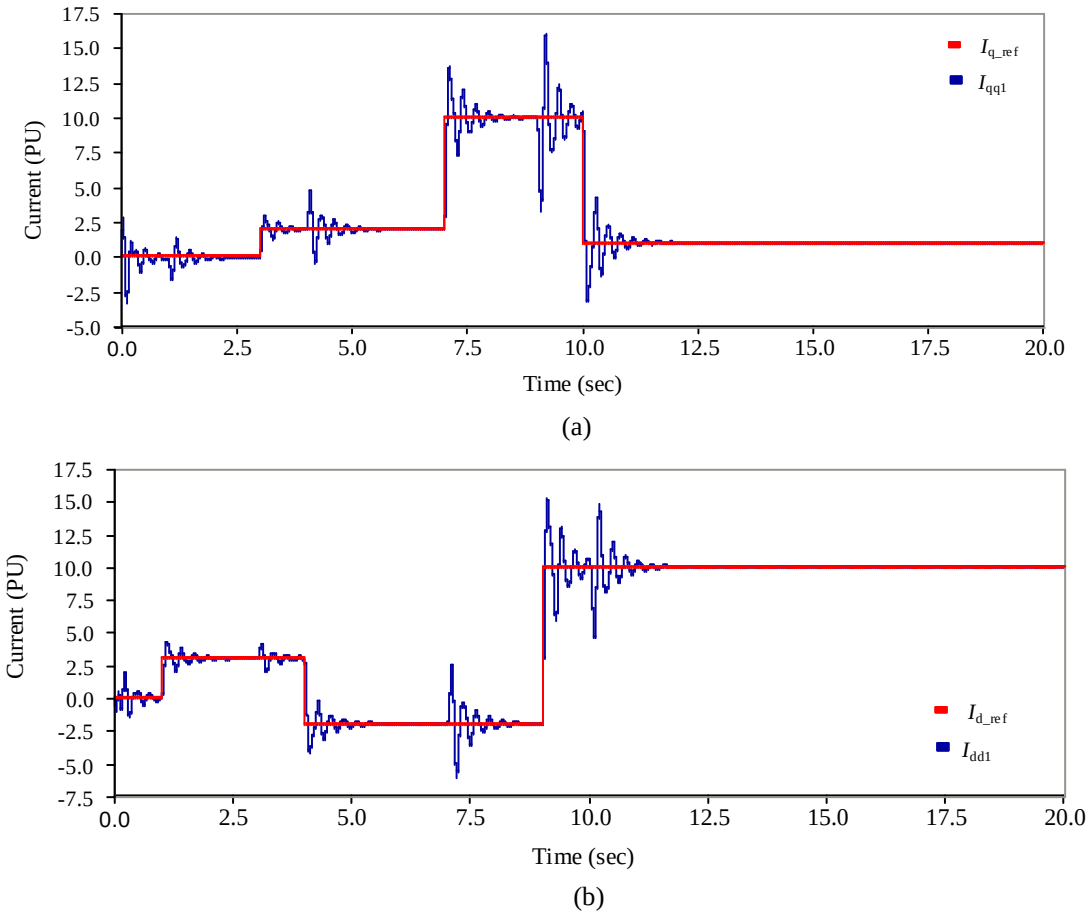

Figure 4-21 - Reference currents and the system currents (a) in q axis, (b) in d axis when the classical controller is used (with 5% inductance change and without adding the filter)

I_{dd1} and I_{qq1} are the system current in dq0 frame when the I_{d_ref} and I_{q_ref} are given as the reference current inputs to the classical controller. Comparing Figure 4-21 with Figure 4-7 it can be observed that, with the 5 percent inductance change in the system, the classical

controller has given unexpected results comprised of unpredicted fluctuations in the output and lack of decoupling capability.

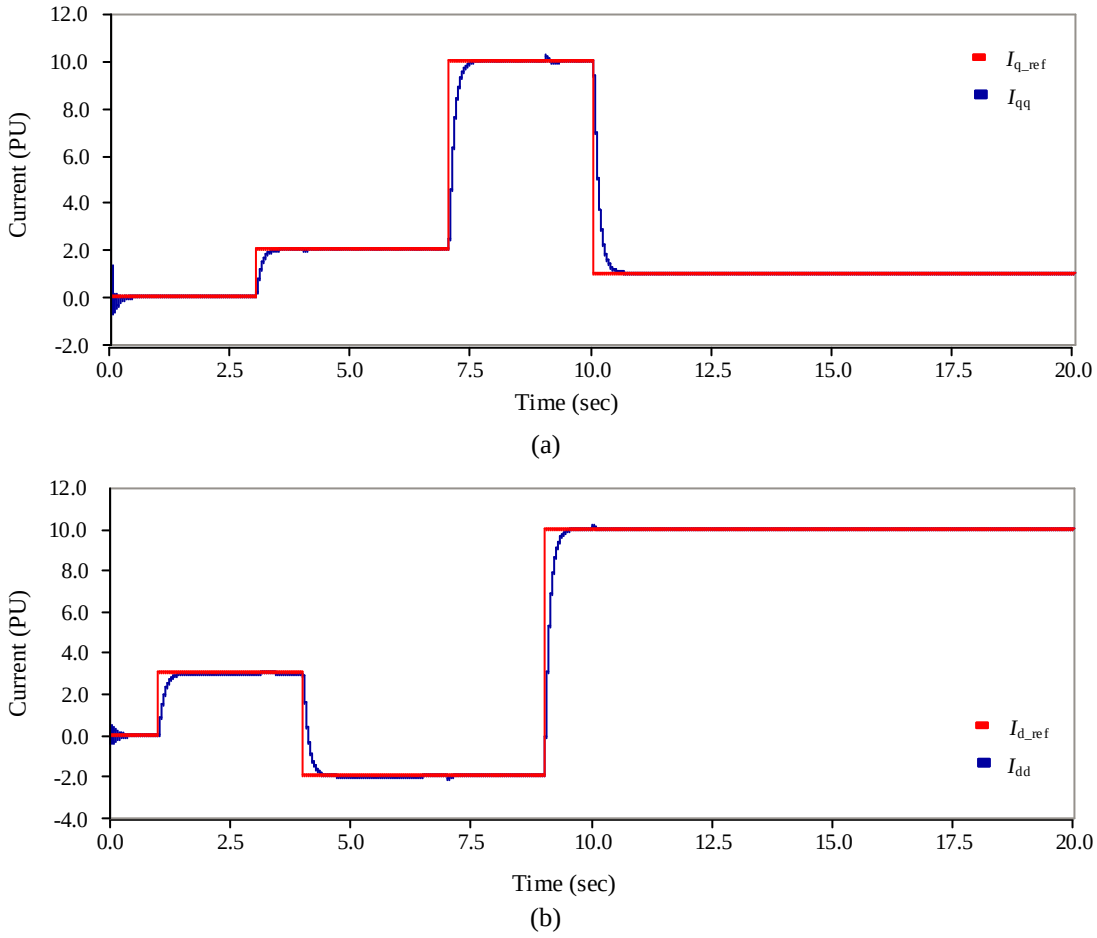

Figure 4-22 - Reference currents and the system currents (a) in q axis, (b) in d axis, of the modified controller designed using method 1 (with 5% inductance change and without adding the filter)

I_{dd} and I_{qq} are the system currents in dq0 frame when the I_{d_ref} and I_{q_ref} are given as the reference current inputs to the modified controller which was designed using the calculations described by method 1. The inductance has been changed by 5 percent from their original values. Comparing Figure 4-22 with Figure 4-10 it can be observed that, even with the inductance change in the system by 5 percent, the modified controller has given the expected results.

4.5.4 System current behavior after changing the inductance of the system by 10 percent without adding the filter

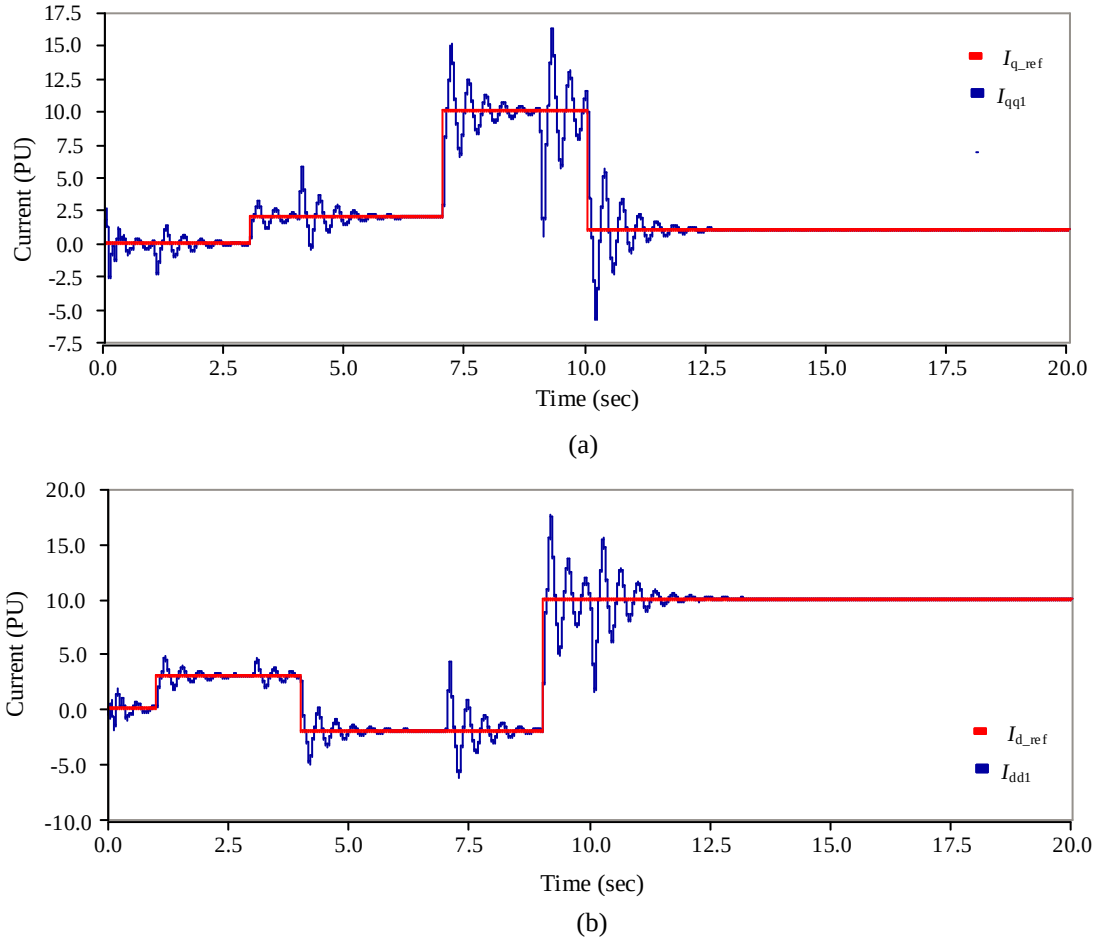

Figure 4-23 - Reference currents and the system currents (a) in q axis, (b) in d axis when the classical controller is used (with 10% inductance change and without adding the filter)

I_{dd1} and I_{qq1} are the system current in dq0 frame when the I_{d_ref} and I_{q_ref} are given as the reference current inputs to the classical controller. Comparing Figure 4-23 with Figure 4-7 it can be observed that, with the 10 percent inductance change in the system, the classical controller has given unexpected results comprised of unpredicted fluctuations and lack of decoupling capability. When comparing the system current performances

with 5 percent inductor change and 10 percent inductor change, it can be clearly seen that when the change of the system parameter increased, the unexpectancy of the controller results has also increased.

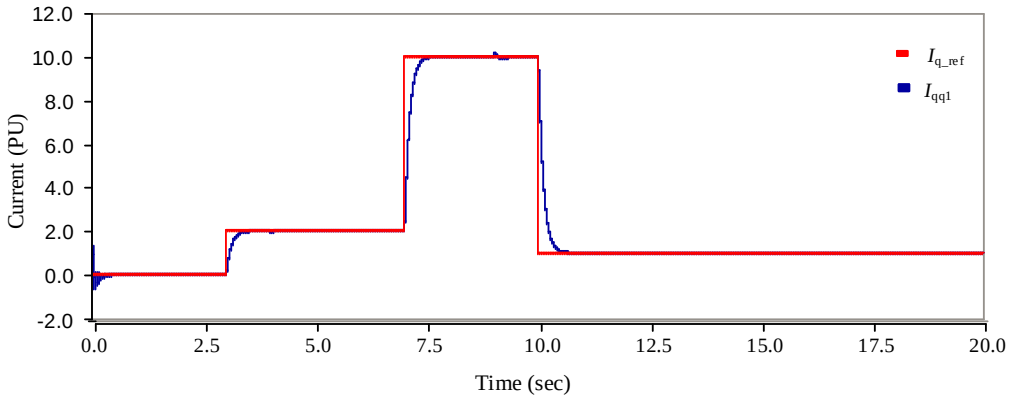

(a)

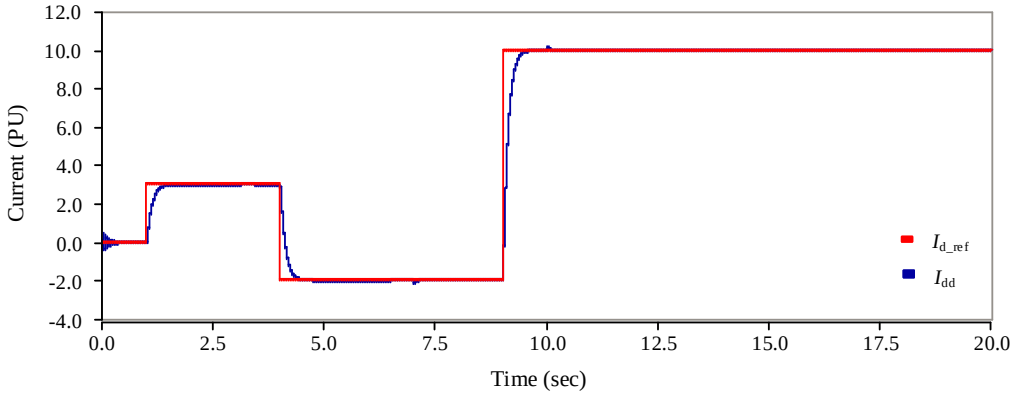

(b)

Figure 4-24 - Reference currents and the system currents (a) in q axis, (b) in d axis, of the modified controller designed using method 1 (with 10% inductance change and without adding a filter)

I_{dd} and I_{qq} are the system current in dq0 frame when the I_{d_ref} and I_{q_ref} are given as the reference current inputs to the modified controller which was designed using the calculations described by method 1. The inductance has been changed by 10 percent from its original value. Comparing Figure 4-22 with Figure 4-10 it can be observed that, even

with the inductance change in the system by 10 percent, the controller modified using method 1, has given the expected results.

4.5.5 System current behavior after changing the inductance of the system by 10 percent with the filter

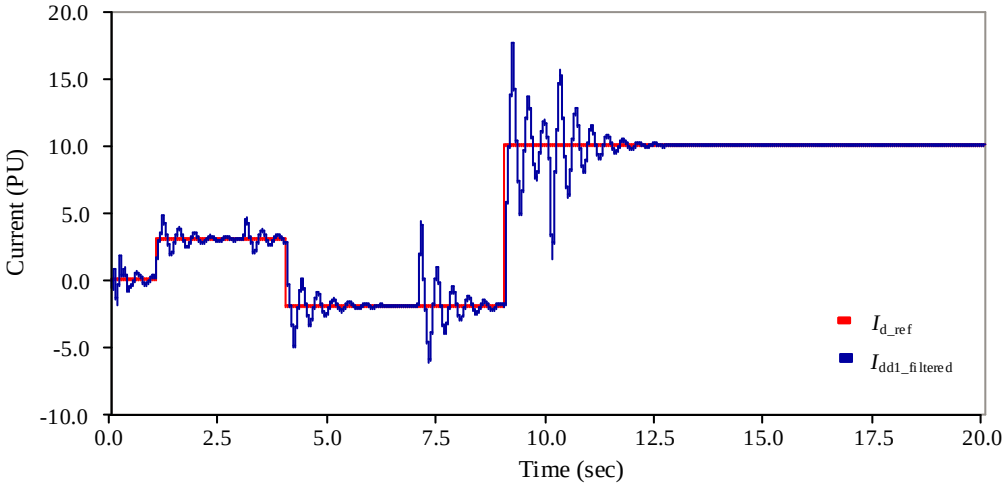

(a)

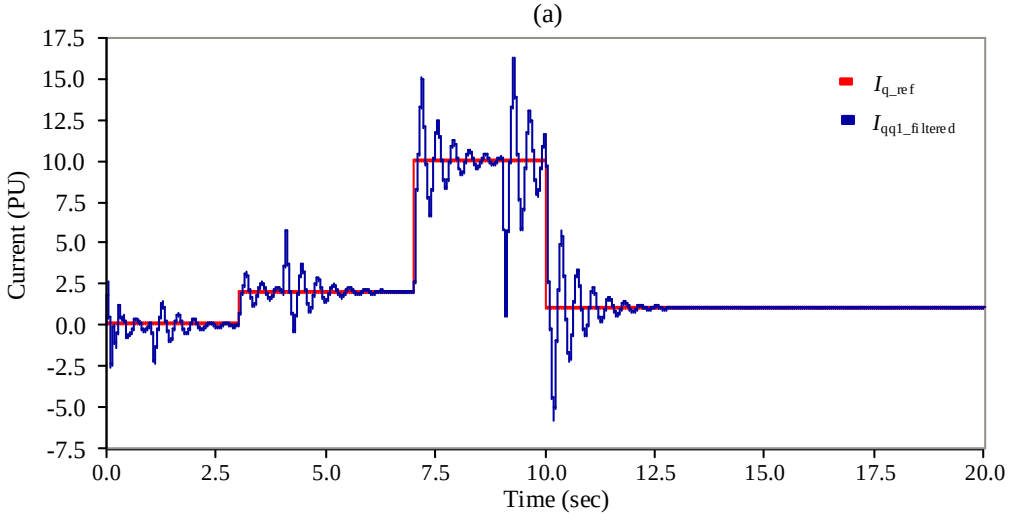

(b)

Figure 4-25 - Reference currents and the system currents (a) in q axis, (b) in d axis when the classical controller is used (with 10% inductance change and after adding a filter)

I_{dd1} and I_{qq1} are the system currents in dq0 frame when the I_{d_ref} and I_{q_ref} are given as the reference current inputs to the classical controller. Comparing Figure 4-25 with Figure 4-7, it can be observed that, with the 10 percent inductance change and addition of the filter in the system, the classical controller has given unexpected results including unpredicted fluctuations and poor decoupling capability. Comparing Figure 4-25 with Figure 4-23 it can be seen that when the filter is added the classical control system output includes a large amount of unexpected fluctuations.

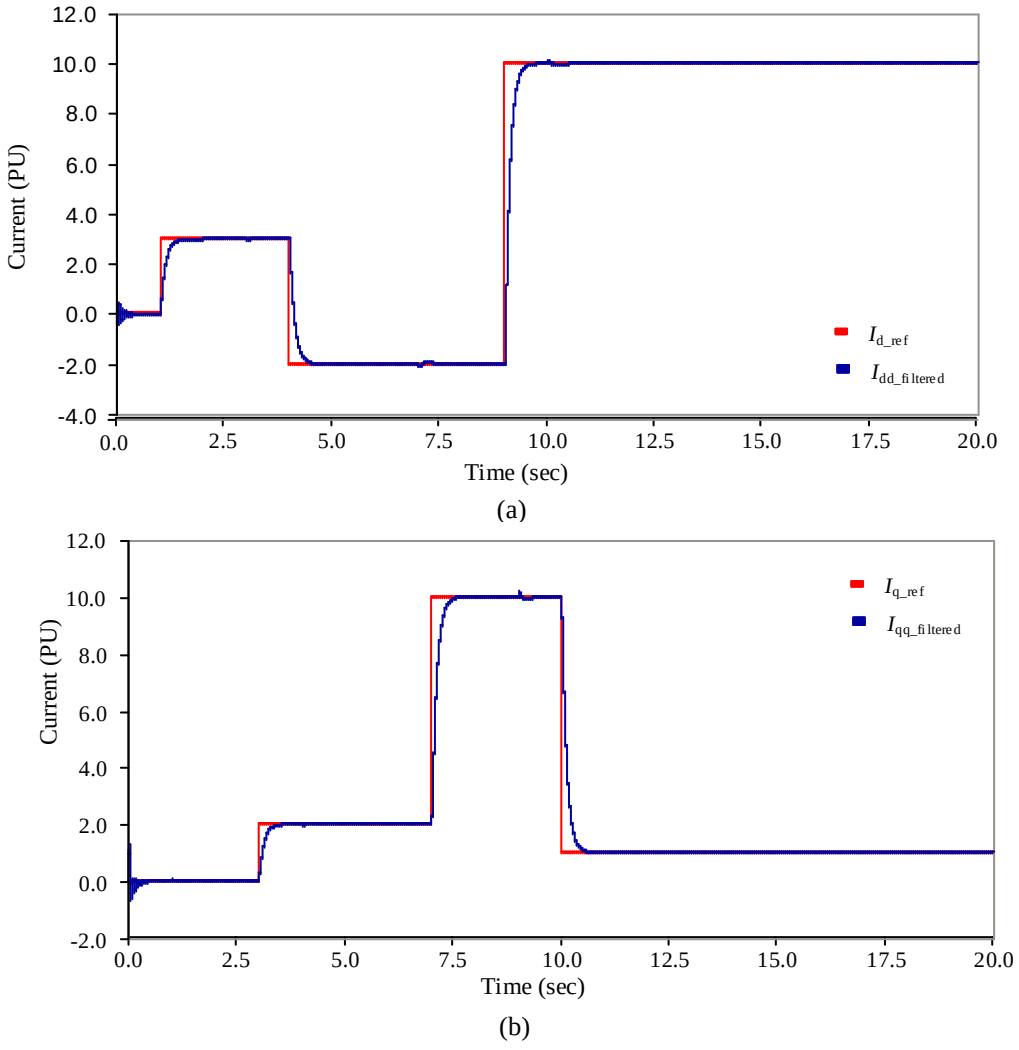

Figure 4-26 - Reference currents and the system currents (a) in q axis, (b) in d axis when the modified controller (using method 1) is used

I_{dd} and I_{qq} are the system current in dq0 frame when the I_{d_ref} and I_{q_ref} are given as the reference current inputs to the modified controller which was designed using the calculations described by method 1. The inductance has been changed from 10 percent and a 0.5ms delay was added to the feedback system. Comparing Figure 4-26 with Figure 4-10 it can be observed that, even with the inductance change in the system by 10 percent with the filter, the modified controller has given expected results.

As per the simulation results shown in this chapter, it can be concluded that the internal model based tracking technique which has been developed for this particular application has the capability of handling uncertainties in the plant parameters as well as the changes of the trajectory. Time delays caused by exogenous conditions such as adding filters to the system can also be compensated. More over the new controller can provide expected results even when there is simultaneous system unexpected conditions.

Chapter 5

Vector Controlled Induction Motor Drives

Electric motors are used in a wide spectrum of power applications ranging from fraction of a Watt to several Mega-Watts and are available in different forms such as ac or dc, and single phase or three phase. DC motors are efficient and because of their characteristics and controllability, have a large presence in motion control applications. However dc motors use physical contacts such as commutators and brushes, which frequently require maintenance due to wear and tear [42]. With the enhancements of power electronic control strategies, advanced control methods of controlling the torque and speed of ac machines have been used in many power system applications. Induction motors are commonly used in most of the industrial applications, due to the simplicity, high efficiency, solid construction and other appealing features [43].

Induction motor drives can usually be categorized as the ones based on the steady state model of the machine and the ones rooted in the dynamic model of the machine. Induction motor controllers designed based on steady state observations of the machine provide acceptable performance only in steady state conditions [44]. The induction motor controllers developed using a transient model of the machine provide acceptable performance under both steady and transient conditions. These control techniques are referred to as field oriented or vector control methods and allow the electromagnetic torque to follow a reference torque providing higher dynamic performance and faster response [44]-[49].

5.1 Induction machine model

To develop the machine model a three phase two pole induction machine has been used and it is assumed to have sinusoidally distributed windings both on the rotor and stator.

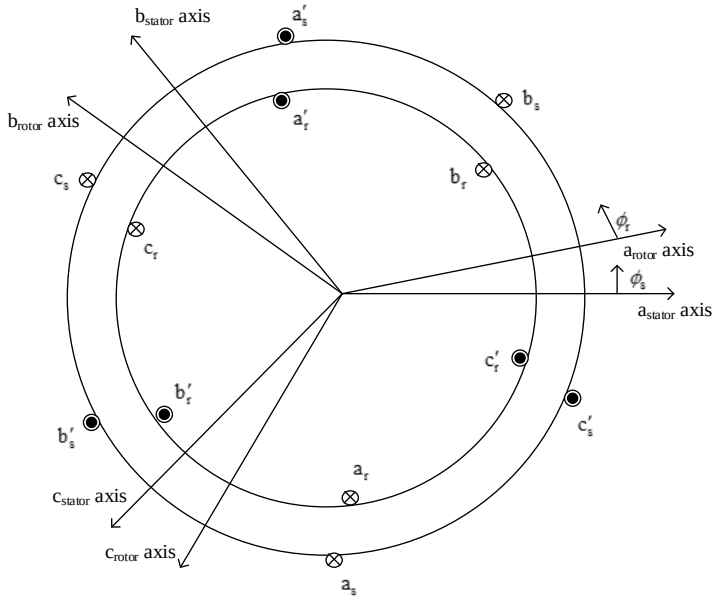

Figure 5-1 – A three phase two pole induction machine

The flux linkages of the stator and the rotor windings can be expressed by the following equation:

$$\begin{bmatrix} \lambda_{abcs} \\ \lambda_{abcr} \end{bmatrix} = \begin{bmatrix} L_s & L_{sr} \\ (L_{sr})^T & L_r \end{bmatrix} \begin{bmatrix} i_{abcs} \\ i_{abcr} \end{bmatrix} \tag{5.1}$$

where the stator flux linkage is $\lambda_{abcs} = [\lambda_{as}\ \lambda_{bs}\ \lambda_{cs}]^T$ and the rotor flux linkage is:

$\lambda_{abcr} = [\lambda_{ar}\ \lambda_{br}\ \lambda_{cr}]^T$.

The voltage equations can be expressed as shown below:

$$V_{abcs} = r_s i_{abcs} + p\lambda_{abcs} \tag{5.2}$$

$$V_{abcr} = r_r i_{abcr} + p\lambda_{abcr} \tag{5.3}$$

where r_r and r_s are the rotor and stator resistance and *p* is the time derivative.

Using Park's transformation the above two sets of equations can be transformed into a dq0 frame where the location of the frame is specified by ɵ as per the Figure 5-2.

The transformation matrix for the stator quantities and rotor quantities can be shown by the following matrices:

$$K_s = \frac{2}{3}\begin{bmatrix} \cos(\theta) & \cos(\theta - \frac{2\pi}{3}) & \cos(\theta + \frac{2\pi}{3}) \\ \sin(\theta) & \sin(\theta - \frac{2\pi}{3}) & \sin(\theta + \frac{2\pi}{3}) \\ \frac{1}{2} & \frac{1}{2} & \frac{1}{2} \end{bmatrix} \text{ and } K_r = \frac{2}{3}\begin{bmatrix} \cos(\beta) & \cos(\beta - \frac{2\pi}{3}) & \cos(\beta + \frac{2\pi}{3}) \\ \sin(\beta) & \sin(\beta - \frac{2\pi}{3}) & \sin(\beta + \frac{2\pi}{3}) \\ \frac{1}{2} & \frac{1}{2} & \frac{1}{2} \end{bmatrix}$$

where $\beta = \theta - \theta_r$ is the angle between the rotor a axis and the q axis of the reference frame.

Let the rotor speed and the stator speed be ω_r and ω_s (elect. rad/s), respectively.

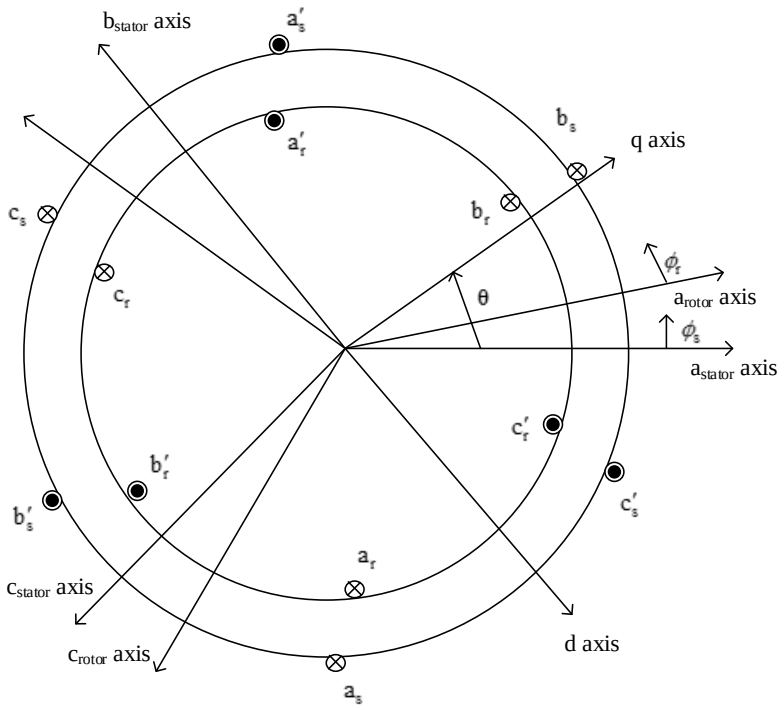

Figure 5-2 – Reference frame for transformation

Using equation (5.1) and the transformation matrices the following equations can be derived:

$$\lambda_{qd0s} = K_s L_s K_s^{-1} i_{qd0s} + K_s L_{sr} K_r^{-1} i_{qd0s}$$

$$\lambda_{qd0r} = K_r L_{sr}^{T} K_s^{-1} i_{qd0s} + K_r L_r K_r^{-1} i_{qd0s}$$

$$\lambda_{qs} = (L_{ls} + L_M) i_{qs} + L_M i_{qr} \tag{5.4}$$

$$\lambda_{ds} = (L_{ls} + L_M) i_{ds} + L_M i_{dr} \tag{5.5}$$

$$\lambda_{0s} = L_{ls} i_{0s} \tag{5.6}$$

$$\lambda_{qr} = (L_{lr} + L_M) i_{qr} + L_M i_{qs} \tag{5.7}$$

$$\lambda_{dr} = (L_{lr} + L_M) i_{dr} + L_M i_{ds} \tag{5.8}$$

$$\lambda_{0r} = L_{lr} i_{0r} \tag{5.9}$$

The rotor and stator voltage equations can be derived as shown below:

$$V_{qs} = r_s i_{qs} + \omega \lambda_{ds} + \frac{d}{dt}\lambda_{qs} \tag{5.10}$$

$$V_{ds} = r_s i_{ds} - \omega \lambda_{qs} + \frac{d}{dt}\lambda_{ds} \tag{5.11}$$

$$V_{0s} = r_s i_{0s} + \frac{d}{dt}\lambda_{0s} \tag{5.12}$$

As the rotor is short circuited its voltage equations will be identical to zero.

$$V_{qr} = r_r i_{qr} + (\omega - \omega_r)\lambda_{dr} + \frac{d}{dt}\lambda_{qr} = 0 \tag{5.13}$$

$$V_{dr} = r_r i_{dr} - (\omega - \omega_r)\lambda_{qr} + \frac{d}{dt}\lambda_{dr} = 0 \tag{5.14}$$

$$V_{0r} = r_r i_{0r} + \frac{d}{dt}\lambda_{0r} \tag{5.15}$$

The torque equation can be derived in the new reference frame as below:

$$T_e = \frac{3}{2}\frac{P}{2}\frac{L_M}{L_M + L_{lr}}(i_{qs}\lambda_{dr} - i_{ds}\lambda_{qr}) \tag{5.16}$$

where P is the number of poles.

5.2 Vector control methodology

When one closely examines the torque equation (5.16) of the induction machine, it can be seen that the electric torque is generated by the interaction between the stator current vector $i_s = \begin{bmatrix} i_{qs} & i_{ds} \end{bmatrix}$ and the rotor flux $\lambda_r = \begin{bmatrix} \lambda_{qr} & \lambda_{dr} \end{bmatrix}$. In this vector control strategy the d ax-

is of the reference frame is aligned with the d axis of the rotor flux vector. Rotor flux is a single entity; therefore the q component of the rotor flux becomes zero.

$$\lambda_{qr} = 0$$

Therefore equation (5.16) can be simplified to:

$$\mathrm{T_e} = \frac{3}{2}\frac{\mathrm{P}}{2}\frac{L_\mathrm{M}}{L_\mathrm{M} + L_\mathrm{lr}}(i_{qs}\lambda_{dr}) \tag{5.17}$$

As per this equation it can be observed that the torque is produced as a result of the armature current and the rotor flux which are 90° apart. The stator current consists of two current components i_{ds} and i_{qs}. The d axis current component (i_{ds}) will be along with the rotor flux and adjusts the field, whereas the q axis current component (i_{qs}), which is perpendicular to the flux, will regulate the torque.

Given $\lambda_{qr} = 0$ let $i_{dr} = 0$

By substituting values for equation (5.8), the following expression can be obtained.

$$\mathrm{T_e} = \frac{3}{2}\frac{\mathrm{P}}{2}\frac{L_\mathrm{M}^2}{L_\mathrm{M} + L_\mathrm{lr}}(i_{qs}i_{ds}) \tag{5.18}$$

With the two assumptions made earlier it can be seen that the induction machine behaviour has become similar to a DC machine, and the following equations can be derived:

$$V_{dr} = r_r i_{dr} + \frac{d}{dt}\lambda_{dr} - (\omega - \omega_r)\lambda_{qr} = 0 \tag{5.19}$$

From equation (5.8) and (5.19),

$$r_r i_{dr} + \frac{d}{dt}((L_{lr} + L_M)i_{dr} + L_M i_{ds}) = 0 \tag{5.20}$$

$$r_r i_{dr} + (L_{lr} + L_M)\frac{d}{dt} i_{dr} = -L_M \frac{di_{ds}}{dt} \tag{5.21}$$

As per the equation (5.21) it can be seen that, to adjust the field at a given value if the d-axis stator current (i_{ds}) is kept constant then the d-axis rotor current will tend to zero.

5.3 Implementation of the vector control strategy

To implement this control methodology, correct placement of the reference frame has obtained using the rotor voltage equations as shown below:

$$r_r i_{qr} + \frac{d}{dt}\lambda_{qr} + (\omega - \omega_r)\lambda_{dr} = 0 \tag{5.22}$$

Therefore,

$$\omega = \omega_r - r_r \frac{i_{qr}}{\lambda_{dr}} \tag{5.23}$$

where ω is the instantaneous speed of the reference frame in electrical rad/s.

With the two assumptions made earlier using equation (5.7):

$$\lambda_{qr} = (L_{lr} + L_M) i_{qr} + L_M i_{qs} = 0$$

Therefore,

$$i_{qr} = \frac{-L_M}{L_{lr} + L_M} i_{qs} \tag{5.24}$$

From equation (5.8),

$$\lambda_{dr} = L_M i_{ds} \tag{5.25}$$

After combining equations (5.23), (5.24) and (5.25),

$$\omega = \omega_{\mathrm{r}} + \frac{r_{\mathrm{r}}}{L_{\mathrm{lr}} + L_{\mathrm{M}}} \frac{i_{\mathrm{qs\_ref}}}{i_{\mathrm{ds\_ref}}} \tag{5.26}$$

where $i_{\mathrm{qs\_ref}}$ and $i_{\mathrm{ds\_ref}}$ are the reference values provided to the converter to drive the motor.

$\omega = \frac{d\theta}{dt}$ Therefore by integrating the speed (ω) over time, the required angle for transformation can be obtained.

By substituting the expression to speed from equations (5.22) and (5.14) following equations can be derived:

$$r_{\mathrm{r}} i_{\mathrm{qr}} + \frac{d}{dt}\lambda_{\mathrm{qr}} + \frac{r_{\mathrm{r}}}{L_{\mathrm{lr}} + L_{\mathrm{M}}} \frac{i_{\mathrm{qs\_ref}}}{i_{\mathrm{ds\_ref}}} \lambda_{\mathrm{dr}} = 0 \tag{5.27}$$

$$r_{\mathrm{r}} i_{\mathrm{dr}} + \frac{d}{dt}\lambda_{\mathrm{dr}} - \frac{r_{\mathrm{r}}}{L_{\mathrm{lr}} + L_{\mathrm{M}}} \frac{i_{\mathrm{qs\_ref}}}{i_{\mathrm{ds\_ref}}} \lambda_{\mathrm{qr}} = 0 \tag{5.28}$$

By finding i_{qr} and λ_{dr} from equations (5.7) and (5.8):

$$i_{\mathrm{qr}} = \frac{1}{L_{\mathrm{lr}} + L_{\mathrm{M}}} \lambda_{\mathrm{qr}} - \frac{L_{\mathrm{M}}}{L_{\mathrm{lr}} + L_{\mathrm{M}}} i_{\mathrm{qs\_ref}} \tag{5.29}$$

$$\lambda_{\mathrm{dr}} = (L_{\mathrm{lr}} + L_{\mathrm{M}}) i_{\mathrm{dr}} + L_{\mathrm{M}} i_{\mathrm{ds\_ref}} \tag{5.30}$$

Using the above equations, the following system equations can be derived,

$$\frac{d\lambda_{\mathrm{qr}}}{dt} = \frac{-r_{\mathrm{r}}}{L_{\mathrm{lr}} + L_{\mathrm{M}}} \lambda_{\mathrm{qr}} - r_{\mathrm{r}} \frac{i_{\mathrm{qs\_ref}}}{i_{\mathrm{ds\_ref}}} i_{\mathrm{dr}} \tag{5.31}$$

$$\frac{di_{\mathrm{dr}}}{dt} = \frac{-r_{\mathrm{r}}}{(L_{\mathrm{lr}} + L_{\mathrm{M}})^2} \frac{i_{\mathrm{qs\_ref}}}{i_{\mathrm{ds\_ref}}} \lambda_{\mathrm{qr}} - \frac{r_{\mathrm{r}}}{L_{\mathrm{lr}} + L_{\mathrm{M}}} i_{\mathrm{dr}} - \frac{L_{\mathrm{M}}}{L_{\mathrm{lr}} + L_{\mathrm{M}}} \frac{di_{\mathrm{ds\_ref}}}{dt} \tag{5.32}$$

As per the above equations it can be seen that the d axis current of the rotor and the q axis flux of the rotor will vanish to zero when the stator d-axis current is kept constant. This will satisfy the conditions for the vector control as it is assumed the q-axis rotor flux is zero, and the d-axis rotor current is zero resulting in the d-axis stator current being the only means to adjust the field. A simple block diagram of the control method is shown below. To yield the required angle for the qd0 transformation speed can be integrated over time. This methodology only measures the speed of the machine and other parameters are estimated. Torque command is generated as a function of speed error ($\omega_{\_ref}$ - ω_r) as shown below.

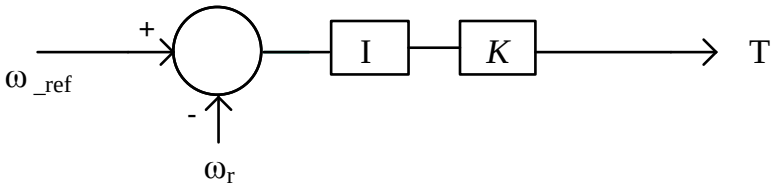

Figure 5-3 – Torque command generator

A simple block diagram of the indirect vector control is shown Figure 5-4.

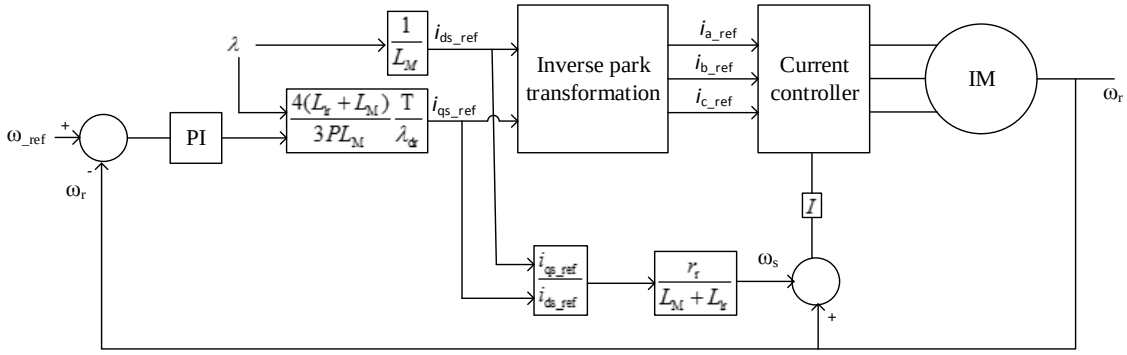

Figure 5-4 – Induction vector control schematic diagram

Figure 5-4 illustrates a summary of generating a three phase stator current to the induction motor. The above case has been designed and simulated using the PSCAD/EMTDC software and the induction machine drive system parameters are given bellow.

Table 5-1 - Induction motor Drive system parameters

Parameter	Value
Machine Voltage	2300 V
Machine Power	500 hp
Machine Frequency	60 Hz
J	11.06 $Kg.m^2$
Stator resistance - R_s	0.262 Ω
X_{ls}	1.206 Ω
X_M	54.02 Ω
X_{lr}	1.206 Ω
Rotor resistance - R_r	0.187 Ω
Pole	4
Input Voltage	3900 V
Input Frequency	60 Hz

Two major parameters in a machine drive system are the machine speed and the torque, which are regulated using a PI controller in this control strategy. Therefore the gain and the time constant of the controller should be carefully tuned to obtain the expected results which is to follow the changes in a reference frame in this particular drive system.

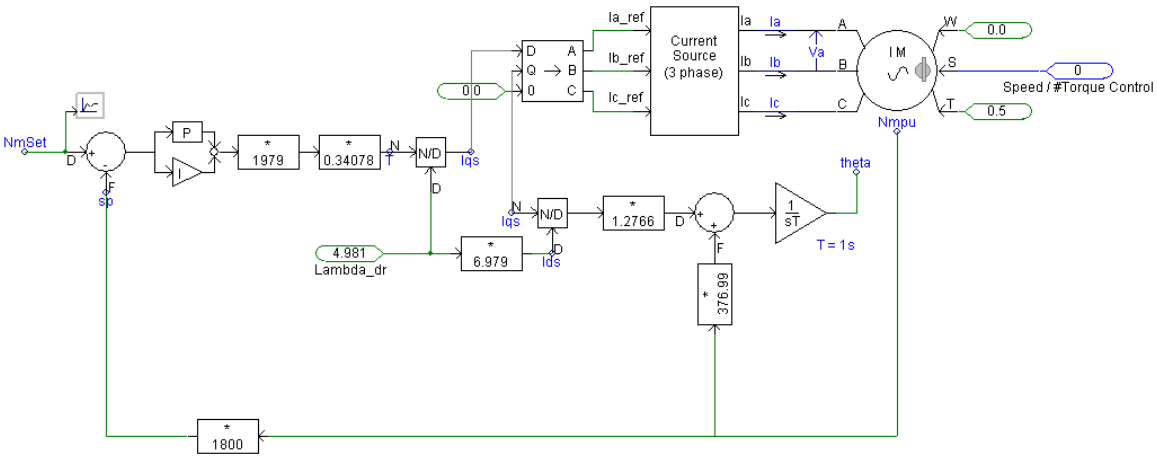

Figure 5-5 – PSCAD/EMTDC simulation for indirect vector control of induction motor

When the case study shown in Figure 5-5 is simulated using the PSCAD/EMTDC software, the following results were obtained.

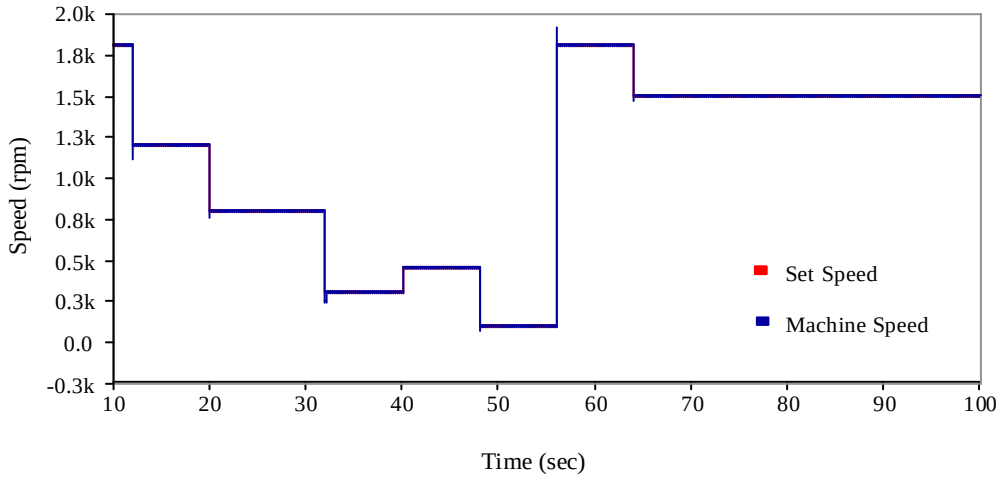

Figure 5-6 – Set speed and the machine actual speed

As per Figure 5-6 it can be seen that the machine speed has followed the set speed. Therefore it can be concluded that the PI controller is well tuned. When the machine speed is closely examined it can be seen that every time the set speed changes there is a transient in the machine speed as shown in Figure 5-7.

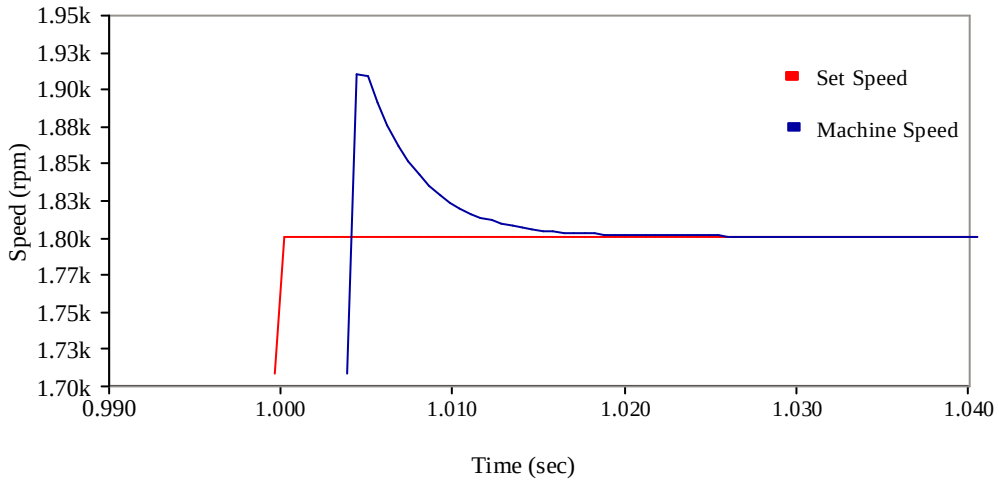

Figure 5-7 – Set speed and the actual speed of the machine

As per Figure 5-7, the reference machine set speed has changed to 1800 rpm but it can be seen that the machine speed has increased up to 1925 rpm before settling to the reference point and it has taken 0.022 seconds to get settled.

5.3 Addition of the internal model to the indirect vector control of the induction machine

As described in Chapter 3 a controller designed with an internal model is able to secure asymptotic decay to zero of the tracking error for every possible trajectory and it can perform robustly with respect to parameter uncertainties of the system. a simple internal model was added to the induction machine controller which is discussed in Section 5.2 to improve its performance. As described in Section 3.2, the internal model design is designed for the induction motor.

Referring to equation (3.15),

$$u(t) = -K_1 \int_0^t e(\tau)\, d\tau - \mathbf{K}_2\mathbf{x}(t)$$

where $u(t)$ is the input to the system and $e(t)$ is the error of that particular time and $\mathbf{x}(t)$ is the state of the system. In this scenario the speed of the machine is considered to be the state. Therefore the modification shown in Figure 5-8 has been made in the control system.

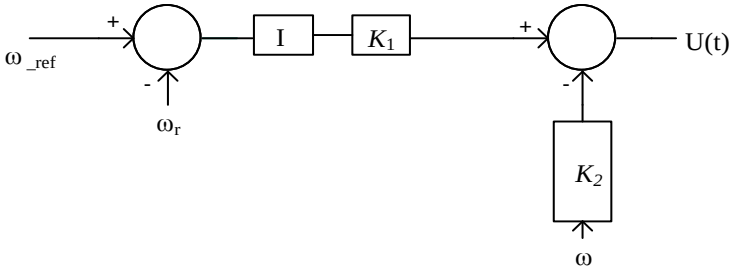

Figure 5.8 - Modified input to the system

Then the gains of the modified controller were tuned to achieve the expected results and following simulations results shown in Figure 5-9 were obtained.

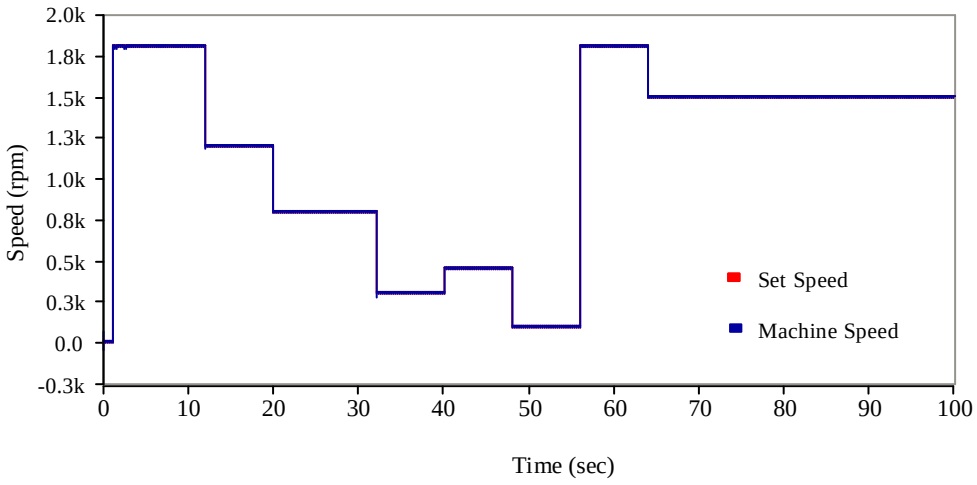

Figure 5-9 - Set speed and the machine actual speed with the modified controller

As per Figure 5-9 it can be seen that the machine speed has followed the set speed. With close examination of the machine speed it can be seen that every time when the set

speed changes there is not much of a transient compared to Figure 5-6. This can be clearly seen in Figure 5-10.

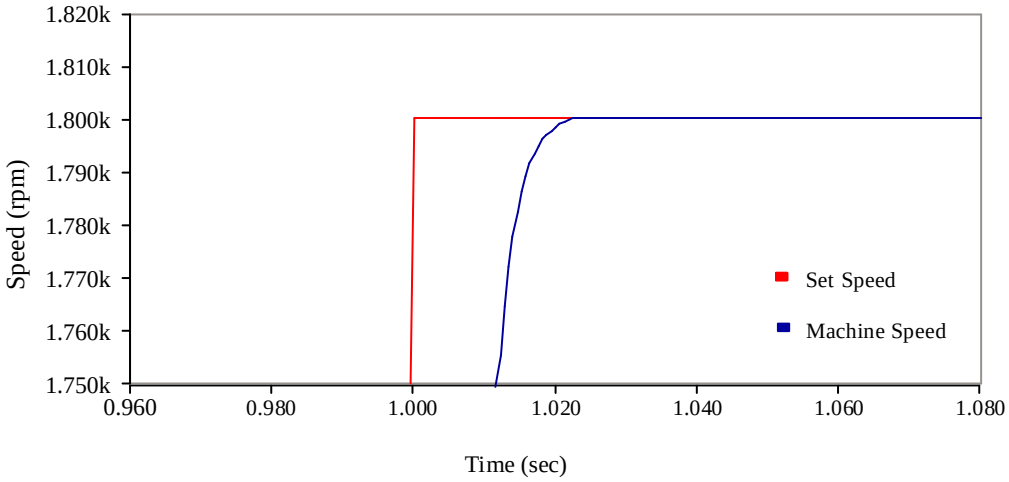

Figure 5-10 - Set speed and the actual speed of the machine with the modified

As per the Figure 5-10, the reference machine set speed has changed to 1800rpm and it can be seen that the machine speed follows the exact reference value and it has taken only 0.018 seconds to get settled. When the two control systems are compared, it can be clearly seen that the modified control system provides faster response and it closely follows the reference speed.

5.4 Controller response with and without internal model to internal parameter change of the machine

When controllers are designed for any power system application or machine drive, most of the system uncertainties that can occur in real time implementation are not considered. Therefore those controllers may need to be re tuned to achieve the expected results under unexpected conditions. In this example, rotor resistance of the machine may change from

its original value. Therefore to check the controller performance, rotor resistance was changed from half of its value to 1.5 times and the following results were obtained.

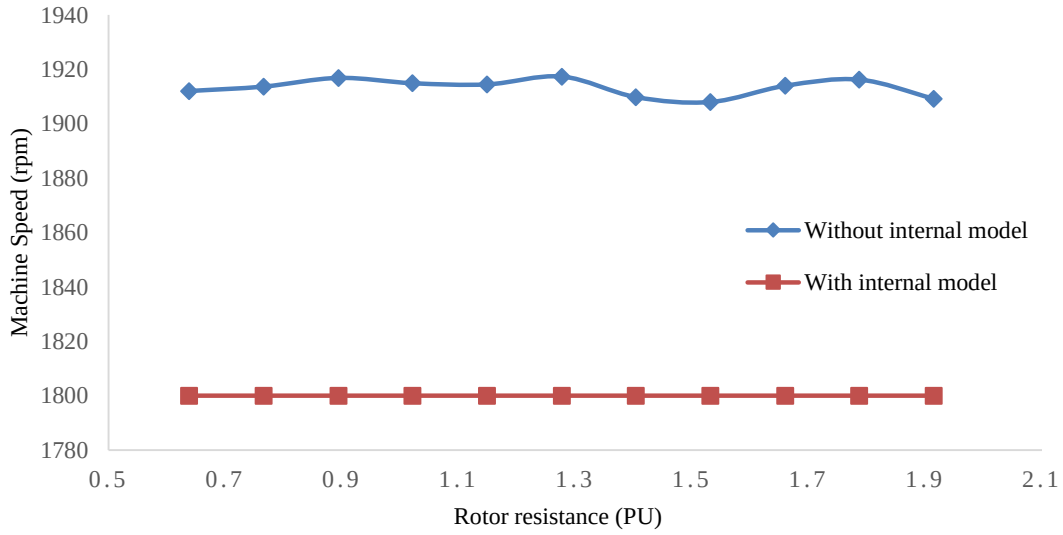

Figure 5-11 – Machine speed variation with the rotor resistance change

Figure 5-11 illustrates how the speed of the machine changes with the change of the rotor resistance. As per the above graph it can be seen that the rotor resistance has been reduced to 50 percent and then increased by 10 percent until 1.5 percent of the original resistance. The reference input speed for the controller is 1800 rpm. The maximum transient machine speed has changed with the rotor resistance change when the normal controller regulate the machine. But with the internal model design it can be seen that the machine has taken the expected speed for every resistance change.

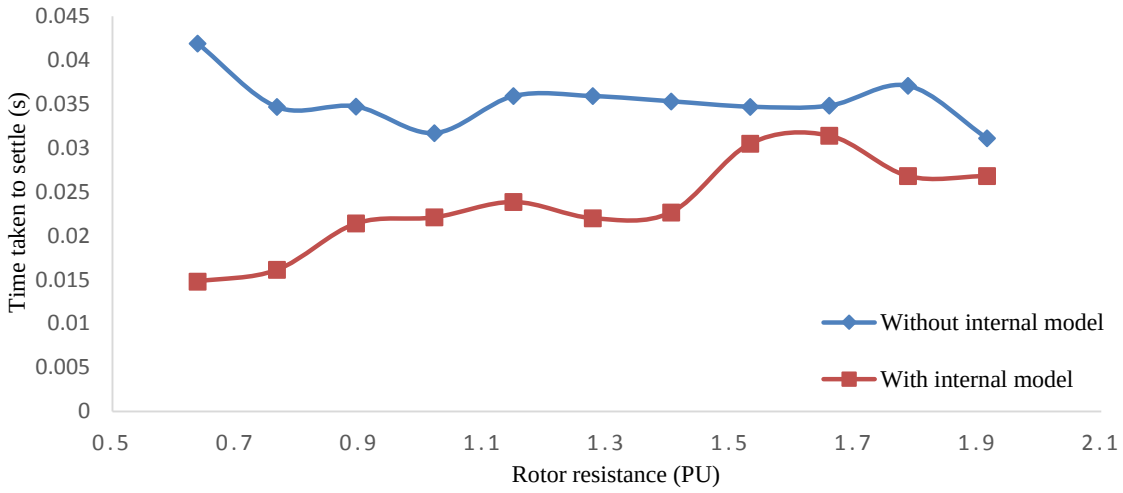

Figure 5-12 – Time taken to settle with the rotor resistance change

Figure 5-12 illustrates how the time taken to obtain the reference speed of the machine changes with the change of the rotor resistance. Settling time has changed with the change of the rotor resistance and when comparing the two cases it can be seen that with the internal model design, the machine has obtained the expected results much faster than the classical controller.

Chapter 6

Conclusions, Contributions and Future Work

6.1 Conclusions and Contributions

Designing a feedback controller to track a reference trajectory for a given power system application is a dominant problem in control theory. In this research a control methodology which consists of an internal model design has been developed to control a voltage source converter and an induction machine. Based on the simulation results of the examples described in Chapter 3 and applications described in Chapter 4 and 5, the following conclusions can be made.

1. In Chapter 3, first-order and second-order system model examples were used to exemplify the internal model design concept. First, classical control systems were developed for both examples to track a reference input given to the con-

trollers and then the classical control systems were modified with internal model designs. Three different controllers were developed for each example. The first controller was a classical control system and the other two controller strategies were designed using internal models. As described in Chapter 3, an internal model controller has an internal state feedback which can be either directly obtained from the system or estimated using a state observer method. The other two controllers were designed by modifying the classical control system and including internal model designs. To compare the response of the classical controller and the modified controllers, similar reference inputs were given to all three cases. Controller performance was checked under normal system conditions and after introducing a disturbance to the system.

According to the simulation results in Chapter 3, it was concluded that all the three cases followed the reference input as desired. However the controllers with the internal model design provided a faster response when the reference was changed compared to the classical controller. Even with the presence of the disturbance, the modified controllers with internal model designs gave better and faster response compared to the classical controller.

2. In Chapter 4, a modified advanced decoupled control system was designed to control a voltage source converter. In this application, the controller was designed to improve the stability of the VSC by providing the real and reactive power. First a basic decoupled controller was designed to achieve independent control of active and reactive power transferred through the converter. Then the

classical control system was modified by adding an internal model design. To check the performance of the modified controller against the classical control system, system parameters were changed up to 10 percent from their original values and a filter was added, which provided 5ms time delay in the system. Controller performance was checked under normal system conditions as well as the resulting unexpected system conditions.

As per the simulation results in Chapter 4, it was concluded that the modified controller with an internal model design has the capability of handling uncertainties in the plant parameters as well as changes of the trajectory. Time delays caused by adding a filter to the system can also be compensated. More over the new controller can provide expected results even when there are simultaneous unexpected conditions. It was shown by simulating the modified decoupled controller that it was able to secure asymptotic decay to zero of the tracking error for every possible trajectory. Therefore the designed internal model controller is a very promising.

3 In Chapter 5, a control system using indirect vector control strategy, was developed to track a set machine speed of an induction motor. This case was implemented in PSCAD/EMTDC and all the proportional and integral gains were carefully tuned to obtain expected performance. Then an internal model controller was added to the existing control system. Controller performance was checked with and without internal model design and after changing the rotor

resistance of the machine to observe its response with system parameter changes.

According to the simulation results of the induction machine controller it was concluded that the modified controllers with the internal model design provided faster response compared to the classical controller. Not only that but also the modified controllers did not involve large transients when the reference value was changed. Furthermore, compared to the classical controller it was seen that the modified controller provides satisfactory results even when the system parameters were changed.

6.2 Future Work

Some related advances that can be considered as possible expansions of this research are;

1 When designing the internal model, a different state observer method such as Kalman filter, can be used to estimate the internal state and compare the performance with the classical control system or with the modified controllers designed with other possible state observer methods.

In this research, Luenberger state observer technique and a state estimator calculated using the system model equations have been used to design the internal model controller. The control strategy developed in this thesis does not provide satisfactory results when there is noise in the system. State observer methods designed using Kalman methodology might be expected to provide satisfactory results in such noisy environments.

2 When designing the controller for the induction motor, few states of the system can be estimated and have more than one internal model designs in the controller.

In this thesis, when the controller was designed using the internal model, only one internal state feedback was used. Adding few internal models with more estimated states within one controller might provide better performance compared to the controllers with one internal model design.

References

[1] R Maglie, A Engler, "Radiation prediction of power electronics drive system for electromagnetic compatibility in aerospace applications," *Power Electronics and Applications (EPE 2011), Proceedings of the 2011-14th European Conference on* ,vol., no., pp.1,9, Aug. 30 2011-Sept. 1 2011

[2] V.G. Agelidis, "Introducing power electronics technologies into the aerospace engineering undergraduate curriculum," *Power Electronics Specialists Conference, 2004.PESC 04. 2004 IEEE 35th Annual*, vol.4, no., pp.2719, 2724Vol.4, 2004 doi: 10.1109/PESC.2004.1355262

[3] K.Shenai, "Silicon carbide power converters for next generation aerospace electronics applications," *National Aerospace and Electronics Conference, 2000. NAECON 2000.Proceedings of the IEEE 2000*, vol., no., pp.516, 523, 2000 doi:10.1109/NAECON.2000.894955

[4] L.J Feiner, "Power electronics for transport aircraft applications," *Industrial Eletronics, Control, and Instrumentation, 1993. Proceedings of the IECON '93, International Conference on* , vol., no., pp.719,724 vol.2, 15-19 Nov 1993 doi: 10.1109/IECON.1993.338992

[5] Ying Xiao, H.N Shah, R Natarajan, Rymaszewski, J.Eugene, T.P Chow, R.J Gutmann, "Integrated flip-chip flex-circuit packaging for power electronics applications," *Power Electronics, IEEE Transactions on* , vol.19, no.2, pp.515,522, March 2004 doi: 10.1109/TPEL.2003.820586

[6] C. G. Hodge, "Modern applications of power electronics to marine propulsion systems," *Power Semiconductor Devices and ICs, 2002. Proceedings of the 14th International Symposium on*, vol., no., pp.9, 16, 2002 doi: 10.1109/ISPSD.2002.1016160

[7] R. Jayabalan, B. Fahimi, A Koenig, S. Pekarek, "Applications of power electronics-based systems in vehicular technology: state-of-the-art and future trends," *Power electronics Specialists Conference, 2004. PESC 04. 2004 IEEE 35th Annual*, vol.3, no., p.1887, 1894 Vol.3, 20-25 June 2004 doi: 10.1109/PESC.2004.1355405

[8] L. Moran, "Power electronics applications in utility systems," *Industrial Electronics Society, 2003. IECON '03. The 29th Annual Conference of the IEEE* , vol.3, no.,pp.3027,3028 Vol.3, 2-6 Nov. 2003 doi: 10.1109/IECON.2003.1280733

[9] T. Curcic, Wolf, A. Stuart, "Superconducting hybrid power electronics for military systems," *Applied Superconductivity, IEEE Transactions* on , vol.15, no.2, pp.2364,2369, June 2005 doi: 10.1109/TASC.2005.849667

[10] R.Radzuan, M.A.A Raop, M.K.M. Salleh, M.K. Hamzah, R.A. Zawawi, "The designs of low power AC-DC converter for power electronics system applications," *Computer Applications and Industrial Electronics (ISCAIE), 2012 IEEE Symposium on* , vol., no., pp.113,117, 3-4 Dec. 2012 doi: 10.1109/ISCAIE.2012.6482080

[11] K.H. Edelmoser, F.A. Himmelstoss, "Analysis of a new high-efficiency DC-to-AC inverter," *Power Electronics, IEEE Transactions on*, vol.14, no.3, pp.454, 460, May 1999 doi: 10.1109/63.761689

[12] Hyunchul Eom, Youngjong Kim, Yongsang Shin, "A TRIAC dimmable driver design for high dimmer compatibility in low power LED lighting," *Power Electronics and Applications (EPE), 2013 15th European Conference* on , vol., no., pp.1,5, 2-6 Sept. 2013

doi: 10.1109/EPE.2013.6631916

[13] Zhijun Jiang, Xiaoling Huang, Na Lin, "Simulation study of heavy motor soft starter based on discrete variable frequency," *Computer Science & Education, 2009. ICCSE '09. 4th International Conference on*, vol., no., pp.560, 563, 25-28 July 2009 doi: 10.1109/ICCSE.2009.5228368

[14] A.A Shepherd, "The properties of semi-conductor devices," *Radio Engineers, Journal of the British Institution* of, vol.17, no.5, pp.255, 273, May 1957 doi: 0.1049/jbire.1957.0024

[15] R.A Hamilton, Lezan, R. George, "Thyristor Adjustable Frequency Power Supplies for Hot Strip Mill Run-Out Tables," *Industry and General Applications, IEEE Transactions* on , vol.IGA-3, no.2, pp.168,175,March 1967 doi: 10.1109/TIGA.1967.4180756

[16] R.W. Roberts, G.R. Mallory, R.C Blackmond, "Thyristor Controlled, 4300-kW Power Supply System for a Mixed Melter Glass Furnace," *Industry Applications, IEEE Transactions on* , vol.IA-12, no.5, pp.516,523, Sept. 1976 doi: 10.1109/TIA.1976.349463

[17] P.K. Dash, A.M. Sharaf, E.F Hill, "An adaptive stabilizer for thyristor controlled static VAR compensators for power systems," *Power Systems, IEEE Transactions on*, vol.4, no.2, pp.403, 410, May 1989 doi: 10.1109/59.193809

[18] H. Mitlehner, J. Sack, H. Schulze, "High voltage thyristor for HVDC transmission and static VAr compensators," *Power Electronics Specialists Conference, 1988. PESC '88 Record., 19th Annual IEEE* , vol., no., pp.934,939 vol.2, 11-14 April 1988 doi: 10.1109/PESC.1988.18228

[19] C. A Brough, C.C. Davidson, J. D. Wheeler, "Power electronics in HVDC power transmission," *Power Engineering Journal*, vol.8, no.5, pp.233, 240, Oct. 1994 doi: 10.1049/pe: 19940510

[20] A.K Chattopadhyay, "An Adjustable-Speed Induction Motor Drive with a Cycloconverter-Type Thyristor-Commutator in the Rotor," *Industry Applications, IEEE Transactions on* , vol.IA-14, no.2, pp.116,122, March 1978 doi:10.1109/TIA.1978.4503505

[21] Dechuan Chen; Meifang Wang, "Soft Variable Structure Control for Sealing Temperature of Bag Making Machine," *Control and Automation, 2007. ICCA 2007. IEEE International Conference on*, vol., no., pp.720, 723, May 30 2007-June 1 2007 doi: 10.1109/ICCA.2007.4376449

[22] Lianfa Yang; Miaomiao Zhang; Yihong Jiang, "A new approach for temperature control of medical air insulation blanket," *Intelligent Computing and Intelligent Systems, 2009. ICIS 2009. IEEE International Conference on*, vol.2, no., pp.261, 263, 20-22 Nov. 2009 doi: 10.1109/ICICISYS.2009.5357958

[23] C. Meyer, R.W. De Doncker, "Solid-state circuit breaker based on active thyristor topologies," *Power Electronics, IEEE Transactions on* , vol.21, no.2, pp.450,458, March 2006 doi: 10.1109/TPEL.2005.869756

[23] M. Azuma, M. Kurata, "GTO thyristors," *Proceedings of the IEEE* , vol.76, no.4, pp.419,427, Apr 1988 doi: 10.1109/5.4427

[24] Z. Zhao, M.R. Iravani, "Application of GTO voltage-source inverter for tapping HVDC power," *Generation, Transmission and Distribution, IEE Proceedings* , vol.141, no.1, pp.19,26, Jan 1994 doi: 10.1049/ip-gtd:19949604

[25] A Balestrino, F. B Verona, A. Landi, “On-line process estimation by ANNs and Smith controller design”. *IEE proceedings - Control theory and applications, 1998*, 145(2):231-235.

[26] Zhang Zhi-Gang; Zou Ben-Guo; Bi Zhen-Fu, "Dahlin algorithm design and simulation for time-delay system," *Control and Decision Conference, 2009. CCDC '09. Chinese*, vol., no., pp.5819, 5822, 17-19 June 2009 doi: 10.1109/CCDC.2009.5195239

[27] Introduction to Estimation and the Kalman Filter Hugh Durrant-Whyte Australian Cenre for Field RoboticsThe University of Sydney NSW 2006 Australia hugh@acfr.usyd.edu.au January 2, 2001Version 2.2

[28] K. Warwick and D. Rees, Industrial Digital Control Systems, IET, 1988

[29] T.H. Lee, T.S. Low, A. Al-Mamun, and C.H. Chen, "Internal model control (IMC) approach for designing disk drive servo-controller," IEEE Trans. Ind. Electron., Vol. 42, no. 3, pp. 248-56, 1995.

[30] A Two Degrees of Freedom Control Design For Robot Manipulator Using Internal Model Structure.

[31] Shu-fen Qi; Yong Yang; Chong Zhao, "Study of Internal Model Control Based on Feed forward Compensation," *Intelligent Systems and Applications, 2009. ISA 2009. International Workshop on*, vol., no., pp.1, 4, 23-24 May 2009 doi: 10.1109/IWISA.2009.5073124

[32] H. R. TeimooriPota, M. Garratt, M.K. Samal, "Helicopter flight control using inverse optimal control and backstepping", *Control Automation Robotics & Vision (ICARCV), 2012 12th International Conference on* page(s): 978 – 983

[33] Colasanto, L.; Tsagarakis, N.G.; Zhibin Li; Caldwell, D.G., "Internal model control for improving the gait tracking of a compliant humanoid robot," Intelligent Robots and Systems (IROS), 2012 IEEE/RSJ International Conference on , vol., no., pp.5347,5352, 7-12 Oct. 2012 doi: 10.1109/IROS.2012.6385978

[34] Robust Adaptive Control by Petros A. Ioannou, Jing Sun Publisher: Prentice Hall PTR 1995 ISBN/ASIN: 0134391004 ISBN-13: 9780134391007

[35] I. Papic, P. Zunko, D. Povh, M. Weinhold, "Basic control of unified power flow controller," *Power Systems, IEEE Transactions on*, vol.12, no.4, pp.1734,1739, Nov 1997 doi: 10.1109/59.627884

[36] R.E Kalmon, "A New Approach to Linear Filtering and Prediction Problem," *SIAM J, Control*, Vol. 1, 1963, pp. 152-193.

[37] R.E Kalman and R.S Bucy, "New Results in Linear Filtering and Prediction Theory," *Transactions of American Society of Mechanical Engineering, Series D, Journal of Basic Engineering*, 1961,pp.95-108

[38] M. Bodson, "High Performance Control of a Permanent Magnet Stepper Motor," *IEEE Transactions on Control Systems Technology*, March 1993, pp.5-14.

[39] Luenberger, D.G., "Observing the State of a Linear System," *Military Electronics, IEEE Transactions on*, vol.8, no.2, pp.74, 80, April 1964, doi: 10.1109/TME.1964.4323124

[40] Modern Control System, 11th addition by Richard C. Dorf and Robert H. Bishop

[41] Schauder, C.; Mehta, H., "Vector analysis and control of advanced static VAr compensators," *Generation, Transmission and Distribution, IEE Proceedings C*, vol.140, no.4, pp.299, 306

[42] P.C. Sen, Principles of Electric Machines and Power electronics, 2nd edition, Wiley, 1996

[43] B.K Bose, Modern Power electronics and AC drives, Englewood Cliffs, NJ: Prentice-Hall, 2001.

[44] R. Krishnan, Electric Motor Drives: Modeling, Analysis, and control, Upper Saddle River, NJ: Prentice-Hall Inc,2011

[45] F.Boldea, S.A. Nasar, Vector control of ac drives, CRC Press Inc. Boca Roaton, FL, 1992

[46] Yen-Shin Lai, "Modeling and vector control of induction machines-a new unified approach," *Power Engineering Society 1999 Winter Meeting, IEEE* , vol.1, no., pp.47,52 vol.1, 31 Jan-4 Feb 1999 doi: 10.1109/PESW.1999.747424

[47] A. M Trzynadlowski, "The Field Orientation Principle in Control of Induction Motor," Kluwer Academic Publishers, Hingham, MA, 1994

[48] N. P. Quang and J. Dittrich, Vector Control of Three-Phase AC Machines: System Development in the Practice, Springer, 2008

[49] R.D. Lorenz, "Tuning of Field-Oriented Induction Motor Controllers for High-Performance Applications," *Industry Applications, IEEE Transactions* on , vol.IA-22, no.2, pp.293,297, March 1986 doi: 10.1109/TIA.1986.4504717